BRNO UNIVERSITY OF TECHNOLOGY
VYSOKÉ UČENÍ TECHNICKÉ V BRNĚ

FACULTY OF MECHANICAL ENGINEERING
FAKULTA STROJNÍHO INŽENÝRSTVÍ

INSTITUTE OF MACHINE AND INDUSTRIAL DESIGN
ÚSTAV KONSTRUOVÁNÍ

THE EFFECT OF VISCOELASTICITY AND OPERATING CONDITIONS ON FRICTION OF COMPLIANT CONTACTS
VLIV VISKOELASTICITY A PROVOZNÍCH PODMÍNEK NA TŘENÍ PODDAJNÝCH KONTAKTŮ

MASTER'S THESIS
DIPLOMOVÁ PRÁCE

AUTHOR
AUTOR PRÁCE

Bc. Cheney Quinn

SUPERVISOR
VEDOUCÍ PRÁCE

Ing. David Nečas, Ph.D.

BRNO 2021

BRNO UNIVERSITY OF TECHNOLOGY
FACULTY OF MECHANICAL ENGINEERING

Assignment Master's Thesis

Institut:	Institute of Machine and Industrial Design
Student:	**Bc. Cheney Quinn**
Degree programm:	Mechanical Engineering
Branch:	Mechanical Engineering Design
Supervisor:	**Ing. David Nečas, Ph.D.**
Academic year:	2020/21

As provided for by the Act No. 111/98 Coll. on higher education institutions and the BUT Study and Examination Regulations, the director of the Institute hereby assigns the following topic of Master's Thesis:

The effect of viscoelasticity and operating conditions on friction of compliant contacts

Brief Description:

Within the area of biotribology, an increased attention has been paid to the issue of compliant contacts in recent years. The eye/lens contact, friction between tongue and palate during food processing, tooth brushing, or application of cosmetics may be mentioned as the representative examples. The research studies are usually focused on the evaluation of friction coefficient, while it seems to be apparent that the behaviour of soft–matter contacts is influenced by material viscoelasticity to some extent. The master thesis is thus going to be aimed at the analysis of friction within compliant contact while various materials and operating conditions will be applied. The attention will be later paid to the role of lubricant viscosity.

Type of the thesis: Research
Output of the thesis: Publication (J, D)
Project: Czech Science Foundation (GACR)

Master's Thesis goals:

The main goal is to assess the effect of material viscoelasticity and lubricant viscosity on the coefficient of friction of compliant contact with the use of ball–on–disc tribometer. Various operating conditions will be applied, aiming on the mimicking of real biotribological applications of compliant contacts.

Sub–aims of the master thesis:

– to conduct research study of recent publications dealing with biotribology of soft contacts,

– to design suitable material couples mimicking usual biotribological applications of compliant contacts,

– to define operating conditions approaching real applications,

– to analyse the effect of material, viscoelasticity, operating conditions, and lubricant viscosity,

– to discuss obtained results in context of recent papers.

Required outputs: report.

Thesis range: approx. 72,000 characters (40 – 50 pages excluding figures).

Time schedule, thesis structure and the template of the report must follow:
http://ustavkonstruovani.cz/texty/magisterske–studium–ukonceni/

Recommended bibliography:

PUTIGNANO, C. and D. DINI, 2017. Soft Matter Lubrication: Does Solid Viscoelasticity Matter? ACS Applied Materials & Interfaces. 9(48), 42287-42295.

SADOWSKI, P. and S. STUPKIEWICZ, 2019. Friction in lubricated soft-on-hard, hard-on-soft and soft-on-soft sliding contacts. Tribology International. 129, 246-256.

DE VICENTE, J, J. R. STOKES and H. A. SPIKES, 2006. Rolling and sliding friction in compliant, lubricated contact. Proceedings of the Institution of Mechanical Engineers, Part J: Journal of Engineering Tribology. 220(2), 55-63.

Deadline for submission Master's Thesis is given by the Schedule of the Academic year 2020/21

In Brno,

L. S.

prof. Ing. Martin Hartl, Ph.D.
Director of the Institute

doc. Ing. Jaroslav Katolický, Ph.D.
FME dean

ABSTRACT

Compliant contacts containing polymer or rubber members may be found in both technical and biological applications. Despite the development in the field, certain effects influencing the tribological performance of these contacts are yet to be investigated. This work investigates the effects of kinematic conditions, configuration, viscoelasticity, and lubricant viscosity on friction in lubricated compliant contacts. Experimental data were also used to develop a numerical simulation capable of predicting fluid friction in compliant contacts. Mini Traction Machine (MTM) in the ball-on-disc configuration was used to successfully gain insight into the behaviour of compliant contacts, allowing the investigation of the mentioned effects. Findings in the technical applications have confirmed that viscoelastic effects are present in all configurations, being soft-on-hard, hard-on-soft and soft-on-soft, where they seem to be more profound in the configurations using compliant discs. The experimental data also suggest that the slide-to-roll ratio affects rolling friction in all configurations which is contrary to current literature. Data from the biological applications suggest that native lubricants may be substituted by simple lubricants under certain conditions. These findings have the potential to lay the ground for further investigations of compliant contacts.

KEYWORDS

Compliant contact, configuration, friction, kinematic conditions, viscosity, viscoelasticity

ABSTRAKT

Poddajné kontakty obsahující polymerní nebo pryžové členy lze nalézt v technických i biologických aplikacích. I přes vývoj v této oblasti existují efekty, které ovlivňují tribologické aspekty těchto kontaktů, a je třeba je dále zkoumat. Tato práce se zabývá vlivy kinematických podmínek, konfigurace, viskoelasticity a viskozity maziva na tření v mazaných poddajných kontaktech. Výsledky byly použity k vývoji numerického modelu pro predikci kapalinového tření v poddajných kontaktech. K objasnění chování poddajných kontaktů bylo použito zařízení Mini Traction Machine (MTM) v konfiguraci ball-on-disc, což umožnilo zkoumání zmíněných vlivů. Z poznatků z technické oblasti bylo zjištěno, že viskoelasticita se projevuje ve všech konfiguracích, tedy soft-on-hard, hard-on-soft a soft-on-soft, a její efekt je nejvýznamnější v konfiguracích s poddajným diskem. Data dále ukazují, že poměr skluzu a valení má vliv na valivé tření což je v rozporu se současnou literaturou. Výsledky z biologické oblasti naznačují, že za určitých podmínek lze nahradit nativní kapalinu jednoduchým mazivem. Tyto poznatky mohou posloužit jako odrazový můstek pro další studie zabývající se poddajnými kontakty.

KLÍČOVÁ SLOVA

Poddajné kontakty, konfigurace, tření, kinematické podmínky, viskozita, viskoelasticita

BIBLIOGRAPHIC REFERENCE

QUINN, Cheney. *The effect of viscoelasticity and operating conditions on friction of compliant contacts.* Brno, 2021, 119 p. Brno University of Technology, Faculty of Mechanical Engineering, Institute of Machine and Industrial Design. Thesis supervisor Ing. David Nečas, Ph.D.

ACKNOWLEDGMENT

There are many people that I would like to thank. Firstly, I am very thankful to my supervisor, Ing. David Nečas, Ph.D. for his invaluable advice, patience and mentorship during my master's studies. The expressed enthusiasm and shared experience have encouraged me during my research. My thanks also go to Ing. Petr Šperka, Ph.D. for his dedicated time, advice, ideas, and doc. Ing. Radek Kalousek, Ph.D. for his help and enthusiasm while solving certain problems. I also thank Dr. Max Marian for the opportunity to participate in the development of numerical simulation which was very interesting. I would also like to thank my friends both from my class and my personal life for their help, joint discussions, and the time spent together, which I truly cherish. Hopefully, this cooperation will continue in my potential further PhD studies.

My biggest thanks go to my girlfriend Tereza and my family for their undying support and for shedding light on my journey of achieving my master's degree.

Thank you all.

AUTHOR'S DECLARATION ON THE ORIGIN OF THE WORK

I hereby declare that I have written the master's thesis *The effect of viscoelasticity and operating conditions on friction of compliant contacts* on my own according to the advice of my supervisor Ing. David Nečas, Ph.D., and using the sources listed in references.

.....

Author's signature

CONTENT

1 INTRODUCTION

Mechanical systems are an integral part of today's ever-improving world, where one of the most closely monitored parameters is efficiency. These systems mostly transfer energy through contacts in which it is estimated to be lost up to 23% of the world's total energy [1]. This makes tribology an important discipline with the potential of significant savings in lost energy. The development of these devices entails the use of many new materials including polymers, which are extensively used for their simple design providing a range of different mechanical and tribological properties while being cost-efficient. These materials are beginning to appear in several applications such as bearing [2], tires [3], wipers, gears [4] and sealings. Nevertheless, these materials are also extensively used in biological implants [5], contact lenses [6], joint replacements [7], and smart devices [8] as biocompatibility is one of their many properties. This creates several tribological interfaces that are called by many names such as compliant contacts, soft contacts or isoviscous-elastohydrodynamic (i-EHL) contacts.

The downside of these contacts is that viscoelastic effects may be present. These effects can be negligible or they have the potential to increase or modify friction. A better understanding of the compliant contact's behaviour could lead to fine-tuning their behaviour and thus, improving the comfort of wearing contact lenses, decreasing wear in artificial joints or improving traction of tyres. The list of potential improvements could go on and on.

Investigation of these contacts brings new challenges which do not exist in typical rigid (i.e. metal-on-metal) contacts. Rheology of the material has to be accounted for, meaning mechanical properties such as elastic modulus becomes a function of loading frequency for example. This makes the compliant contact a complex interplay of many mechanisms which are still being revealed.

This work mainly investigates the effects of kinematic conditions, viscoelasticity of the material, contact configuration, and lubricant viscosity on friction in lubricated compliant rolling-sliding contacts in pursuit of further describing the behaviour of compliant contacts, as some effects are yet to be investigated.

2 STATE OF THE ART

2.1 Compliant contact

Compliant contact is a contact of two bodies where one of them is made of a material whose modulus of elasticity is lower than 1 GPa. These materials usually have high surface roughness, limited reflectivity, and a large contact area. Considering the conditions, the contact is usually operated in the isoviscous-elastohydrodynamic (i-EHL) lubrication regime (Fig. 2-1). This regime is accompanied by significant elastic deformations in the contact surfaces considerably affecting the film thickness of the lubrication film, whereas the viscosity of the lubricant isn't affected due to low contact pressure [9, 10].

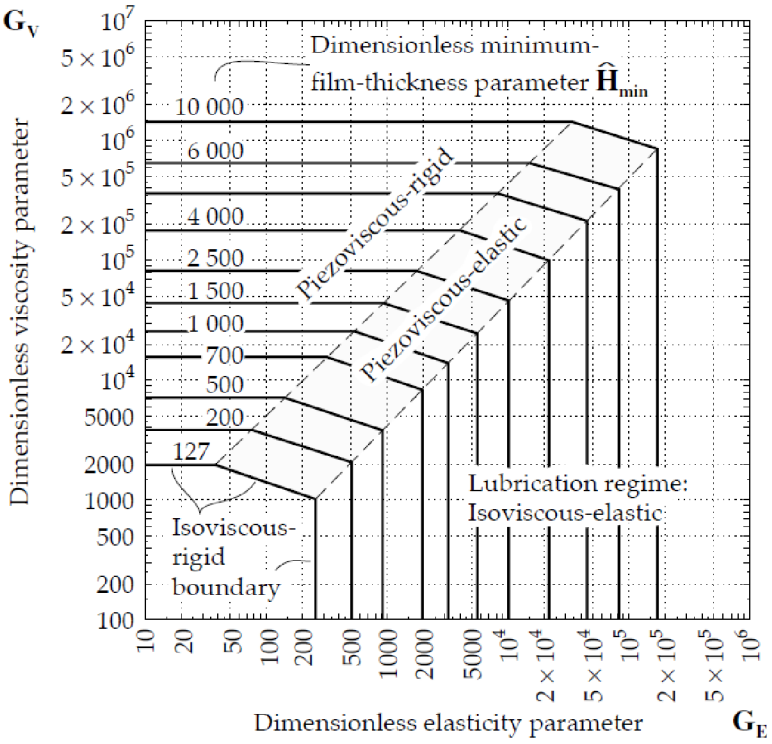

Fig. 2-1 Map of lubrication regimes [10].

2.2 Viscoelasticity

A viscoelastic material has the properties of both elastic and viscous materials. When a force is applied to the elastic material, stress and strain occur simultaneously, whereas for the viscous material, stress and strain experience a lag between one another, which is called phase difference (δ) and is equal to 90°. Viscoelastic material also has a phase difference, which is lower than 90°, as it combines both elastic and viscous material properties [11].

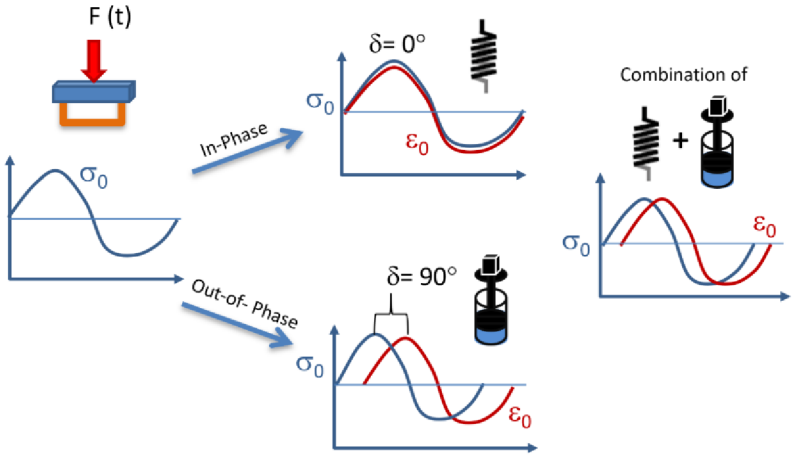

Fig. 2-2 Illustration of the elastic, viscous and viscoelastic behaviour [41].

This material is described using a dynamic modulus denoted by E(ω) - Complex modulus, which consists of E'(ω) - Storage modulus and E''(ω) - Loss modulus. The proportion of loss and storage moduli determines the tangent of phase difference (δ), which can be used to determine elastic hysteresis. The storage modulus describes the stiffness of the measured material and as the name suggests, is a measure of stored elastic energy. The loss modulus describes the proportion of the lost energy due to damping by the viscous part [11].

$$E(\omega) = E'(\omega) + E''(\omega)$$

To determine the dynamic moduli, Dynamic Mechanical Analysis (DMA) can use two approaches: transient or dynamic oscillatory tests. The transient approach uses creep and relaxation, where for the creep test the sample is loaded by a constant force (stress) and deformation is measured in time. After unloading the sample its recovery is measured. The relaxation test deforms the sample by a constant value and stress is measured in time [12, 13].

Measuring the viscoelastic properties may be restrained to a certain range of loading frequency by the device, which is limiting when one wants to evaluate the viscoelastic effects for high frequencies. This can be resolved by using the time-temperature superposition, where temperature and time (frequency) are interchangeable to an extend, so measuring at different temperatures can be used to describe viscoelasticity through a wider spectrum of frequencies than the measuring apparatus is limited to [14].

2.3 Friction in compliant contacts

2.3.1 Compliant contacts in technical applications

Compliant contacts have been predominantly investigated in experimental studies, however, recently numerical solutions have been applied to tackle the problem of lubricated soft contacts. This work mainly focuses on the experimental part so most of the literature also focuses on the experimental measurements.

Bongaerts et al. [15] examined the influence of roughness and the effects of hydrophobicity on lubrication using a Mini Traction Machine (MTM), where both the ball and disc were made of polydimethylsiloxane (PDMS). The influence of surface roughness and hydrophobicity was found to be negligible in the EHL regime. The increase of surface roughness expands the boundaries of boundary and mixed regimes. Hydrophobicity largely affects both boundary and mixed regimes also.

The next research group investigating friction in compliant contacts was led by de Vicente. In one of his work [16], the authors combined both experimental and numerical studies in a rolling-sliding soft-EHL contact. The experimental study was carried out using the MTM in a hard-on-soft configuration, being a steel ball loaded by 3 N against a silicone elastomer over a wide entrainment speed range from 4 mm/s to 1200 mm/s at a fixed slide-to-roll ratio of +/- 50%. The contact was lubricated by a corn syrup-water solution of different concentrations to ensure various viscosities and thus measuring at lubrication regimes from boundary to full-film. The numerical study of the i-EHL circular contact was used to then derive a predictive equation of Couette and Poiseuille friction components. The Couette friction component arises from sliding in the contact and the Poiseuille friction component can be also called rolling friction. The experimental data were averaged using data from positive and negative slide-to-roll ratio, however, this methodology made it unable to directly compare the Poiseuille friction component with the predictions, thus only the Couette friction component was compared with theory, showing good agreement. However, the Poiseuille friction component cannot be neglected even in pure sliding contact, as this component is comparable to the Couette components, making rolling friction a significant part of the whole measured friction.

In the author's next work [17], de Vicente et al. separated the mentioned friction components, being rolling (Poiseuille) friction and sliding (Couette) friction, using a novel experimental technique. Rolling friction occurs when surfaces are in motion relative to the contact. Sliding friction takes place when two contacting surfaces are in relative motion. In a non-conform hard-on-hard contact rolling friction can be neglected due to its size. In the case of compliant contacts rolling friction is comparable to sliding friction and thus must be considered. The measurements were performed on the MTM, where a stainless-steel ball was loaded against a 4.5 mm thick silicone elastomer disc that was clamped against a supporting stainless-steel disc as shown in fig. 2-3.

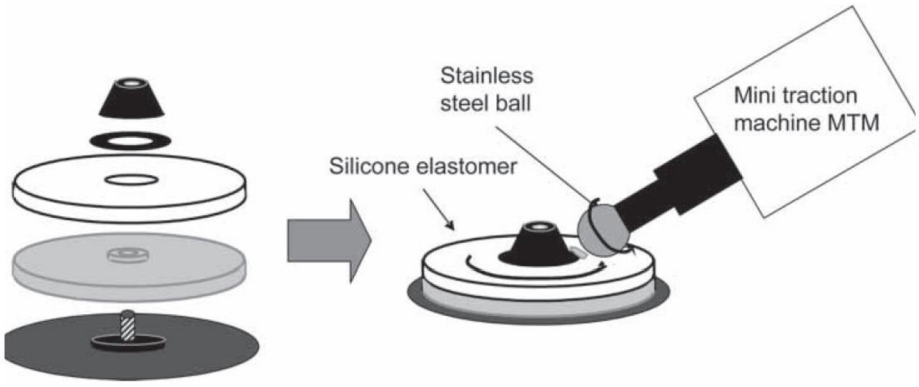

Fig. 2-3 Scheme of the MTM configuration using a silicone disc [17].

Most of the tests had a set value of slide-to-roll ratio to 50%, over a wide range of entrainment speed from 4 mm/s to 1200 mm/s. Thanks to the author's novel approach it was possible to separate rolling and sliding friction. Rolling friction was found to mostly be a product of Poiseuille flow and elastic hysteresis. Also, for high reduced velocities an unexplained rolling friction component was observed. The author also proved that friction is mostly independent of sliding speed due to surface adhesion, elastic hysteresis, and Poiseuille flow. However, Couette flow was found to be proportional to the slide-to-roll ratio.

Myant et al. [18] studied the influence of load and elastic properties on the rolling and sliding friction using MTM with a steel ball that was loaded against a PDMS. Loads were varied during the measurements and three discs were used with different elastic modulus across three orders of magnitude with a constant load. The viscoelastic behaviour of the soft discs was determined using Greenwood's model [19]. The measured Stribeck curves were used to validate the numerical models developed by de Vicente et al [17]. The influence of load on the isoviscous-elastic sliding friction coefficient was in quite close agreement with the numerical models for all three polymers as shown in fig. 2-4a. However, the author states that within the i-EHL regime the friction coefficient increases with decreasing elastic modulus, which does not support the prediction made by de Vicente et al. [17] that says the influence of elastic modulus should be negligible. The author's model is not capable of predicting the i-EHL rolling friction coefficient accurately as a function of applied load. The rolling friction coefficient converges to a constant value of 0.1 at high entrainment speeds, as shown in fig. 2-4b, making rolling friction quite significant.

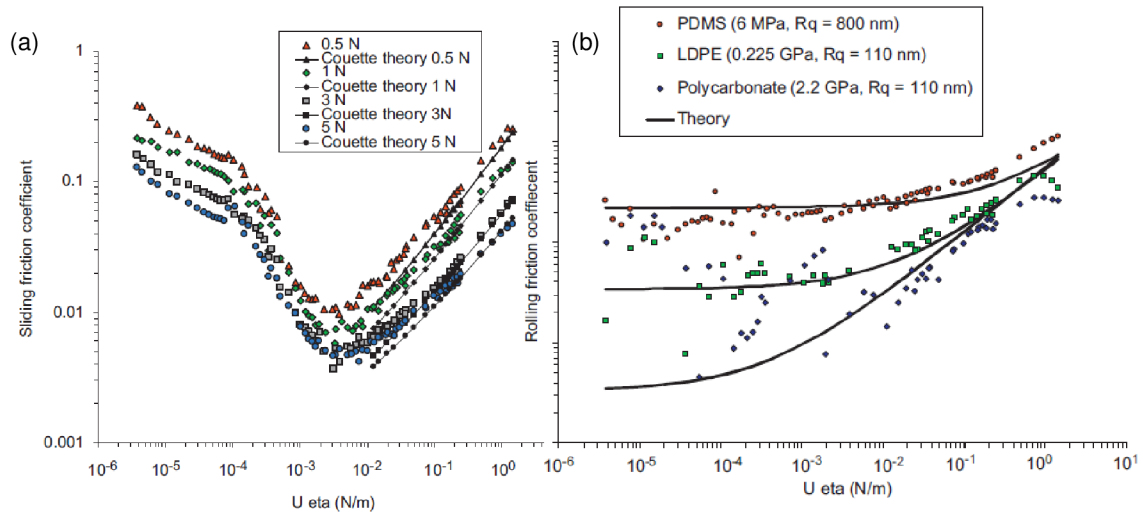

Fig. 2-4 Influence of elastic modulus on: (a) Sliding friction vs. reduced speed in log-log axis (b) Rolling friction vs reduced speed in log-log axis. Solid lines show theoretical predictions of: (a) Couette friction coefficient, (b) Poiseuille friction coefficient + hysteresis [18].

The work of Putignano and Dini [20] investigated both lubrication and friction in compliant contacts with an emphasis on the viscoelastic behaviour using numerical methods. The authors proposed a new lubrication regime called the visco-elasto-hydrodynamic lubrication regime, where the existence of this regime can be relatively simply predicted using a coupling parameter $\Gamma = h_{hydro}/\delta_{cr}$, where h_{hydro} is minimum film thickness in hydrostatic conditions and δ_{cr} is the solid penetration at a critical speed. The mentioned critical speed can be easily predicted when knowing E_0, E_∞ and τ, being rubber modulus, elastic modulus at high frequencies and relaxation time, respectively. To observe the proposed visco-elastohydrodynamic lubrication regime, $\Gamma \approx 1$ and lower.

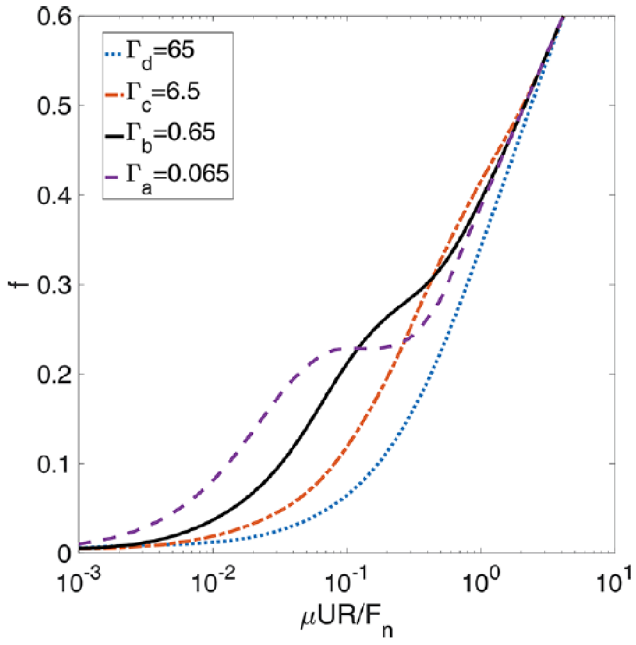

Fig. 2-5: Friction coefficient vs. log Hersey number demonstrating the effect of viscoelasticity using the coupling parameter Γ on the Stribeck curve [20].

In other words, the critical speed must fall into the EHL regime, where the deformation in the contact is comparable to film thickness. If the critical speed falls into the full-film regime, then no viscoelastic effects should be observed and classical EHL theory can be used to describe the contact. Fig. 2-5 demonstrates the effects of viscoelasticity on the Stribeck curve with different values of the coupling parameter, where viscoelasticity causes greater dissipation of energy resulting in a modified Stribeck curve. As the authors state, this is a powerful and yet simple parameter that can determine the presence of viscoelastic effects, which are important when designing mechanisms with repeatedly loaded and lubricated rubber parts.

The work of Selway et al. [21] focused on the effects of lubricant viscosity and the wetting effects in a lubricated rolling-sliding soft contact. The measurements were carried out using MTM with a ball-on-disc configuration with two material pairs, being PTFE-PDMS and PDMS-PDMS with different orders of surface roughness. The experimental data were also used to validate the theoretical model proposed by Scaraggi and Persson [22]. An interesting observation was made, where with increasing surface roughness friction coefficient decreased over the whole measured speed spectrum, most notably at the transition from boundary to mixed lubrication regime, which can be seen in the following figure (fig.2-6).

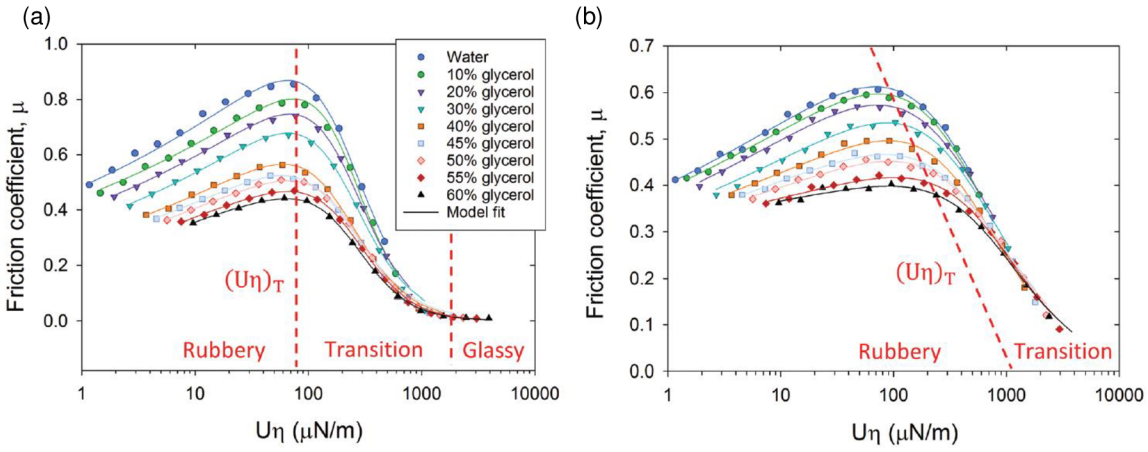

Fig. 2-6 The friction coefficient plotted as a function of reduced velocity (Entrainment speed · viscosity), where graph (a) shows the smooth and (b) rough configuration. The red lines show the individual regime regions depending on the viscoelastic response of the PDMS disc [21].

The rough surface enables the fluid to enter the contact more easily and thus promoting film formation by introducing fluid to the contact. Also, fewer adhesive bonds are created compared to smooth surfaces which create more adhesive bonds that increase solid contact friction and thus additional bulk. A smooth surface tends to entrap the fluid in the contact.

The Scaraggi and Persson [22] model suggest the maximum friction coefficient is followed by a decrease to a minimum friction coefficient does not necessarily indicate the transition from boundary to mixed lubrication regime. The authors suggest that the effect can be a product of contact "stiffening", meaning that with increasing loading frequency the material changes its viscoelastic properties which cause the drop in friction coefficient.

The authors hypothesise two reasons why the friction coefficient decreases with increasing lubricant viscosity, which is also a notable deviation from the Scaraggi and Persson model [22]. The first being, that an increase in lubricant viscosity could lead to weaker interfacial interactions making the solid-rolling friction component also weaker and thus the viscoelastic effect should not be as profound. The second reason is associated with dewetting (nucleation of dry contact regions on the top of the asperities) and squeeze-out dynamics (rate of fluid being removed from the contact). These two processes are shown to increase the contact area and thus supporting the solid-contact friction. To describe these processes, it is important to introduce static contact angle θ_s. The authors have found that glycerol-water solution has an unchanging static angle regardless of the glycerol concentration, suggesting that glycerol has a weak association with PDMS. This changes when dynamic conditions are introduced, which are typical for a tribo-contact, where the wetting angle becomes a function of fluid viscosity which is an important attribute for wetting. The dynamic contact angle also increases with the sliding velocity. Also, the squeeze-out of fluid from the asperities in the contact decreases with increasing lubricant viscosity. The friction also depends on the rate of dewetting and squeeze-out against the rate of fluid being replenished in the contact. This can be seen at lower speeds, where the fluid has more time to squeeze out and dewet the contact area and thus supporting the solid-contact friction. As the lubricant viscosity increases these mechanisms are inhibited and shifted to very low speeds, which means that the lubricant is still present in the contact, thus reducing the solid-contact friction.

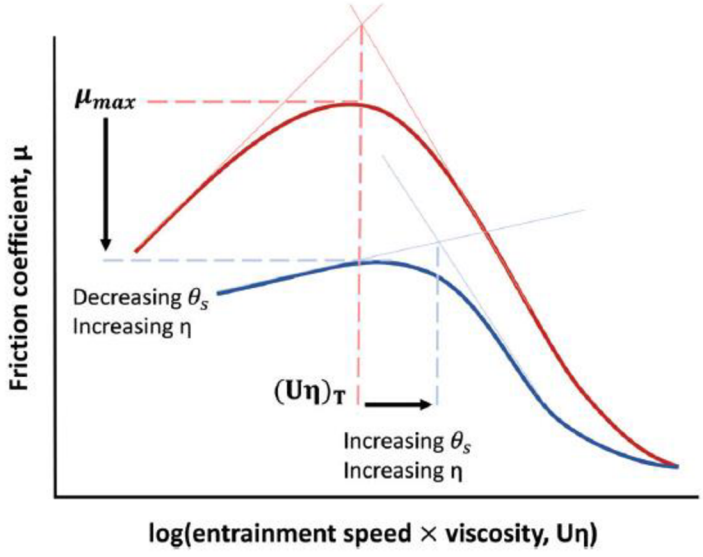

Fig. 2-7 A generalized behaviour of the compliant contact with the influences of the lubricant viscosity and static contact angle [21].

The study of Selway et al. [21] uses a well-defined model created by Scaraggi and Persson [22] which shows that asymmetrical pressure arising in the contact is generated by the viscoelastic hysteresis and thus reshapes the Stribeck curve. To describe lubricated soft contacts, the model divides friction into four components, which can be seen in fig. 2-8.

1. Solid-contact sliding friction - μ_{Sc}
2. Solid-contact rolling friction - μ_{Rc}
3. Wet-contact sliding friction - μ_{Sf}
4. Wet-contact rolling friction - μ_{Rf}

The solid-contact sliding and rolling components arise from the adhesive shear stress and rubber deformation losses. Wet-contact sliding friction is generated within the fluid contact region including Poiseuille and Couette flow, whereas the wet-contact rolling friction is produced by a combination of viscous losses and fluid-induced rubber deformation.

The resulting Stribeck curve is divided into several regions (labelled 1-5 in fig.2-8) describing each region's properties. It could be said that each region is described by a competition of the loading/unloading of the disc against the relaxation of the disc material. As the disc rotates the contact moves around the disc, leaving behind a trail of relaxing material.

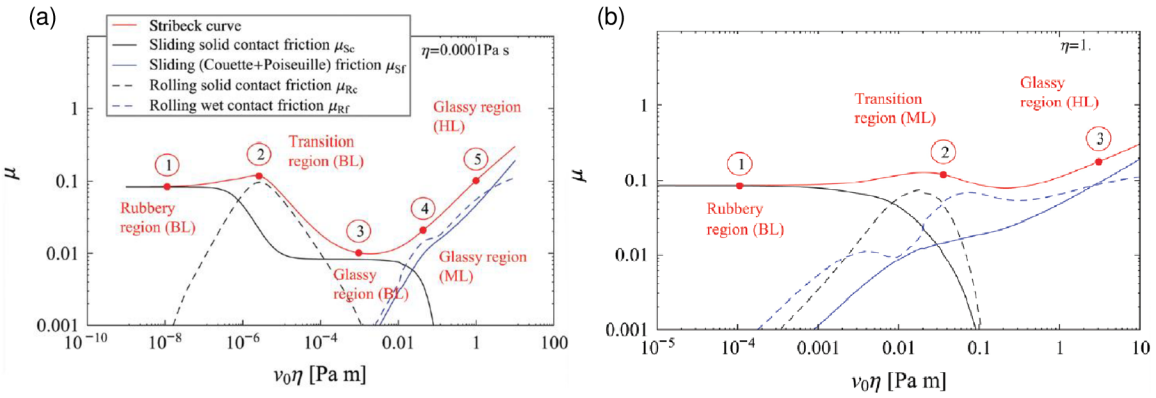

Fig. 2-8 Scaraggi and Persson's model for viscoelastic lubrication for (a) low and (b) high viscosity lubricant. The four distinct friction components are also shown in the legend of the graph. The resulting Stribeck curve is divided into regions using labels 1-5 [22].

The first described region in the model is the rubbery region (1) located in the low reduced velocity range, where accumulated contact stress has time to dissipate through relaxation of the material. As the reduced velocity increases a peak in friction facilitated by the solid contact rolling friction component can be observed bringing the tribological contact to a transition region (2) which is determined by the viscoelastic properties of the material. For smooth contacts, this corresponds to the maximum in loss modulus, whereas for rough contacts, it's the maximum in loss tangent.

As this reduced velocity increases, the trail left behind the contact does not have enough time to relax before entering the contact again and therefore, a decrease in solid-contact rolling friction follows and is called critical speed. The relaxation of the material decreases further as the reduced velocity increases, eventually leading to a point where no relaxation is possible, thus no contribution from the solid-contact rolling friction component which brings the contact to the glassy region (3-5).

To summarise the last paragraph, the solid-contact promotes the boundary lubrication (BL), whereas wet-contact friction promotes mixed lubrication (ML) and finally pure wet-contact friction promotes hydrodynamic lubrication (HL).

The model also predicts that the contribution of solid- and wet-contact friction is affected by lubricant viscosity across the whole reduced velocity range which affects the resulting Stribeck curve (fig.2-9). The model predicts that with increasing lubricant viscosity the rubber hysteresis also rises due to fluid pressure acting on asperities, leading to a rise in wet-rolling friction. Rough contact promotes the fluid-asperity interactions and thus shifting the wet-contact rolling friction to lower values of reduced velocities, eventually the wet- and solid-contact rolling friction coincide and altering the resulting Stribeck curve shape and shifting the friction peak to higher values of reduced velocity.

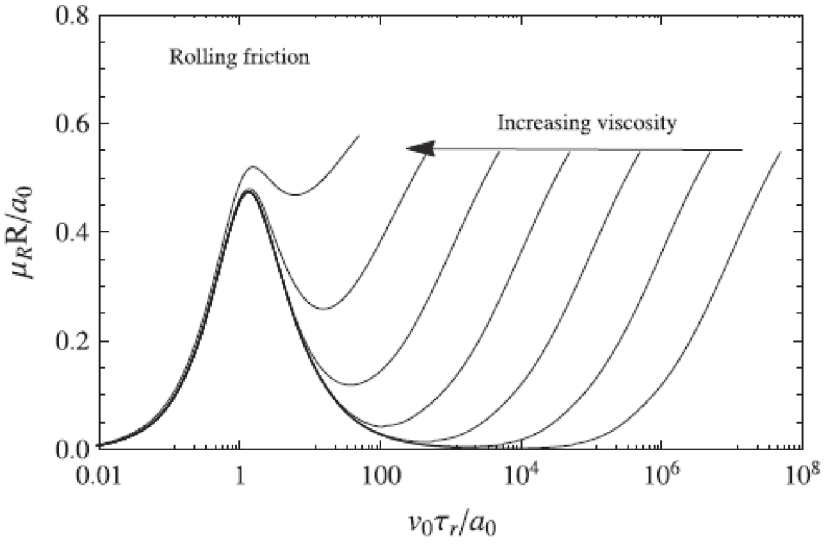

Fig. 2-9 Total rolling friction as a function of dimensionless sliding velocity for different values of lubricant viscosity [22].

The published paper of Sadowski et al. [23] studies friction in a lubricated pure sliding compliant contact created by a ball-on-disc configuration. The authors used all three possible configurations, being soft-on-hard, hard-on-soft and soft-on soft (ball-on-disc order). This has made it possible to study the effect of configurations directly, which has not been yet done in a single study to the paper's date. The work also studies the effect of surface roughness using discs with varying surface roughness. Since the soft specimens are viscoelastic, this means that the configurations using soft discs, being hard-on-soft and soft-on-soft, experience additional hysteresis while being measured. To correct this phenomenon Persson's [24] theoretical model was used to determine these effects. The raw data (data not being corrected for hysteresis) showed a linear increase in friction with increasing reduced velocity and when compared to the theoretical predictions of de Vicente et al. [17] (not including the viscoelastic effects) a reasonable agreement was observed in the full-film regime. When the data were corrected for hysteresis the difference of hard-on-soft and soft-on-hard configurations were negligible in the full-film lubrication regime. What is also interesting is that in the full-film regime friction coefficients merged into a single line for all configurations, which can be seen in fig. 2-10a. Moving on to the effects of roughness, with increasing surface roughness the shift from full-film lubrication to mixed lubrication is shifted to higher U_η as theory predicts. When the lubrication parameter $\lambda>10$, surface roughness has a negligible effect on friction. When $3<\lambda<10$ the specimen surfaces are still separated, however, the flow of the lubricant is affected by surface roughness.

At $\lambda\approx3$ breakdown of the lubrication, the film begins leading to contacts of asperities increasing the friction coefficient. Fig. 2-10b shows minimum film thickness as a function of composite roughness, where individual configurations show a reasonable agreement, mostly below the dashed line.

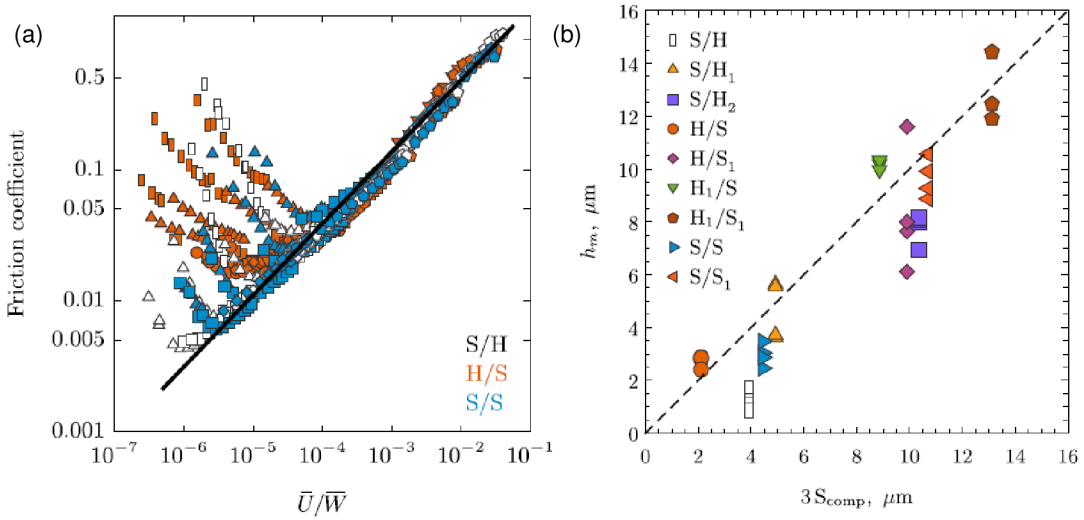

Fig. 2-10: (a) friction coefficient as a function of the Hersey number using the corrected data (b) relation between the minimum film thickness and composite roughness, where dashed line corresponds to $h_m = 3S_{comp}$ [23].

Putignano et al. [25] proposed a generalized numerical methodology to determine both lubrication and friction in soft contacts, where friction predictions were compared with the measurement of Sadowski et al [23]. In fig. 2-11, the model showed good agreement with the experimental data for most of the speed range except for low values, where a transition from full-film lubrication to mixed lubrication regime led to the deviation between the predicted friction and experimental data. At the mixed regime, lubrication is heavily affected by surface roughness, which was not incorporated in the author's work, as it was out of its scope.

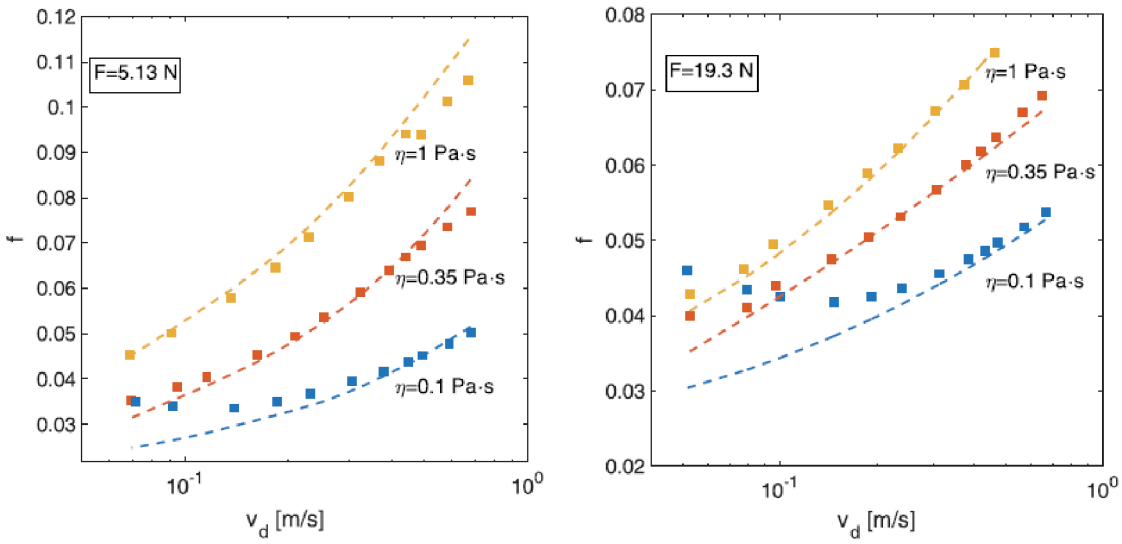

Fig. 2-11 Friction coefficient as a function of disc speed for different loads and lubricant viscosities [25].

Kim et al. [26] studied the influence of viscoelastic material properties on friction coefficient in dry and lubricated sliding soft contact mainly in the boundary lubrication regime. The soft samples were made from PDMS and the various viscoelastic properties were achieved by tunning weight ratios of PDMS and curing agent, creating four different specimens in the process. Glycerol and water were used to lubricate the contact and then exposed to different values of loading, from 0.245 N to 1.962 N, and a range of sliding speed, from 0.004 mm/s to 0.1 mm/s. The work uses an assumption that the lubricating film thickness is less than 10 nm thick and thus, does not play a significant role in the viscoelastic effects. The measurements were carried out on a universal macro-tribometer (UMT2). The friction coefficient was lower for the lubricated contact even at the boundary lubrication regime, suggesting that lubricant was still present in the contact and thus, reducing the number of adhesive bonds supporting the hysteretic losses. The authors were able to create regression equations for both dry and lubricated contacts, where key parameters are sliding velocity, lubricant viscosity, and load. The influence of the loss modulus on the friction coefficient was found to be around six times higher in the dry contact compared to the lubricated contact.

The work of Moyle et al. [27] investigates possible ways of modulating sliding lubrication friction in compliant contacts. To do so, the author used a spherical glass indenter with radii of 0.5 mm, 2 mm and 3 mm loaded against three different flat specimens. The first one being a two-phase periodic structure (TPPS), the second one called stiff control and the last compliant control (fig.2-12a). The TPPS is created by two parts, one being the stiff part (E = 3 MPa) and the second one the compliant part (E = 190 kPa). The specimens are made from PDMS using different mixing ratios to achieve different elastic moduli. The contact is loaded by a normal force from 18.6 mN to 238 mN while being lubricated with an unreacted PDMS base with a viscosity of 5.1 Pa·s over a sliding speed range from 0.025 mm/s to 1 mm/s.

To address the possible effects of material elastic hysteresis and adhesive bonds created due to fluid film breakage, the author added fluorescent particles to the used lubricant which were then tracked in the measurements. These data were then used to precisely describe the flow of the lubricant in the contact. The author suggests that a sudden local transition in compliance provides a mechanism of energy dissipation in a new form of elastic hysteresis, where the energy is dissipated through the fluid in the contact, which can be seen in fig.2-12a. To assess the energy losses by the material hysteresis a finite-element analysis was conducted, however, it was found that the contribution of the material hysteresis was negligible compared to the fluid elastic hysteresis. The newly proposed elastic hysteresis in fluid seems to not rely on the energy dissipated in the material itself. The authors also state, that in the dry and boundary lubrication regimes the elastic hysteresis of the material overwhelms the newly proposed hysteresis by fluid, which can be expected. By using patterns of soft/stiff material regions it is possible to modify the lubrication friction in compliant contacts.

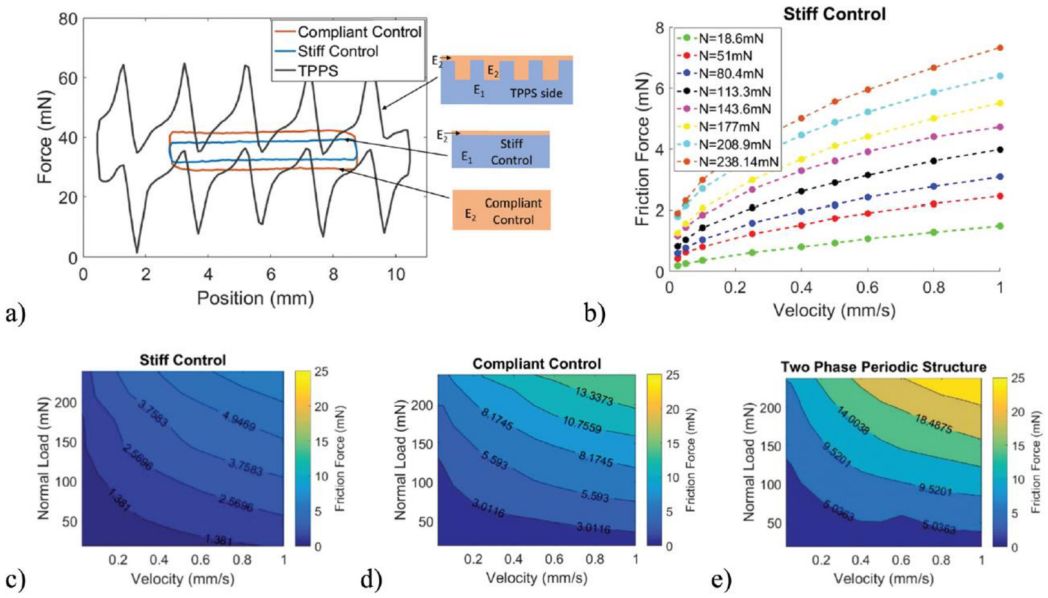

Fig. 2-12 Lubricated sliding friction data for an indenter with a radius of 2 mm (a) raw data for one cycle at a normal load of 113.3 mN and a velocity of 0.5 mm/s with an illustration of the used specimens (b) Plot of friction force, f, for the stiff control specimen (c-e) contour plot of friction values for (c) stiff control (d) compliant control and (e) TPPS in load-velocity space [27].

2.3.2 Compliant contacts in biological applications

Now moving to the world of biotribology. One of the many topics that biotribology investigates is food processing. For example, Masen et al. [28] developed a simple tribological test to evaluate the friction arising between tongue and palate while consuming chocolate. The smoothness and creaminess of the chocolate, being one of the key features of a good chocolate, are assumed to be linked with friction. The measurements are carried out using a High-Frequency reciprocating rig (PCS Instruments) at a stroke of 1.0-1.5 mm at a frequency of 10 Hz. The tongue/palate interface is represented by a flat-on-flat configuration using PDMS and glass specimens loaded by 1 N producing a contact pressure of 30 kPa. The tests used both family and luxury chocolates ranging from 5% to 85% of cocoa.

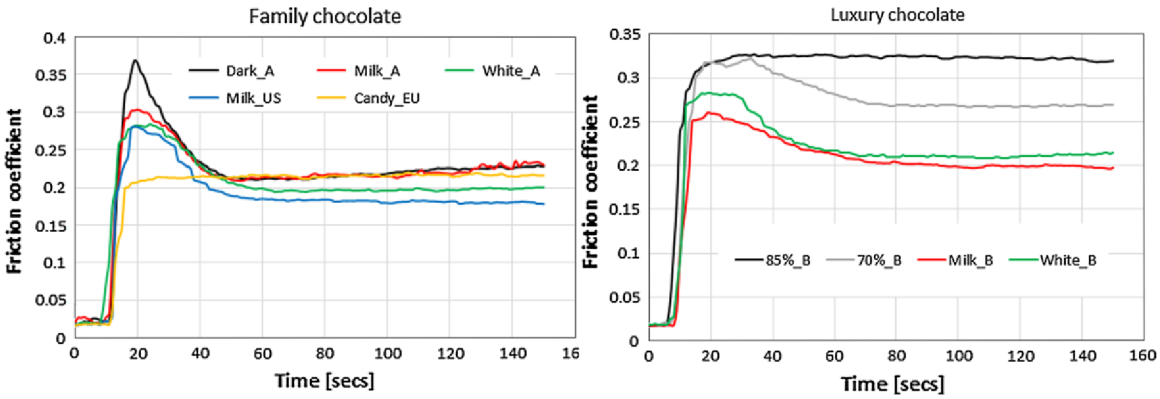

Fig. 2-13 Averaged friction measurements comparison as a function of time of "family" and "luxury" chocolate samples [28].

The melted chocolate is a non-Newtonian fluid, however, as the chocolate is sheared in the contact and thins the problem becomes tribological in nature. The results show (fig. 2-13) that most of the chocolate samples (30 – 70% cocoa) produce a similar friction dependence over time. The initial high in friction is most likely produced by the rheological nature of chocolate, as the sugar crystals are still not decomposed. As their degradation takes place a formation of a fat-rich film follows which determines the resulting final friction. The degraded sugar is expelled from the contact at the end of the strokes. The only exceptions were Candy EU with 5% cocoa and the luxury 85% chocolate. After the measurements, the remaining material in the contact was investigated under an optical microscope and infrared spectroscope to identify the component losses or their change. The resulting film thickness is driven by the degradation processes and not the entrainment speed, thus degradation rate determines friction. The author states that further improvements can be done by introducing saliva to the contact, which would also affect the degradation processes and friction.

The next frontier of biotribology is the tribology of the eye. Pult et al.[6] summarized the effects affecting friction while spontaneous blinking while wearing contact lenses and discusses the friction arising between the upper lid and the cornea or contact lense. In the eye, classical lubrication theory may not apply due to high lubricous properties under a wide range of conditions. One of the key parameters is the tear film viscosity, which directly affects shear stress arising in the eye. The tears themselves are a non-newtonian fluid, to be specific shear-thinning, meaning that with shear rate a decrease in viscosity follows. This provides low shear stresses while blinking. Viscosity is not affected by pressure, only large deformations occur in the contact, meaning the lubricated eye is in the i-EHL regime. The author states that the elastic modulus plays an important role in forming fluid film in a hydrodynamic lubrication regime at high loads. Also, friction could be affected by the elastic modulus as discussed in [18]. Wear of the lens may be affected by a combination of the elastic modulus, hydrodynamic forces, and lid pressure.

The next work investigating the effects of normal load on hydrogel tribology in the eye lubrication field was carried out by Urueña et al. [29]. The measurements were carried out using a custom-built high-speed pin-on-disc microtribometer using pAAm (polyacrylamide). The pAAm was used in five different concentrations resulting in different elastic modulus. The contact was fully submerged in ultrapure water and loaded by a normal force ranging from 0.1 mN to 20 mN at a speed range from 0.01 mm/s to 100 mm/s.

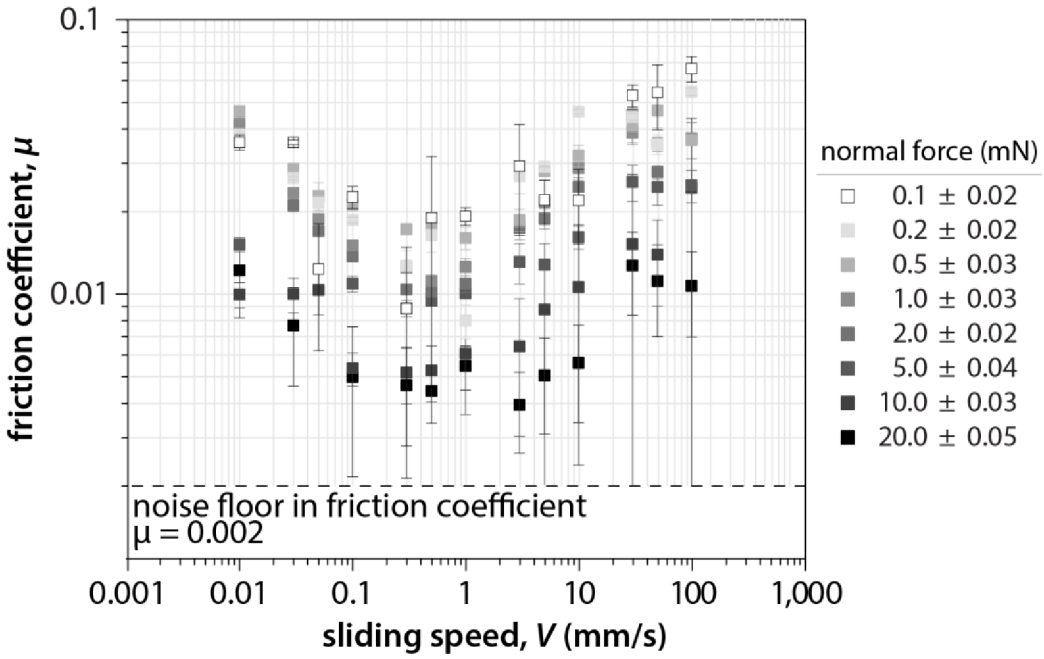

Fig. 2-14 Friction behaviour plotted as a function of sliding speed for different normal loads [29].

The measurements have shown (fig. 2-14) that the friction coefficient decreases with increasing normal load for the whole speed spectrum. In the speed range between 0.01 mm/s and 0.1 mm/s high values of COF can be observed. With an increase in speed to 5 mm/s a speed-independent friction region of low values of friction is formed, where the COF is roughly equivalent to $F_N^{-1/3}$. With a further increase in speed, an increase in COF was observed. However, the calculation of shear stress in the contact was unsuccessful due to the inability of the soft EHL theory to predict the friction coefficient. This suggests that isoviscous fluid shear is not the mechanism governing the energy dissipation observed in the contact.

Murakami et al. [30] studied lubrication in both natural synovial joints and artificial joints using a pendulum test and a simulator test of sliding pairs of stainless-steel spherical components and natural articular cartilage or artificial cartilage. Joints such as knee, ankle and hip are mostly operated in the i-EHL regime with large deformation of the compliant surfaces and together with the viscous effects of the synovial fluid ideal conditions are created that are key to low friction and wear. As the film thickness decreases and the lubrication regime transitions to the boundary regime, the cartilage is lubricated by various lubrication mechanisms such as weeping, boundary and gel-film lubrication, serving as a protection of the cartilage.

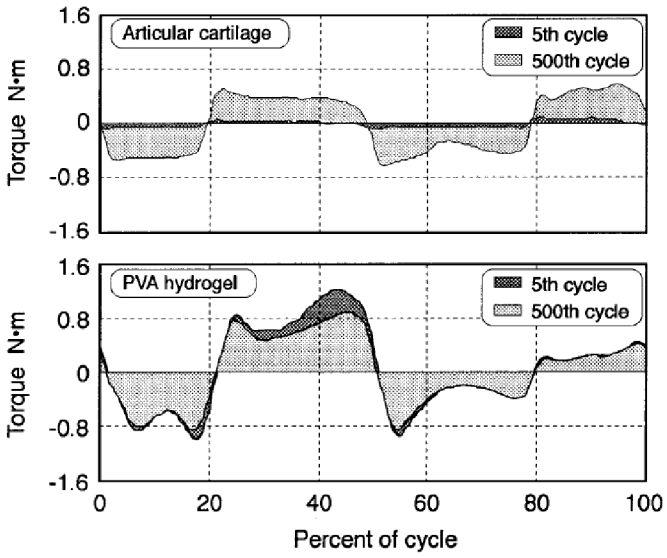

Fig. 2-15 Comparison of the observed friction between cartilage and PVA hydrogel [30].

Mostly ultra-high-molecular-weight polyethylene UHMWPE is used as a joint prosthesis, however, several problems are arising with the use of this material from both tribological and biological standpoints. It is expected that this could be solved by using compliant materials such as silicone rubber or hydrogels on the surfaces of the prosthesis to improve lubrication and thus wear. The synovial joint sample is a PMMA cylindrical sleeve with a 2 mm thick polyvinyl alcohol (PVA) hydrogel with an elastic modulus of 1.1 MPa. It was found that hyaluronic acid and globulin controls the lubricants viscous properties having a direct effect on the lubrication regimes for both PVA hydrogel and artificial cartilage. Also, the PVA hydrogel exhibited greater friction than the artificial hydrogel (fig.2-15) and thus, further investigation of the lubricant solution is required.

The lubrication of articular cartilage was studied by Jahn et al. [31]. Cartilage provides tremendously low friction coefficients that no manmade material can produce making nature the producer of the best material in terms of friction, where friction coefficient can be low as 0.001 under a pressure of 20 MPa. The cartilage covering the ends of the articulating bones is a network of collagen filled with water and highly charged macromolecules and other molecules. Artificial joints lubrication covers the whole lubrication spectrum from boundary to full-film regime lubrication. While in boundary regime, the molecules are present at the surface of the cartilage encounter each other and friction is mostly independent of sliding velocity, whereas friction coefficient in the full-film regime is affected by speed. This is a useful tool to determine the actual lubrication regime, as classical EHL is not as easily applicable in this complex problem.

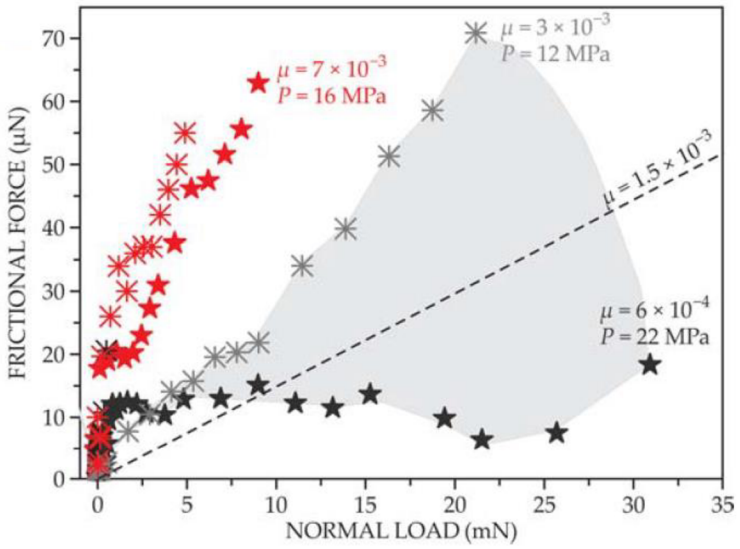

Fig. 2-16 Experimental data obtained by SFB method for various loads and the resulting friction between mica surfaces that are coated with HA-lipid complexed and slid underwater (black) or a salt solution (red); The dashed line show the mean of the data measured underwater [31].

As one could also except, measuring friction in an actual human/animal joint is a major challenge. Surface force balance (SFB) enables the measurement of the normal and frictional surface forces between the complex boundary layers. Hydration lubrication is key to extremely low friction coefficients, as the water molecule itself creates two oppositely charged poles (negative pole by the oxygen molecule and the positive pole by hydrogen atoms). The negative poles are attracted to a positive charge of phospholipids present in the cartilage. This makes it hard to squeeze out the water molecules from the contact as it undergoes shear stress loading and thus provides improved lubrication.

Hilšer et al. [32] investigated friction in the model of human joints, where the main focus was on the effects of hyaluronic acid and phospholipids on friction and producing a new viscosupplement that would be compared to the current ones. The measurements were taken on a pin-on-plate tribometer using different materials such as polyetheretherketone (PEEK), polymethylmethacrylate (PMMA), UHMWPE, glass and mica to form five different pairs at a temperature of 37°C to simulate the biological environment. The first measurements set investigated the static contact angle of hyaluronic acid and phospholipids and its influence on friction at a contact pressure between 10 and 20 MPa. The second measurement set examined the friction between the cartilage-glass and cartilage-mica lubricated by phosphate buffer, hyaluronic acid, a combination of phospholipids and hyaluronic acid and model synovial fluid. The last set compared the newly created viscosupplement with the current ones.

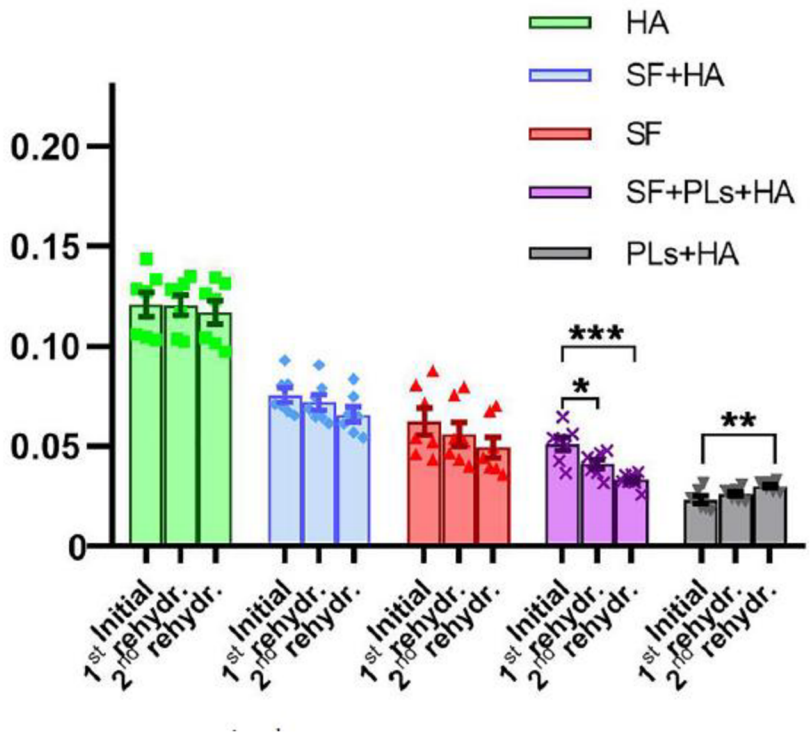

Fig. 2-17: Comparison of different lubricants [32].

It was found that the static contact angle has a significant effect on the resulting friction as it promotes the hydration lubrication regimes which lowers the friction coefficient. A logarithmical increase with entrainment velocity was observed in the cartilage-glass pair for the phosphate buffer, hyaluronic acid and model synovial fluid, which corresponds to the interstitial lubrication regime, whereas for the combination of hyaluronic acid and phospholipids the frictions begin to behave more linearly, from which is evident that hydration lubrication regime takes place. However, for the cartilage-mica pair, a rather constant friction coefficient is observed for all lubricants, indicating the presence of the boundary lubrication regime. In general (fig.2-17), the mixture of hyaluronic acid and the synovial fluid (current viscosupplements) led to an increase in friction coefficient compared to the synovial fluid alone. Nevertheless, mixing hyaluronic acid, phospholipids and synovial fluid (newly proposed viscosupplement) led to a decrease in friction compared to the synovial fluid only.

A recent study by Arshad et al. [7] investigated the effects of adding UHMWPE filler on mechanical and tribological properties in epoxies (SU-8 and Structalit 8801). Recently, epoxies have become more widely used in biomedicine due to their biocompatibility, mechanical properties, and flexibility of manufacturing, including 3D printing. The author states that it is expected that the combination of epoxy and UHMWPE could be promising due to their mechanical properties. The SU-8 epoxy was mixed with hardener ranging from 1 to 9 wt% designated as SU8H1 (SU-8 with 1 wt% hardener). The next set of epoxy samples added 25 wt% of UHMWPE to SU8H5, H7 and H9 designated as SU8H5UH. The Structalit 8801 epoxy is designated as EP and its mixture with 25 wt% UHMWPE is designated as EPUH. The measurements were carried out on a pin-on-disc apparatus at room temperature. The dry contact was loaded by 20 N at a sliding speed of 100 mm/s for a total sliding distance of 3 km.

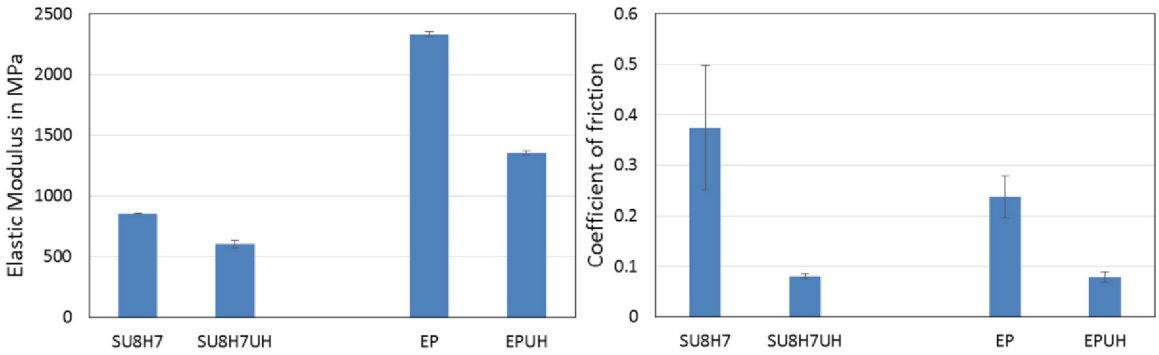

Fig. 2-18 Comparison of different epoxies and their composites, where the left graph shows the effect on the elastic modulus and the right graph the effect on COF [7].

The study found that the addition of UHMWPE significantly enhanced ductility and tribological properties of the SU-8 and Structalit 8801 epoxies, resulting in a 71% and 40% increase in ductility for SU8H7 and EP, respectively. Also, the composites have shown remarkable tribological properties in terms of COF and wear, where COF has dropped by 79 and 67% for SU8H7 and EP, respectively, and the wear rate was reduced by 92% and 58% for SU8H7 and EP, respectively (fig.2-18).

3 PROBLEM ANALYSIS AND AIM OF THE WORK

3.1 Problem analysis

Compliant contacts are currently a very discussed and researched topic due to their increasing utilization in many applications, as today's technology allows to manufacture of a variety of quality polymeric materials, which can be utilized in bearing [2], tires [3], wipers, gears [4] and sealings. Energy in the mechanical systems is transferred through both conformal and non-conformal surfaces. A recent study by Holmberg and Erdemir [1] estimated that 23% of the world's total energy is lost in tribological contacts, which is approximately 119 EJ. The use of these materials is also utilized in medicine concerning biomedical implants [5], contact lenses [6], joint replacements [7], or even smart devices [8], making the presence of compliant contacts more significant by the day.

However, polymer materials are viscoelastic, meaning that a certain amount of energy will be lost while transferring through this material as the viscous component of this material damps energy, thus it is essential to separate individual friction components to better understand the tribology of soft contacts.

The conditions of the measurements must be selected with caution so that the contact is in the i-EHL regime, which is considered in the friction and viscoelastic theories for soft contacts. If the conditions should be chosen incorrectly, this could lead to undesired effects such as a change in viscosity due to high contact pressures, which would make the evaluation of viscosity and viscoelastic effects more challenging, as viscoelasticity is a complex interplay of many mechanisms.

Another crucial component of this puzzle is to obtain or measure the dynamic modulus of the compliant material, as it is key to determine the viscoelasticity contribution to the total friction arising in the contact. Obtaining the necessary data proved to be challenging as the manufacturers of these specimens don't provide these pieces of information as their significance for common use is not essential.

3.2 Analysis and evaluation of the literature review

In the world of tribology, compliant contacts are slowly becoming a major point of interest due to their vast utilization. Considering the aim of this work, let us recapitulate the investigated studies together with the knowledge useful to this work.

Bongaerts et al. [15] studied the influence of roughness and hydrophobicity on lubrication using the MTM. The effects were found to be negligible, only expanding boundaries of boundary and mixed regimes. Next to investigate friction where de Vicente et al. [16, 17] were able to separate rolling and sliding friction using a novel technique and propose a prediction equation for lubrication friction in compliant contacts. The results showed that friction is mostly independent of sliding speed and that friction created by Couette flow is proportional to the slide-to-roll ratio. Myant et al. [18] made a similar study in which they investigated the influence of load on rolling and sliding friction. The measured data also served to validate the work of de Vicente et al. [17]. The authors found that classical models can't predict the rolling friction coefficient accurately as a function of load. Elasticity was also found to affect rolling and sliding friction to a point, where rolling friction is not negligible anymore. Selway et al. [21] studied the influence of fluid viscosity and wetting on different scales of viscoelastic lubrication. The authors found that viscosity and wetting substantially affect the resulting tribological profiles, where for smooth contacts, viscosity is expected to influence dewetting and squeeze-out at an interfacial scale, however, this effect is not as profound for rough contacts. Rough contacts rather produce higher interfacial friction stimulating the viscoelastic hysteresis. Putignano and Dini [20] found that viscoelasticity affects friction, where it adds more dissipation and reshapes the Stribeck curve. Also, the authors defined a new lubrication regime called visco-elastohydrodynamic lubrication, which can be determined using a simple parameter. Sadowski et al. [23] studied friction in a pure-sliding soft contact using three configurations: soft-on-hard, hard-on-soft and soft-on-soft, focusing on the effects of surface roughness and configuration. Configuration showed negligible effects, especially in the full-film regime after being corrected for the viscoelastic effects. Surface roughness affects friction at $\lambda>10$ and film breakdown leading to asperity contacts begins at $\lambda\approx3$. Putignano [25] later proposed a numerical methodology capable of calculating both film thickness and friction coefficient in soft contacts including the viscoelastic effects. Kim et al. [26] found that in both dry and lubricated soft contacts that the loss modulus or loss tangent determines the friction coefficient depending on the lubrication regime. From this observation, a regression equation was further created for both dry and lubricated contact, however, still at the boundary lubrication regime. Moyle et al. [27] showed a possible way of modifying the EHL friction in compliant contacts using patterns of compliant and stiff regions for the compliant specimen and proposes a new form of elastic hysteresis provided by the lubricating fluid in the contact.

Considering the biological applications, Masen et al. [28] developed a novel method to measure friction arising between tongue and palate while consuming chocolate. The initial rapid growth of the friction coefficient was a product of the presence of sugar in the contact. However, the sugar was degraded in the process flooded from the contact, resulting in a decrease to a stable low value of friction coefficient, which was a product of a thin fat-film formation and also determines the final friction. Pult et al. [6] summarized the effects affecting the resulting friction arising while blinking also with contact lenses. Viscosity and elasticity proved to be the main factors affecting the resulting friction, as tears are shear-thinning and reduce the arising friction in the eye and elasticity affecting film formation, which is also an important factor affecting friction.

Urueña et al. [29] investigated the effects of normal load on hydrogel tribology. The measurements have shown that with increasing load friction coefficient decreases for the whole speed spectrum. Also, a speed-independent zone of low friction was observed equal to roughly $F_N^{-1/3}$. Murakami et al. [30] compared friction between natural synovial joints and artificial joints, where the findings show that the artificial joints using PVA hydrogel layers instead of natural cartilage lead to higher friction coefficient. However, PVA is a promising material that could be used instead of UHMWPE due to many complications arising from its use from both biological and tribological standpoints.

Jahn et al. [31] studied the lubrication process in articular cartilage, highlighting the tremendous tribological properties of the cartilage. Joints are exposed to the whole spectrum of lubrication regimes from boundary to full-film lubrication regime, where sliding speed can be used to determine the actual regime. In the boundary regime, hydration lubrication is a key process to ensure low friction even in this regime. Hilšer et al. [32] investigated the effects of hyaluronic acid and phospholipids in viscosupplements. One of the significant factors affecting friction while using viscosupplements is the static contact angle as it promotes film formation. The work has shown that mixing hyaluronic acid and phospholipids with synovial fluid led to a decrease in friction compared to a mixture of hyaluronic acid and synovial fluid, suggesting a novel formula for viscosupplementation that could significantly lower friction in joints. Recent work by Arshad et al. [7] has shown that adding UHMWPE filler to epoxies (SU-8 and Structalit 8801) used in hip replacements significantly decreased friction coefficient (SU8H by 79% and EP by 67%) and increased the ductility (71% and 40% respectively) of the composites. It is possible that the drop in friction can be assigned to the change of viscoelastic properties of the material.

Compliant contacts have been both studied using experimental and numerical methods, where certain configurations were studied but were not directly compared. Sadowski et al. [23] studied all three configurations and compared them together, however, using only sliding conditions. The investigation of the effect of slide-to-roll ratio on friction in compliant contacts has been studied by de Vicente et al. [16, 17], however, only for slide-to-roll ratio up to 50% and not further. Concerning the limitations of the previous studies, this work investigates the effect of different slide-to-roll ratios in compliant rolling-sliding contacts in different configurations and analysing the hysteresis response for each configuration.

3.3 Aim of the work

The main goal is to describe the influence of the material's viscoelasticity and the configuration on friction in a compliant contact considering different operating conditions corresponding to actual applications. Attention has been paid to the influence of kinematic conditions, configuration, material viscoelasticity, and lubricant viscosity. Compliant contacts cover a wide range of material pairs; therefore, this work investigates this problem using the following materials.

To produce the desired contact, PDMS and UHMWPE samples have been used as a soft member of the compliant contact together with steel acting as a hard member of the compliant contact.

The measurements in technical applications used all three possible configurations, soft-on-hard, hard-on-soft and soft-on-soft, to form the compliant contact using PDMS as the soft member and then lubricated by a variety of lubricants with different viscosities.

The rest of the measurements investigates specific case studies from biotribological applications where both PDMS and UHMWPE are used as the soft member. The contact was lubricated by a native and a simple lubricant to determine the possibility of substituting the native lubricant.

The output of this work is going to be an article in a professional journal registered in the Web of Science.

3.3.1 Scientific questions and hypothesis

Question 1:

"What is the effect of viscoelastic response on friction coefficient in compliant contacts?"

Hypothesis 1:

"Relaxation times of the specimen material should play a crucial role as it dictates the hysteresis behaviour whose product is the rolling friction arising in the contact. Thus, the slide-to-roll ratio should also affect the viscoelastic response, as each specimen changes its frequency at which it is loaded."

Question 2:

"What is the proportion of elastic hysteresis to Poiseuille friction component in the i-EHL regime?"

Hypothesis 2:

"It is expected that the thickness of the formed lubricating film should not be as significant in the i-EHL regime. Rolling friction is formed by two components; elastic hysteresis and Poiseuille friction component, where the second component is dependent on film thickness. If we consider that the film thickness is not as significant thus, Poiseuille friction component should also be minor and most of the observed friction in the i-EHL regime should be facilitated by the elastic hysteresis."

4 MATERIALS AND METHODS

4.1 Mini traction machine

Investigation of friction in lubricated soft contacts has been carried out using the aforementioned MTM tribometer. The operation of the device is quite simple. The machine uses a ball-on-disc configuration, where the ball is loaded against the disc, creating the contact (fig. 4-1). The ball specimen is a 19.05 mm diameter sphere with a drilled hole through which a tightening screw is inserted and used to connect the specimen to the holder. The disc specimen has a diameter of 46 mm with a thickness of 6 mm. In the case of a very soft PDMS disc, a supporting disc made from stainless steel is used to support the soft disc during the measuring process. The disc is mounted on a screw connected to the machine and tightened with a nut.

The ball and the disc are driven by two separate motors, which permits independent control over each specimen up to the speed of 4000 mm/s. This allows achieving different slide-to-roll ratios from -200% to + 200% as independent control is possible. The tribometer uses eq.1 to determine entrainment speed where u_b is ball speed and u_d is disc speed. The slide-to-roll ratio is defined by eq.2.

Also, the machine is capable of generating up to 75 N and controlling the temperature of the pot and lubricant. Friction, load and lubricant temperature are measured by a variety of sensors. Both the ball and the disc can be changed for specimens from different materials, making it possible to create different configurations.

$$u = \frac{u_b + u_d}{2} \qquad (1)$$

$$SRR = \frac{2 \cdot (u_d - u_b)}{u_d + u_b} \qquad (2)$$

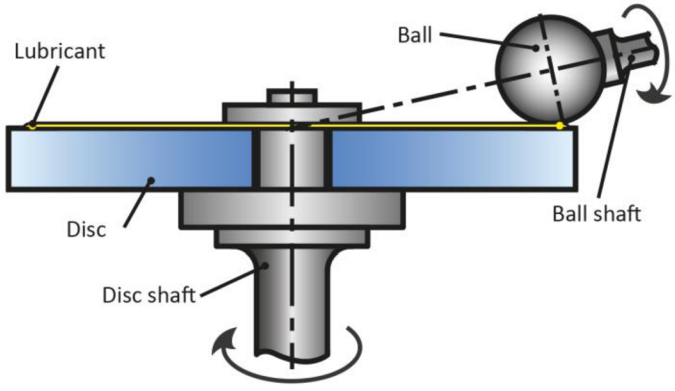

Fig. 4-1 Configurations used for MTM.

4.2 Materials

To create the desired soft contact, one of the bodies in contact has to have an elastic modulus lower than 1 GPa, so the material selection is crucial. For this work, two candidates have been selected, polydimethylsiloxane (PDMS) and ultra-high-molecular-weight polyethene (UHMWPE), both with a different order of elastic modulus. The work uses two PDMS materials having different Shore hardness, where PDMS SH50 is the stiffer material compared to the PDMS SH30. The measurements can be divided into two groups, where the first group represents the selected "Technical applications" and the second covers three typical "Biological applications". The hard specimens are made out of steel for both groups.

The contacts in the "Technical applications" have been lubricated by three different lubricants, being two oils (HC32/100, R834/80) and a glycerol-water solution with 95% glycerol to ensure that the measurements are carried out across a wider range of lubricant viscosities. Each lubricant has been marked with a symbol to distinguish them from one another in the results section. The following table (tab.4-1) presents each lubricant with its symbol and viscosity at different temperatures. The contacts in the "Biological applications" have been lubricated by several lubricants (tab.4-2) as different case studies were conducted and their selection is explained in the following chapter.

Tab. 4-1 Lubricants used in the "Technical applications".

Lubricant	Marker	Dynamic viscosity η (mPa·s)			
		20°C	25°C	30°C	35°C
Glycerol	△	532	350	230	155
R834/80	○	247	176	128	96
HC32/100	□	62	48	38	31

Tab. 4-2 Lubricant used in the "Biological applications".

Lubricant	Marker	Case study	Dynamic viscosity η (mPa·s)
			37°C
Glycerol 40%	△	Eye	2
Eye drops	○		
Model synovial fluid	△	Artificial knee joint	4
PBS	○		
Water	□		
HA 317	△	Fascia	287
TOTM	○		300

The viscoelastic properties of the PDMS SH30 and SH50 samples (tab.4-3) were obtained using the DHR-3 (TA Instruments) for dynamic mechanical analysis. The material was tested over a frequency range from 0.01 to 10 Hz at 30°C for SH50 and 37°C for SH30. The Poisson ratio of the PDMS is expected to be 0.5. The UHMWPE's elastic modulus is estimated to be around 700 MPa with a Poisson ratio of 0.33.

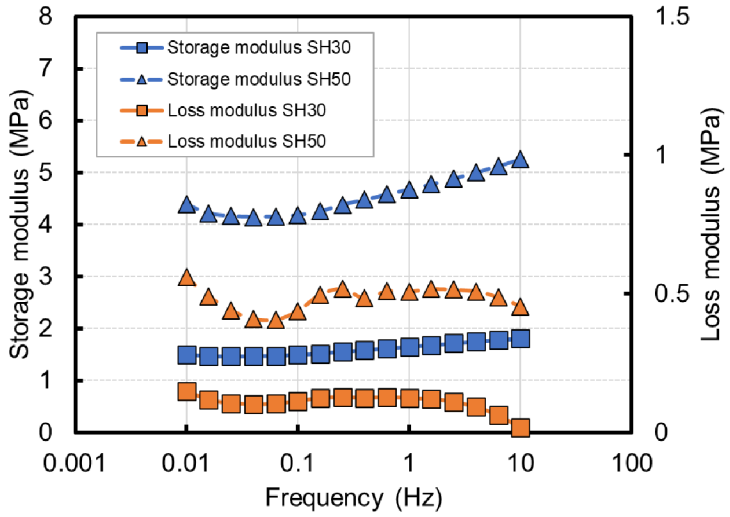

Fig. 4-2 Storage and loss moduli as a function of frequency for SH30 and SH50.

Tab. 4-3 Viscoelastic properties of PDMS SH30 and SH50.

Storage modulus	**Loss modulus**	**tanδ**	**Storage modulus**	**Loss modulus**	**tanδ**	**Frequency**
MPa	MPa	-	MPa	MPa	-	Hz
	SH30 ■			SH50 △		
1.503	0.150	0.100	4.385	0.560	0.128	0.010
1.469	0.118	0.081	4.215	0.492	0.117	0.016
1.462	0.106	0.073	4.161	0.441	0.106	0.025
1.465	0.103	0.070	4.143	0.410	0.099	0.040
1.475	0.104	0.071	4.149	0.407	0.098	0.063
1.491	0.115	0.077	4.176	0.438	0.105	0.100
1.520	0.124	0.081	4.252	0.498	0.117	0.158
1.555	0.128	0.082	4.381	0.518	0.118	0.251
1.584	0.125	0.079	4.478	0.485	0.108	0.398
1.616	0.127	0.079	4.579	0.510	0.111	0.631
1.650	0.124	0.075	4.678	0.509	0.109	1.000
1.681	0.121	0.072	4.776	0.518	0.108	1.585
1.715	0.111	0.064	4.883	0.515	0.106	2.512
1.750	0.093	0.053	5.003	0.509	0.102	3.981
1.782	0.063	0.035	5.127	0.488	0.095	6.310
1.808	0.018	0.010	5.256	0.455	0.087	10.000

4.2.1 Technical applications

Part I

The measurements in the first group mainly serve to study and describe the processes occurring in the soft lubricated contact, while exposed to different kinematic conditions, lubricated by different lubricants with varying viscosities and using PDMS samples with different Shore hardness to assess the individual effects. The specific conditions are presented in tab.4-4. It is worth noting that the slide-to-roll ratios were set to both positive and negative values, which is important as it enables the separation of sliding and rolling friction component in the measurements. The chosen conditions were verified (fig.4-3) to ensure that the contact is in the desired i-EHL regime. The conditions are met for the most part except the lowest speed using glycerol as a lubricant.

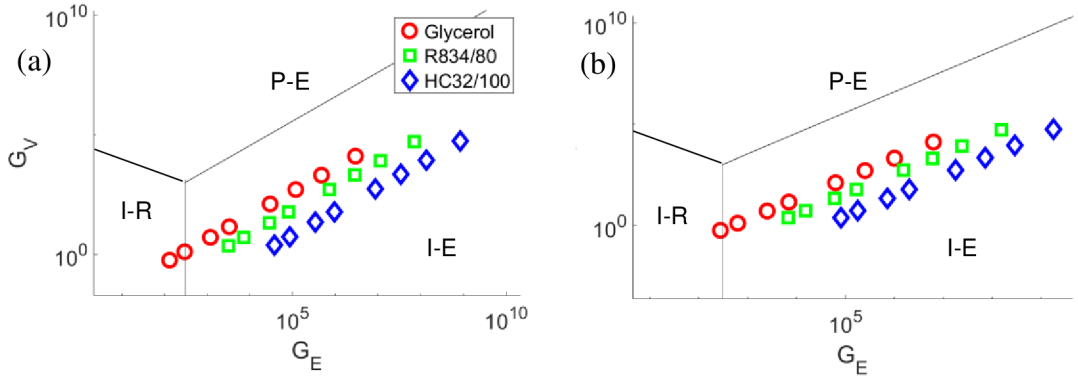

Fig. 4-3 Verification of the i-EHL regime existence for the used lubricants and measurement conditions (a) PDMS H/S, S/H (b) PDMS S/S.

The experiments were then repeated using the PDMS SH30 to determine the veracity of hypothesis n.2 of the work. It should be noted that the repeated experiments only included a slide-to-roll ratio (SRR) set to 50% and the contact was lubricated by R834/80 oil.

The determination of the lubrication parameter λ for the technical applications was carried out using three different equations for film thickness, as the film thickness is needed for the calculation of λ and the measuring device isn't capable of obtaining film thickness. Eq.3 shows the calculation of the lubrication parameter, where h is the film thickness and $R_{a,ball}$, $R_{a,disc}$ are surface roughnesses of the specimens.

Equations 6, 7 [9], 8 [33] were used to determine the film thickness in the measured contact, where u is the entrainment speed, η is the lubricant's viscosity, w is load, E_{red} is the reduced elastic modulus, R'_x is the reduced radius of curvature in the entrainment direction and the parameter k is the ellipticity parameter, where $k=1$ for point contacts. These parameters are used to calculate the dimensionless speed (eq.4) and dimensionless load (eq.5). The resulting lubrication parameters using equations 6, 7, 8 can be found in the attachments together with a description of the eq.8 parameters, as their description is quite lengthy.

$$\lambda = \frac{h}{\sqrt{R_{a,ball}^2 + R_{a,disc}^2}} \qquad (3)$$

$$\bar{U} = \frac{u \cdot \eta}{E_{red} \cdot R'_x} \qquad (4)$$

$$\bar{W} = \frac{w}{E_{red} \cdot R'^2_x} \qquad (5)$$

$$h_c = 7.32(1 - 0.72e^{-0.28k})\bar{U}^{0.64}\bar{W}^{-0.22}R'_x \qquad (6)$$

$$h_{min} = 7.43(1 - 0.85e^{-0.31k})\bar{U}^{0.65}\bar{W}^{-0.21}R'_x \qquad (7)$$

$$h_{nij} = \left\{[\bar{h}_{RIc}^{3/2} + (\bar{h}_{EIc}^{-4} + \bar{h}_{\infty}^{3/2})^{-3/8}]^{2s/3} + (\bar{h}_{RPc}^{-8} + \bar{h}_{EPc}^{-8})^{-s/8}\right\}^{1/s} \cdot \sqrt{R'_x} \qquad (8)$$

Tab. 4-4 Summary of the conducted measurements in the "Technical applications – Part I".

Configuration	Material couple	Load	SRR	Entrainment speed	Lubricant viscosity
		N	%	mm/s	mPa.s
Soft-on-hard	PDMS -on- Steel	1	+/-	10-1500	Glycerol (230)
Hard-on-soft	Steel -on- PDMS		50		R834/80 (120)
			100		
			150		HC32/100 (40)
Soft-on-soft	PDMS -on- PDMS				

The results of the measurements from tab.4-4 are compared with the theory proposed by de Vicente et al. [16] which predicts friction coefficients of Poiseuille (eq.9) and Couette (eq.10) components.

$$\mu_{Poiseuille} = 1.46\bar{U}^{0.65}\bar{W}^{-0.70} \qquad (9)$$

$$\mu_{Couette} = SRR(3.8\bar{U}^{0.71}\bar{W}^{-0.76} + 0.96\bar{U}^{0.36}\bar{W}^{-0.11}) \qquad (10)$$

The elastic hysteresis throughout the whole work is estimated using the simplified equation of Persson (eq.11) [24], where p_a is average contact pressure, E_0 is the low-frequency modulus and tan(δ) is the ratio between loss and storage moduli. The reason why is stated in chapter 6.3. The equation uses an assumption that the frequency of loading is lower than the relaxation time of the viscoelastic material.

$$\mu_{hyst} = 2.34 \cdot \frac{p_a}{E_0} \cdot tan\delta \qquad (11)$$

Also, another comparison has been made with a numerical simulation developed within collaboration with Friedrich-Alexander-University of Erlangen - Nürnberg, Germany. The development of the model was continuously supported by obtained experimental data. The simulations have been carried out for the soft-on-hard and hard-on-soft configurations at SRR of 50%. The main purpose of the simulation is to calculate the film thickness and pressure distribution while taking fluid rheology into account. The proportion of fluid friction is then calculated by integration of the shear stresses τ_{zi} in the centre of the lubricant gap:

$$F_{E,Fluid} = \int_{\Omega_c} \tau_{zi}|_{z=\frac{h}{2}} dxdy \qquad (12)$$

$$\tau_{zi} = \frac{\partial p}{\partial x_i}\left(z - \frac{\int_0^h \frac{z}{\eta} dz}{\int_0^h \frac{1}{\eta} dz}\right) + \frac{1}{\int_0^h \frac{1}{\eta} dz}\left(u_{i,z=h} - u_{i,z=0}\right) \qquad (13)$$

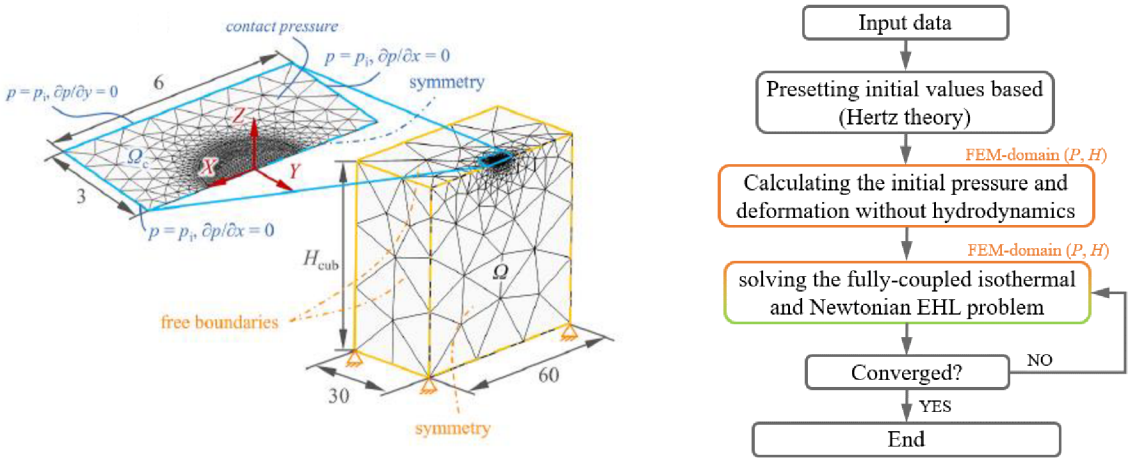

Fig. 4-4 Utilized FEM-domain with boundary conditions [34].

Part II

To take a closer look at the individual friction components, another set of experiments was carried out (tab.4-5). The speed of the soft specimen was fixed at a constant speed and the opposing specimen's speed was increased. These experiments were carried out for the configurations hard-on-soft, soft-on-hard and soft-on-soft. After the experiments were done, the conditions have been reversed, so the hard specimen had a fixed speed and the soft specimen's speed was increasing. This also allows the determination of the individual friction component arising from sliding and rolling. An illustration of the experiment can be found below.

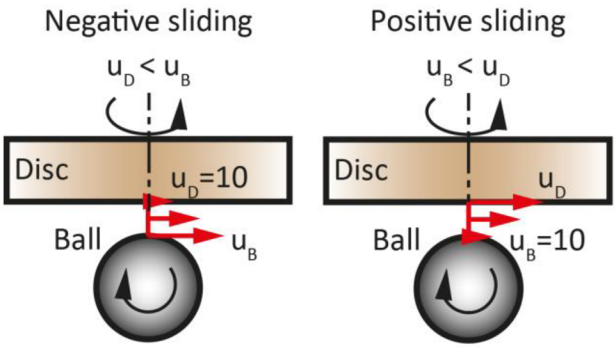

Fig. 4-5 Illustration of the experiment's operating condition fixed disc and ball speed.

Tab. 4-5 Summary of the conducted measurements in the "Technical applications – Part II"
* - Conducted measurements using the opposite SRR.

Configuration	Material couple	Load	Ball speed	Disc speed	Lubricant viscosity
		N	mm/s	mm/s	mPa.s
Soft-on-hard	PDMS SH50 -on- Steel		10 10-1000*	10-1000 10*	
					Glycerol (230)
Hard-on-soft	Steel -on- PDMS SH50	1	10-1000 10*	10 10-1000*	R834/80 (120)
					HC32/100 (40)
Soft-on-soft	PDMS SH50 -on- PDMS SH50		10 10-1000*	1000 10*	

Tab. 4-6 Typical technical applications conditions.

	Entrainment speed	**SRR**	**Contact pressure**	**Material pair E'**	**Lubricant viscosity**
	mm/s	%			mPa.s
O-ring [35]	5-1080	0-200	1300-2100 kPa	FKM/Glass 17.37 MPa	Glycerol-water (5-100)
Wiper - Glass	10-800	200	1 MPa	Rubber/Glass 26.60 MPa	Water (1)
Tyre - Road	0-1000	0-200	3 MPa	Tyre/Concrete 10.00-15.00 MPa	Dry Water (1)

4.2.2 Biological applications

Three case studies (tab.4-7) were conducted to mimic the actual biological interfaces being eye-lid, artificial knee, and fascia. Each case study uses one lubricant that is normally present in its environment and then a second lubricant with similar viscosity is used to reveal if the biological lubricant may be substituted. The loads were chosen to create similar contact pressures, however, in the case of the eye-lid and fascia case studies, the required load was below 1 N, which the MTM is not capable of stably generating and thus the loads were selected as are in the table below. In these case studies, the soft PDMS samples are the PDMS SH30 samples which are more suitable for these conditions. In the case of the artificial knee, the material couple steel-on-UHMWPE was selected as this combination is often used in real artificial knees.

Tab. 4-7 Summary of the conducted measurements investigating biological applications.

Case study	Material couple	Load	SRR	Speed	Lubricant viscosity
		N	%	mm/s	mPa.s
Eye	PDMS -on- PDMS	1	200	5-150	Eye drops Glycerol 40% (2)
Artificial knee	Steel -on- UHMWPE	10	100	10-150	Synovial fluid PBS Water (4)
Fascia	PDMS -on- PDMS	2	200	5-100	HA 317 TOTM (287-300)

5 RESULTS

5.1 Surface roughness measurements

The surface roughness of the used samples was measured using a profilometer Bruker Contour GT-X based on the phase-shifting interferometry technique. Roughness was measured both at the untouched (U) areas, where the samples are not in contact and wear, does not occur and touched (T) areas (tab.5-1). Each area was measured at three different places on the sample and the value was then averaged. The averaged touched values were then compared to the averaged untouched values to determine the amount of wear. The surface roughness of the PDMS samples remained relatively unchanged, whereas the UHMWPE samples were smoothed, especially the UHMWPE disc, where roughness has dropped by 300 nm.

Tab. 5-1 Surface roughness measurements of the used samples.

Sample	U1	T1	U2	T2	U3	T3	$U_{average}$	$T_{average}$	Diff.
	nm	nm	nm	nm	nm	nm	nm	nm	%
PDMS ball	238	298	295	208	132	230	222	250	11.2
PDMS disc	218	133	189	191	140	180	182	170	6.5
UHMWPE ball	549	640	739	910	140	620	794	720	9.3
UHMWPE disc	1230	929	1290	957	1230	970	1250	950	24.0
Steel ball	-	47.76	-	53.20	-	68.00	-	56.32	-
Steel disc	-	9.93	-	9.06	-	9.50	-	9.49	-

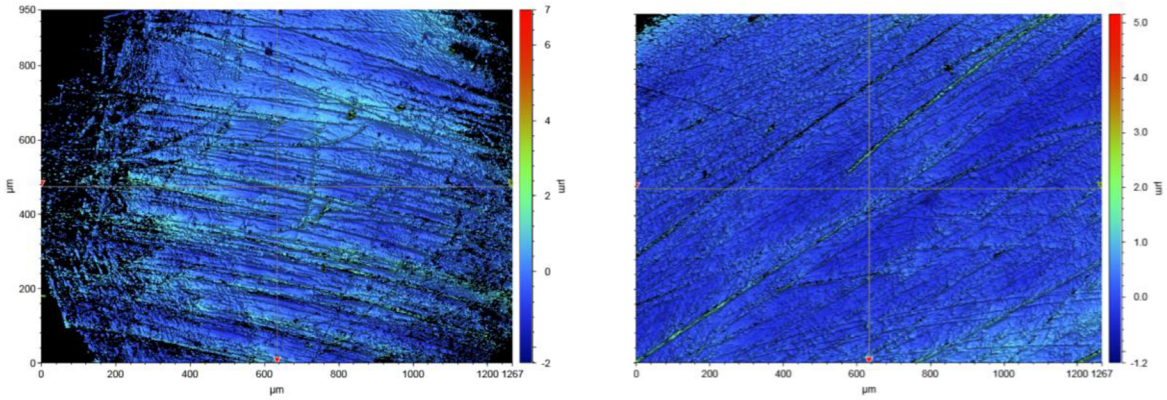

Fig. 5-1 (Left) Touched PDMS ball (Right) Touched PDMS disc.

5.2 Technical application measurements – Part I

The carried out measurements (tab.4-4) are presented in the following subchapters concerning the effects of kinematic conditions, lubricant viscosity, viscoelasticity, material, and comparison of experimental data to the numerical simulation data, respectively. The described effects are also divided into subchapters regarding the actual configuration.

5.2.1 The effects of kinematic conditions

The following figures show the friction coefficient as a function of entrainment speed while using various lubricants for both different configurations, which are as mentioned divided into subchapters, and also a function of SRR, which are coloured by different colours to distinguish its value.

Soft-on-hard configuration

The soft-on-hard configuration's friction coefficient increases with entrainment speed for all three lubricants. Also, with increasing SRR the friction coefficient increases, especially for the friction coefficients obtained at higher entrainment speeds. The friction at low entrainment speed seems to converge to a value of 0.02 for the soft-on-hard configuration for all three SRR measurements and lubricants.

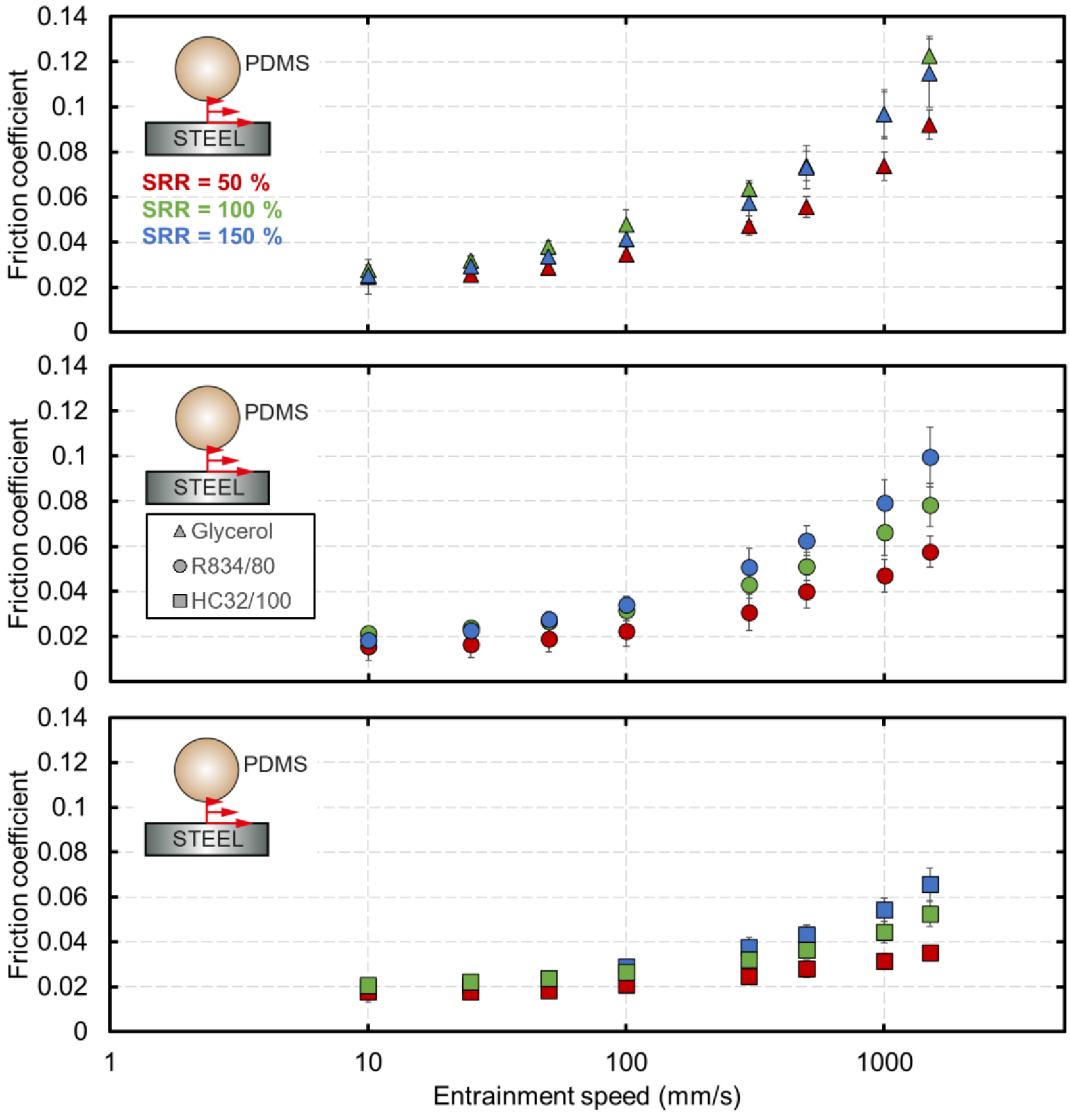

Fig. 5-2 Friction coefficient as a function of log-scale entrainment speed and SRR for the soft-on-hard configuration using specific lubricants.

Hard-on-soft configuration

The hard-on-soft configuration also exhibits the same behaviour, where friction coefficient increases with entrainment speed for all used lubricants. However, the friction coefficient seems to be more sensitive to changes in the SRR, producing higher friction coefficients. Also, at low entrainment speed, the friction coefficient converges to a value of 0.04 for all three slide-to-roll measurements and lubricants.

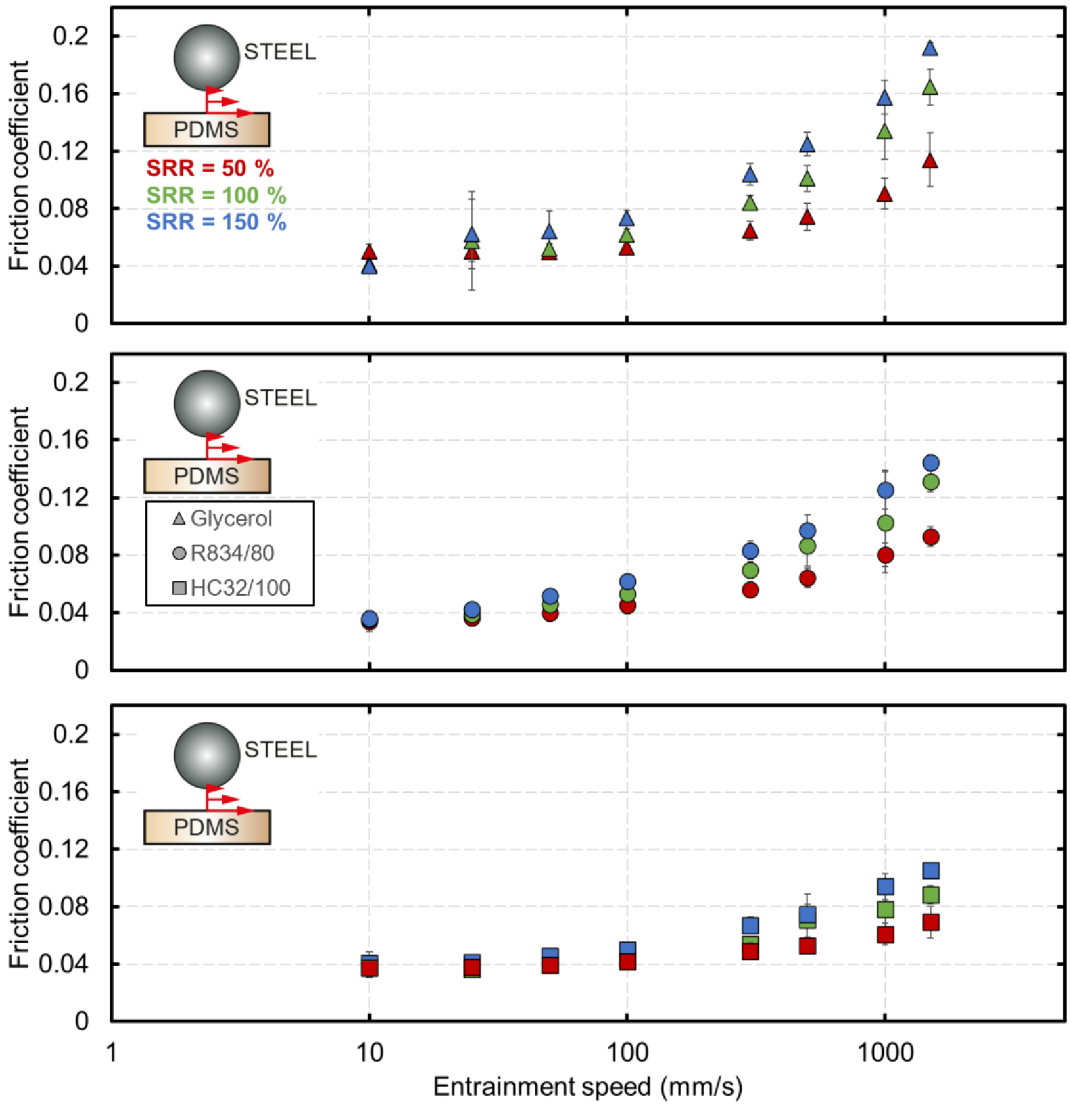

Fig. 5-3 Friction coefficient as a function of log-scale entrainment speed and SRR for the hard-on-soft configuration using specific lubricants.

Soft-on-soft configuration

The soft-on-soft configuration also produces an increase in friction coefficient with entrainment speed in a similar fashion as the hard-on-soft configuration, where the friction coefficient's growth is sensitive to an increase in the SRR. The friction coefficient also converges to a stable value of 0.03 for the soft-on-hard configuration for all three slide-to-roll measurements and lubricants.

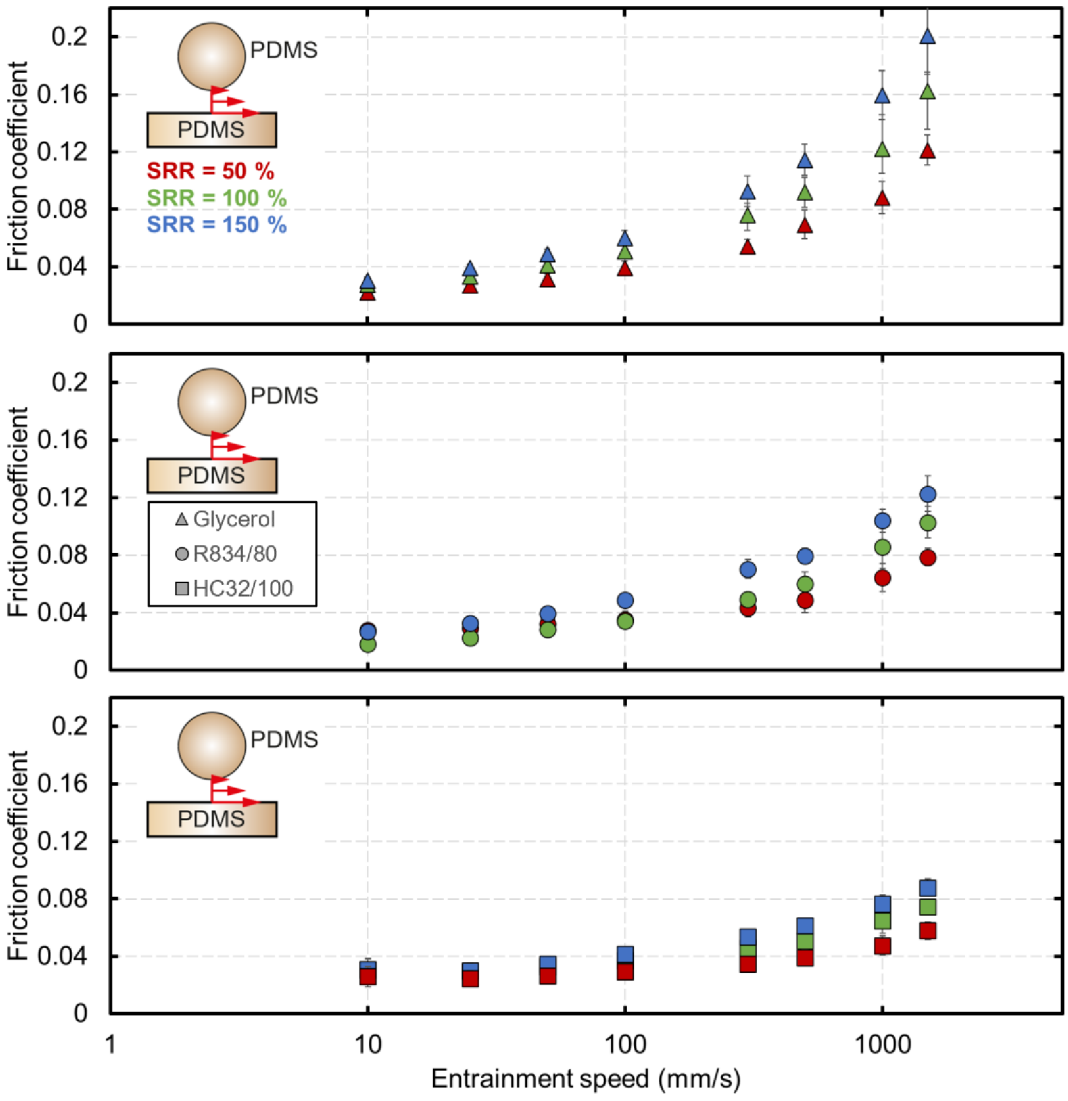

Fig. 5-4 Friction coefficient as a function of log-scale entrainment speed and SRR for the soft-on-soft configuration using specific lubricants.

5.2.2 The effects of lubricant viscosity

When friction coefficient is displayed as a function of reduced sliding speed, experimental data roughly collapse to a "master-curve" which is compared with the theoretical prediction proposed by de Vicente et al. [16] in a form of the regression equation.

Soft-on-hard configuration

From fig. 5-5, it is evident that increasing the lubricant's viscosity leads to an increase in friction coefficient. At high reduced sliding speeds, the experimental data show good agreement with the theory of de Vicente [16]. However, as the reduced sliding speed decreases, so does the degree of agreement. This behaviour applies to all the values of SRRs in this configuration.

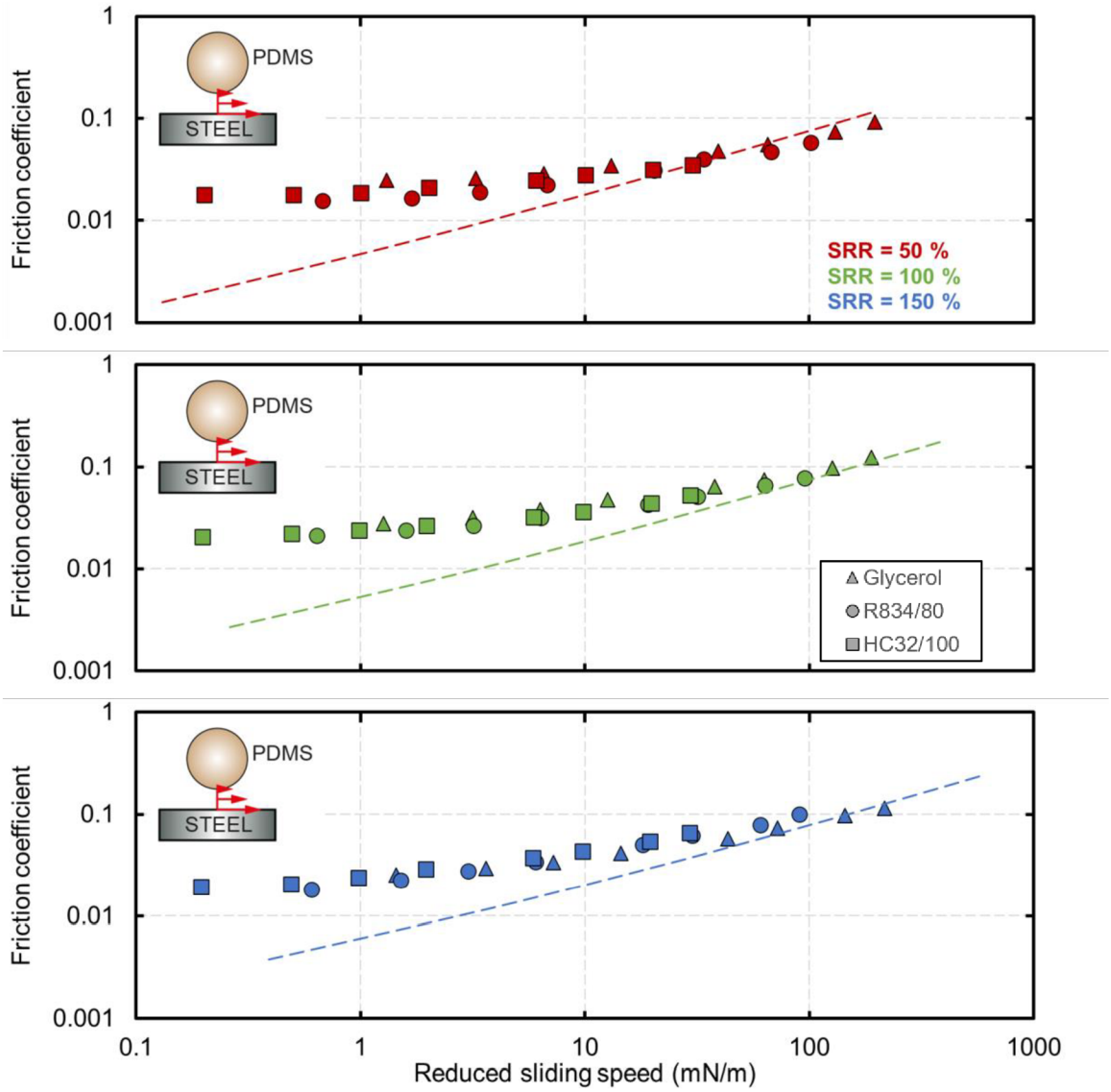

Fig. 5-5 Friction coefficient as a function of reduced sliding speed (viscosity · sliding speed) in log-log scale for the soft-on-hard configuration compared to the regression equations proposed by de Vicente et al. [16] represented by the dashed line.

Hard-on-soft configuration

In the case of the hard-on-soft configuration, similar behaviour is observed, where at high reduced sliding speeds the experimental data for SRR = 50% show good agreement. However, with increasing SRR the degree of the agreement begins to slowly cease. This can be observed in the comparison of experimental data for SRR = 100% and 150%, where the gap between the data points and the dashed line slowly increases. Also, with decreasing reduced sliding speed the deviation from the predicted friction coefficient grows.

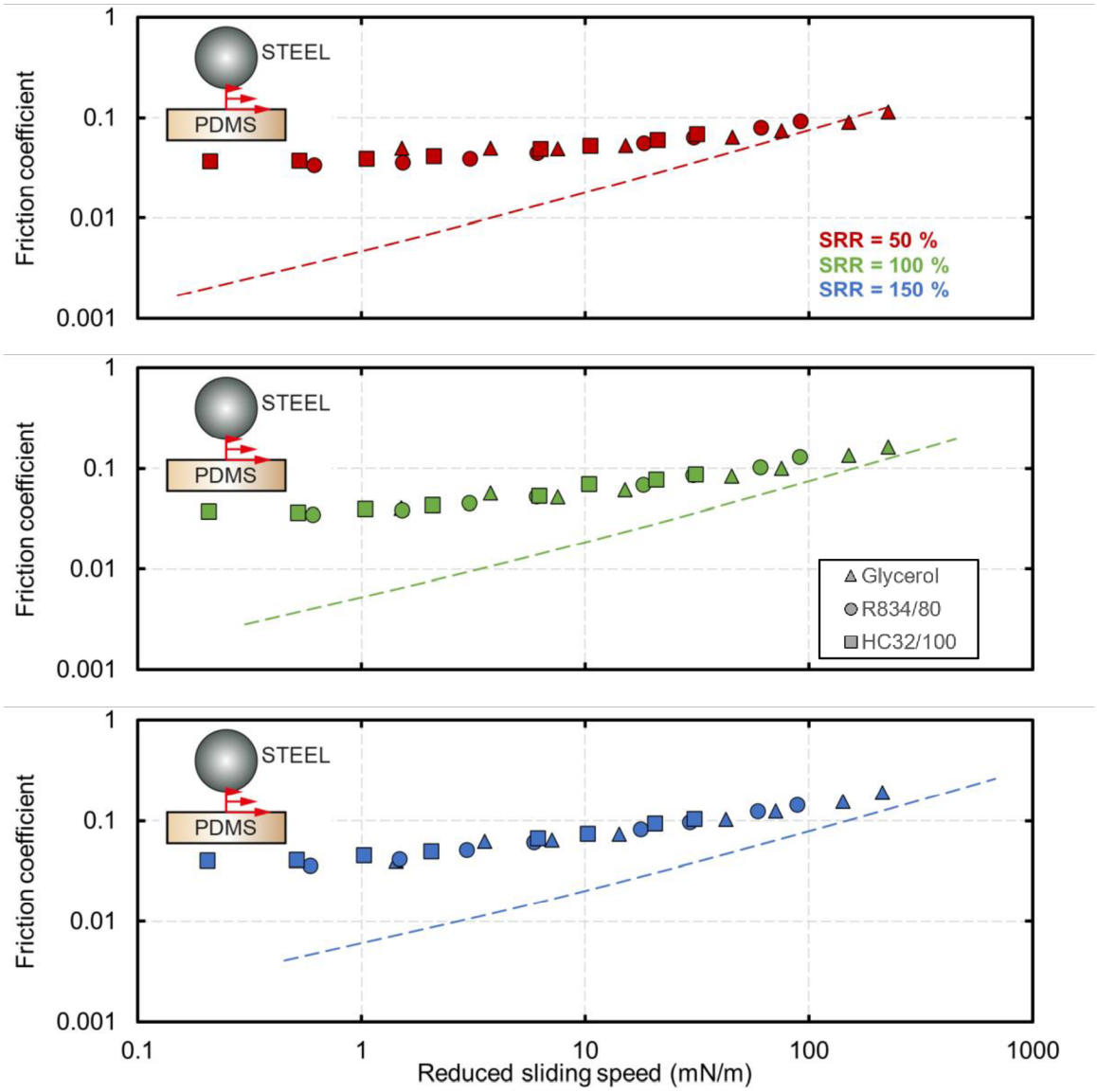

Fig. 5-6 Friction coefficient as a function of reduced sliding speed (viscosity · sliding speed) in log-log scale for the hard-on-soft configuration compared to the regression equations proposed by de Vicente et al. [16] represented by the dashed line.

Soft-on-soft configuration

The soft-on-soft configuration exhibits a similar tendency as the previous configuration, where for SRR = 50% an agreement at high reduced sliding speed is observed and for the higher SRR, the deviation between experimental and theoretical data can be observed. However, the deviation seems to be more pronounced compared to the hard-on-soft. A significant deviation at lower reduced sliding velocities is also observed.

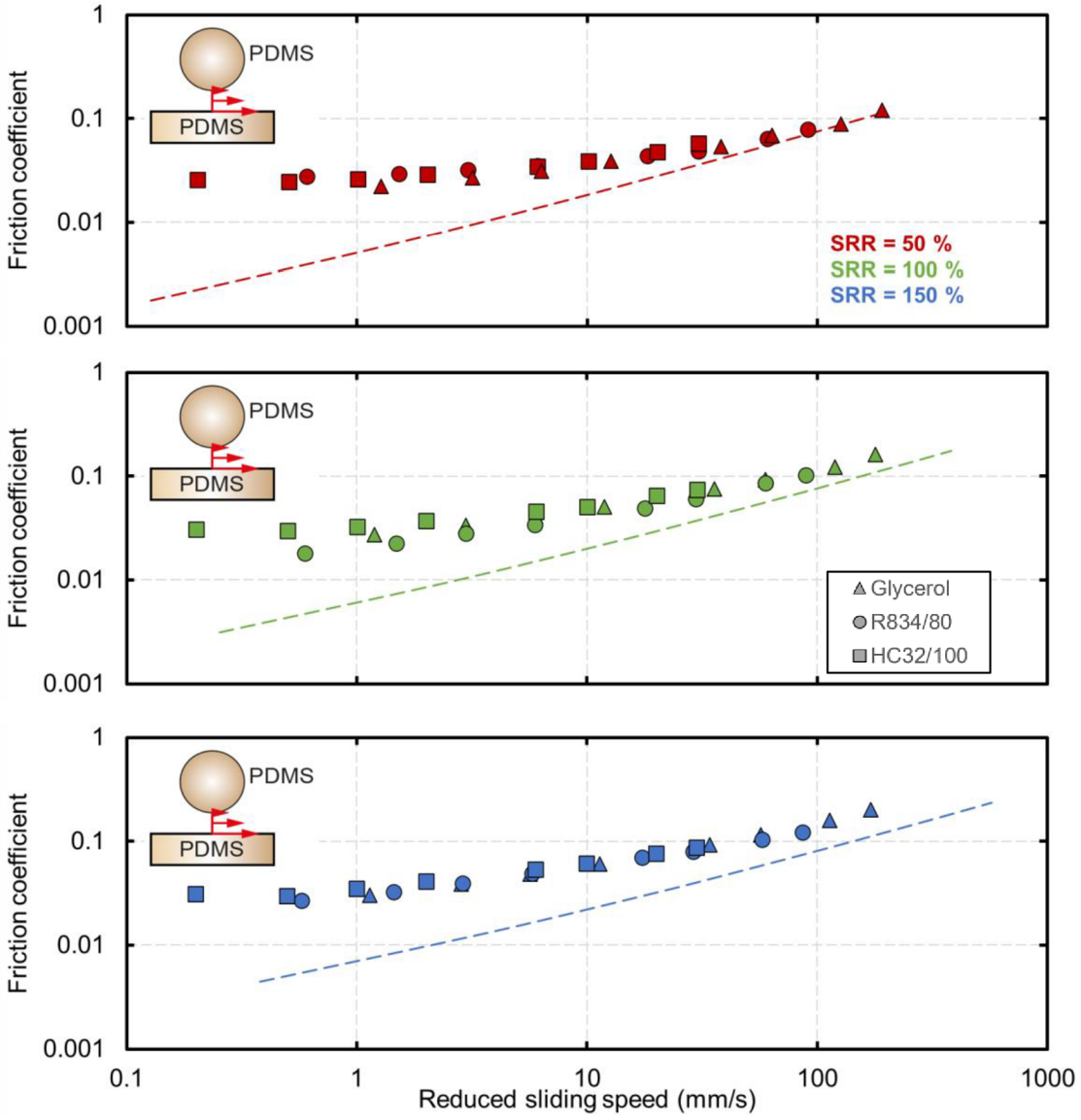

Fig. 5-7 Friction coefficient as a function of reduced sliding speed (viscosity · sliding speed) in log-log scale for the soft-on-soft configuration compared to the regression equations proposed by de Vicente et al. [16] represented by the dashed line.

5.2.3 The effects of viscoelasticity

The following figures compare the sum of the Poiseuille friction component and elastic hysteresis, which corresponds to rolling friction, with the predicted elastic hysteresis using Persson's equation (eq.11). The sum of the two components is displayed as a function of entrainment speed for different lubricants and SRRs.

Soft-on-hard configuration

The experimental data coincide with the hysteresis curve at low entrainment speed for all used lubricants and SRR. With increasing entrainment speed the experimental data begin to recede from the hysteresis curve. This effect is greater with higher lubricant viscosities. The rolling friction coefficient increases as well with increasing SRR.

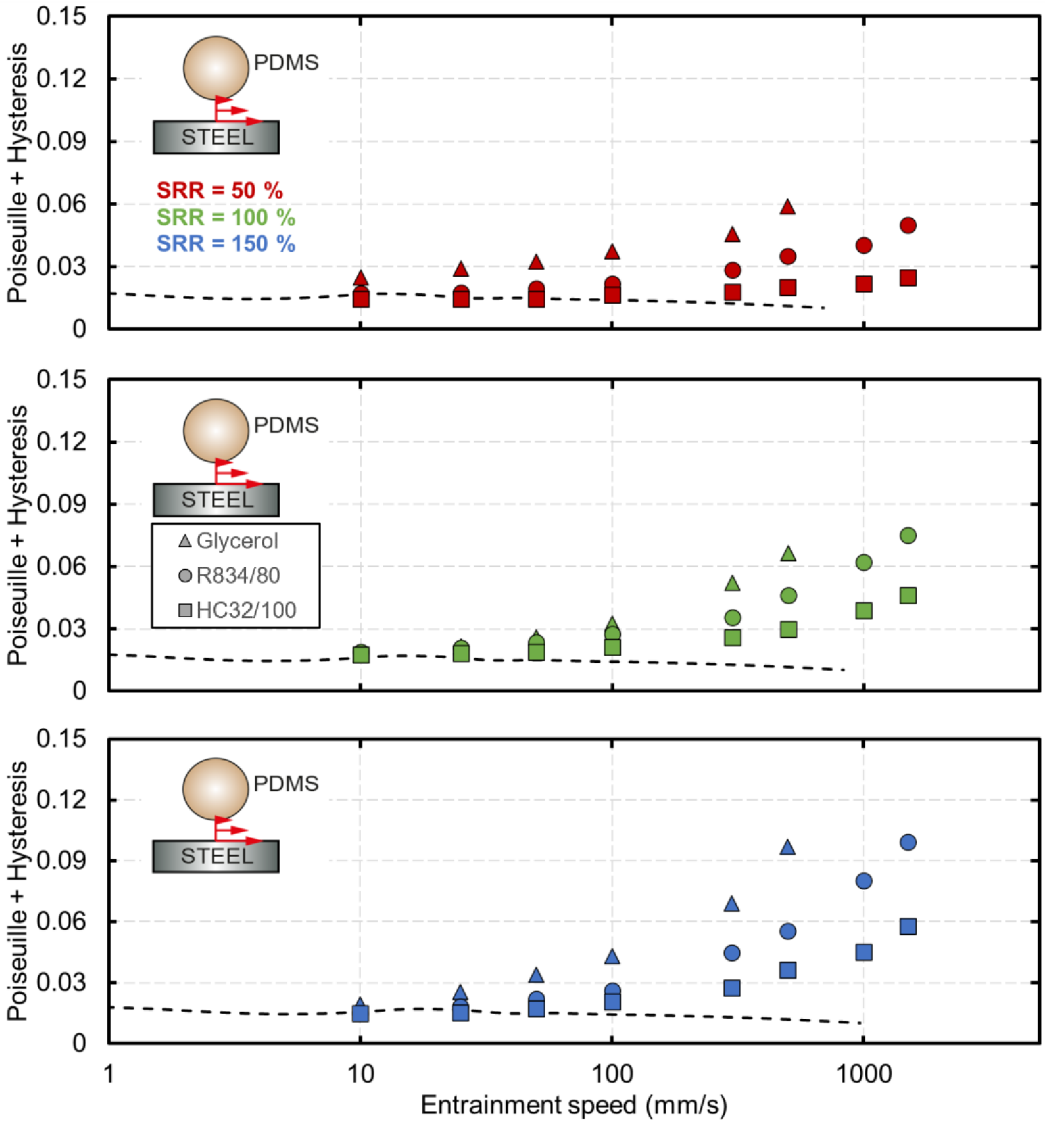

Fig. 5-8 Rolling friction (Poiseuille+Hysteresis) plotted as a function of log-entrainment speed and SRR for the soft-on-hard configuration compared with the elastic hysteresis calculated by using Persson's theory [24].

Hard-on-soft configuration

At low entrainment speeds, the experimental data approach the hysteresis curve, however, with a minor offset. This offset is larger for the low viscosity lubricants than for the high viscosity lubricants. Nevertheless, this behaviour is reversed where with increasing entrainment speed the more viscous lubricants produce higher friction coefficients compared to the less viscous lubricants. This effect is more evident with increasing SRR, which also produced higher rolling friction coefficients.

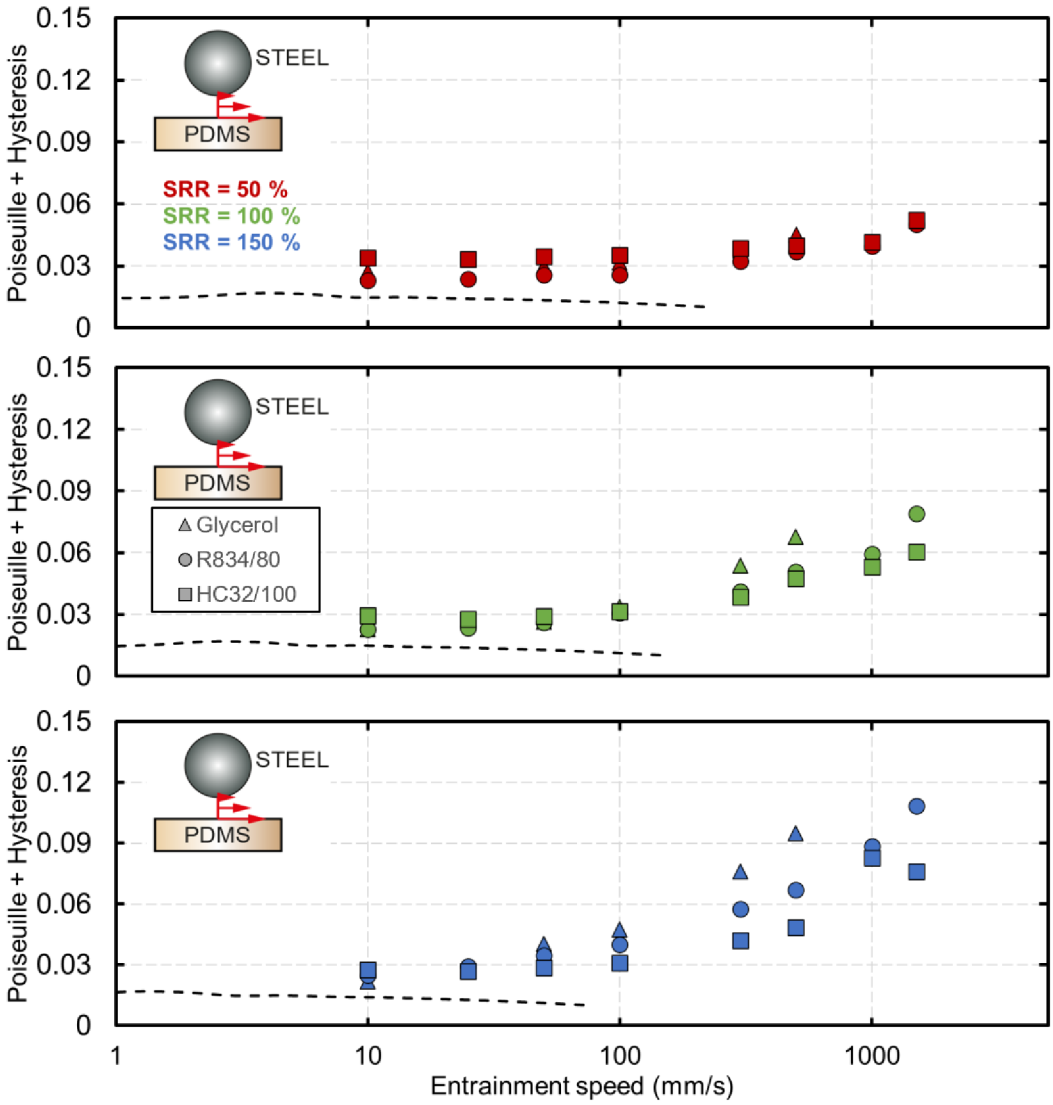

Fig. 5-9 Rolling friction (Poiseuille+Hysteresis) plotted as a function of log-entrainment speed and SRR for the hard-on-soft configuration compared with the elastic hysteresis calculated by using Persson's theory [24].

Soft-on-soft configuration

The soft-on-soft configuration behaves comparably to the soft-on-hard configuration, which is, at low entrainment speed the experimental data converge to a constant value being close to the elastic hysteresis theoretical curve. With increasing entrainment speed friction coefficient increases also. This effect is more profound with lubricants of higher viscosity and with the increase of SRR.

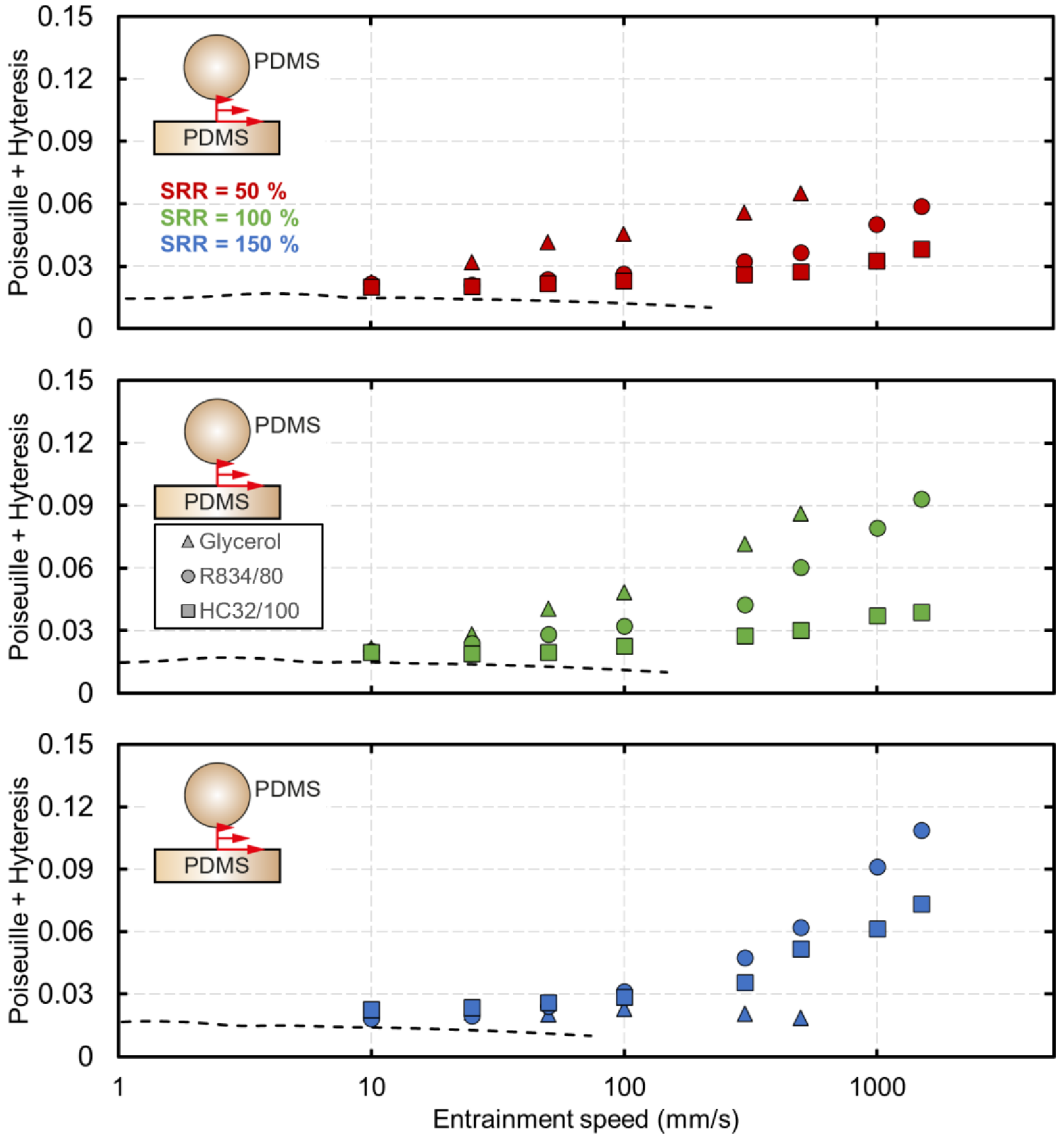

Fig. 5-10 Rolling friction (Poiseuille+Hysteresis) plotted as a function of log-entrainment speed and SRR for the soft-on-soft configuration compared with the elastic hysteresis calculated by using Persson's theory [24].

5.2.4 The effect of material

The following figures show friction coefficient as a function of entrainment speed for the measurements carried out using PDMS SH50 vs. PDMS SH30 with the lubricant R834/80 at SRR = 50%. The next figure displays rolling friction as a function of entrainment speed together with the theoretical prediction using the hysteretic equation (eq.11).

Soft-on-hard configuration

The friction coefficient for both samples increases with increasing entrainment speed. At low entrainment speed, the friction coefficient of the PDMS SH30 is larger than the friction coefficient of the PDMS SH50 sample. This difference disappears with increasing entrainment speed as the experimental data merge.

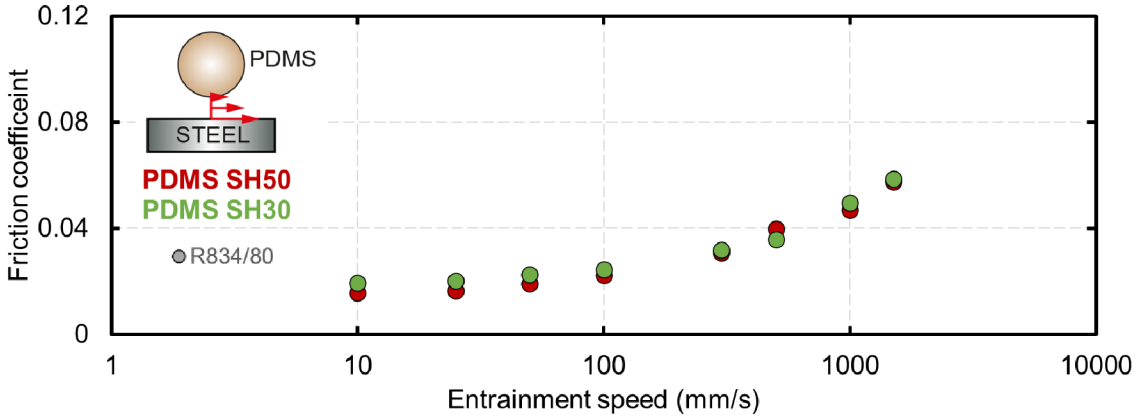

Fig. 5-11 Friction coefficient plotted as a function of log-entrainment speed and Shore hardness for the soft-on-hard configuration lubricated using R834/80 for SRR = 50%.

The rolling friction tends to converge to a stable value for both Shore hardnesses, where the SH50 shows good agreement with the predicted hysteresis, whereas the SH30 slightly deviates from the hysteresis prediction.

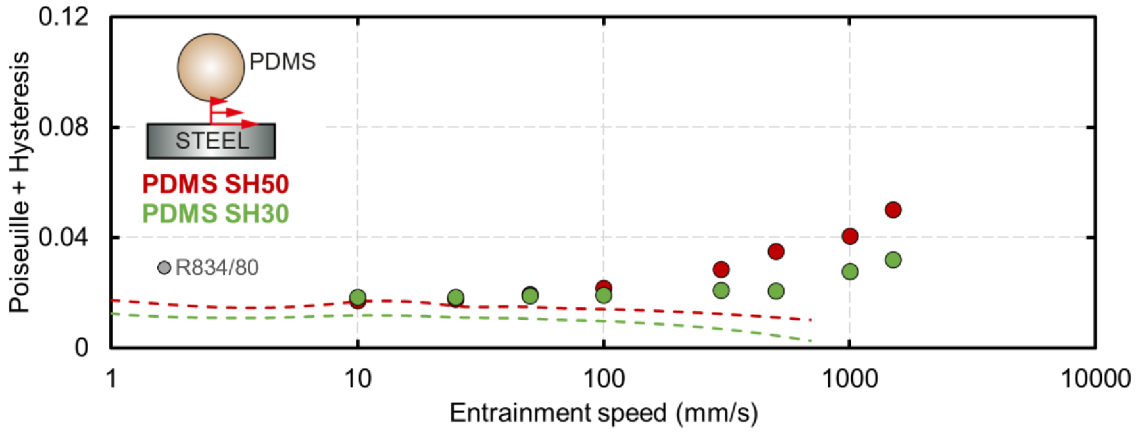

Fig. 5-12 Rolling friction (Poiseuille+Hysteresis) plotted as a function of log-entrainment speed and Shore hardness for the soft-on-hard configuration lubricated using R834/80 and compared with the elastic hysteresis determined by Persson's theory [24].

Hard-on-soft configuration

The hard-on-soft configuration's friction coefficient increases with increasing entrainment speed as well for both PDMS samples. The experimental data also merge at high entrainment speeds, but at low entrainment speeds the behaviour is reversed as the PDMS SH50 sample produces higher friction coefficient compared to the PDMS SH30 sample.

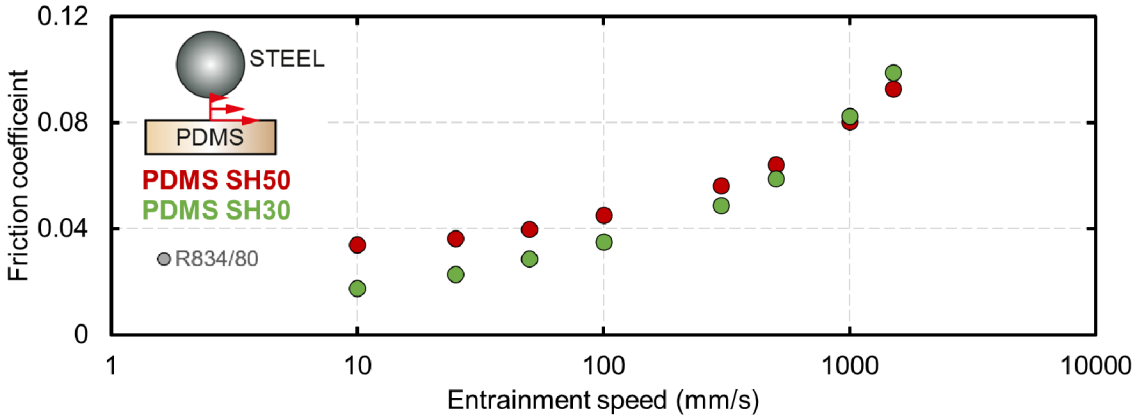

Fig. 5-13 Friction coefficient plotted as a function of log-entrainment speed and Shore hardness for the hard-on-soft configuration lubricated using R834/80 for SRR = 50%.

The hard-on-soft configuration produces slightly more hysteresis at the lowest speed for the SH50 than the SH30. Nevertheless, with increasing entrainment speed the SH30 produces higher rolling friction compared to the SH50. Both SH50 and SH30 show similar deviation from the predicted elastic hysteresis and the prediction of SH50 producing higher amounts of hysteresis were correct.

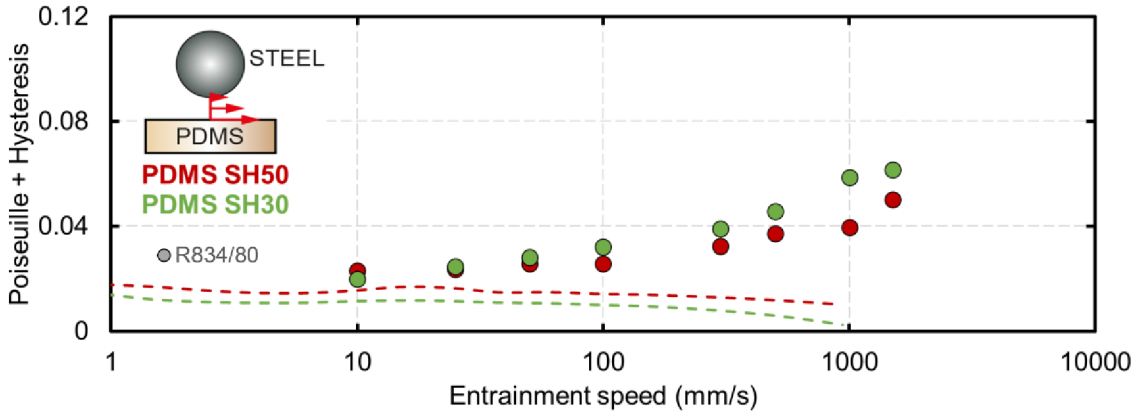

Fig. 5-14 Rolling friction (Poiseuille+Hysteresis) plotted as a function of log-entrainment speed and Shore hardness for the hard-on-soft configuration lubricated using R834/80 and compared with the elastic hysteresis determined by Persson's theory [24].

Soft-on-soft configuration

The friction coefficient of the soft-on-soft configuration also increases with increasing entrainment speed for both PDMS samples. Similarly, at high entrainment speeds, the friction coefficients of both samples merge, however, with decreasing entrainment speed the experimental data begin to separate from each other, where the PDMS SH50 samples produce a higher friction coefficient compared to the PDMS SH30 samples.

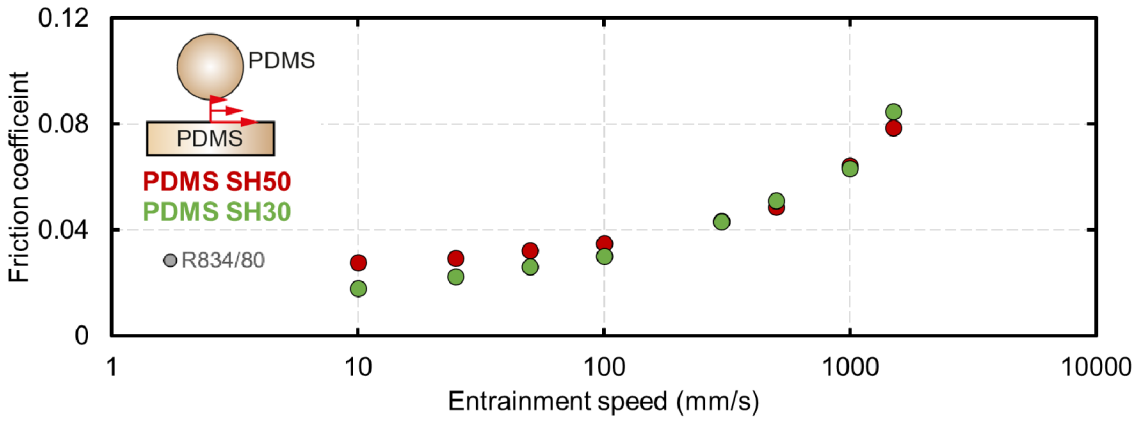

Fig. 5-15 Friction coefficient plotted as a function of log-entrainment speed and Shore hardness for the soft-on-soft configuration lubricated using R834/80 for SRR = 50%.

The rolling friction is almost identical for both SH50 and SH30 except for high entrainment speed, where a small deviation is observed. However, the experimental data converge to the predicted hysteresis of SH50 for both materials.

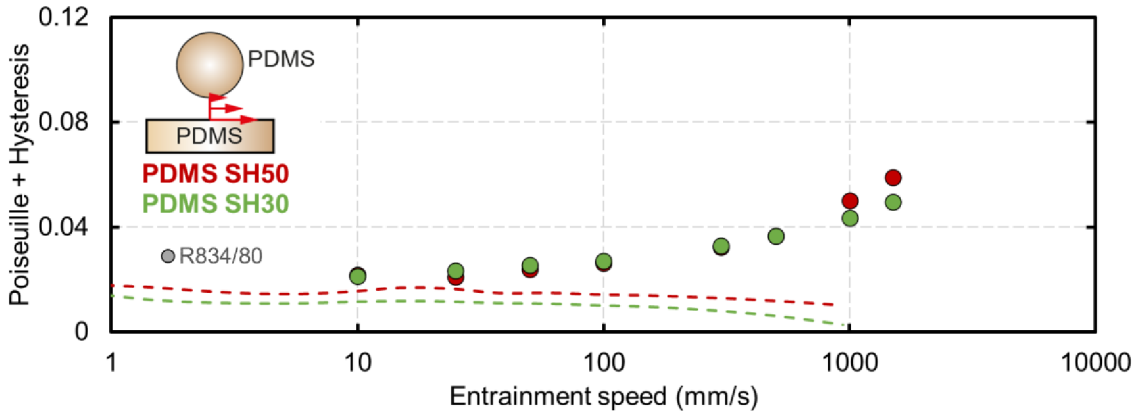

Fig. 5-16 Rolling friction (Poiseuille+Hysteresis) plotted as a function of log-entrainment speed and Shore hardness for the soft-on-soft configuration lubricated using R834/80 and compared with the elastic hysteresis determined by Persson's theory [24].

5.2.5 Experimental vs. Numerical data

The following figures compare the results of experimental measurements with de Vicente's regression equation [16] and the numerical simulation performed in cooperation with FAE Erlangen-Nurnberg for soft-on-hard and hard-on-soft configurations for SRR = 50%.

Soft-on-hard configuration

The experimental data for all three lubricants show good agreement with the numerical simulation performed by FAE Erlangen-Nurnberg (dashed line), where also its slope fits better with the experimental data. Slight deviations at higher speeds can be observed for glycerol and R834/80.

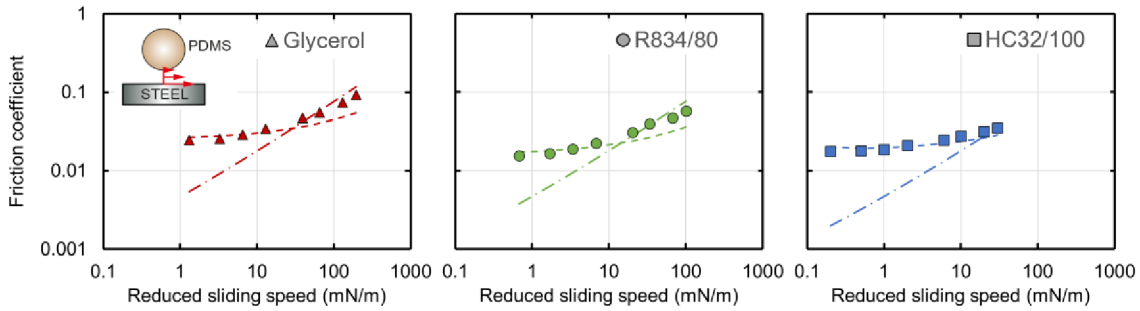

Fig. 5-17 Friction coefficient plotted as a function of reduced sliding speed in log-log scale for the soft-on-hard configuration using different lubricants; The theory proposed by de Vicente et al. [16] is plotted as a dot-and-dashed line and the numerical simulation as a dashed curve.

Hard-on-soft configuration

The numerical simulation (dashed line) also complies with the experimental data for all three lubricants. Slight deviations at higher speeds can be observed for R834/80 and HC32/100.

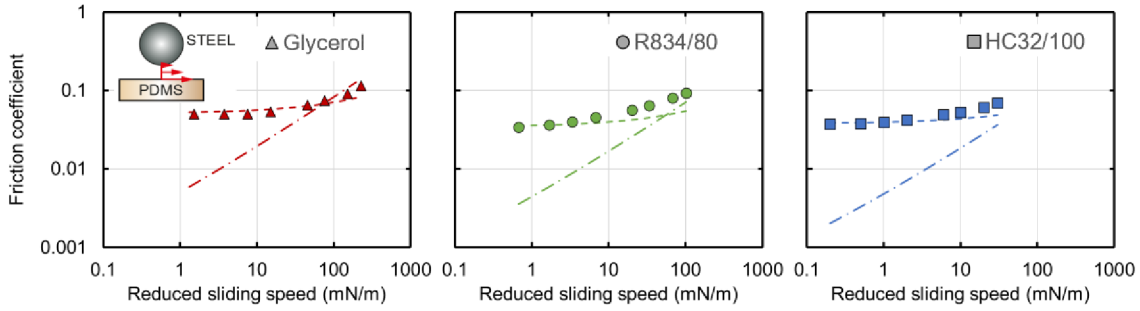

Fig. 5-18 Friction coefficient plotted as a function of reduced sliding speed in log-log scale for the hard-on-soft configuration using different lubricants; The theory proposed by de Vicente et al. [16] is plotted as a dot-and-dashed line and the numerical simulation as a dashed curve.

5.2.6 Summarization

The following figures summarize individual investigated effects.

The effects of kinematic conditions

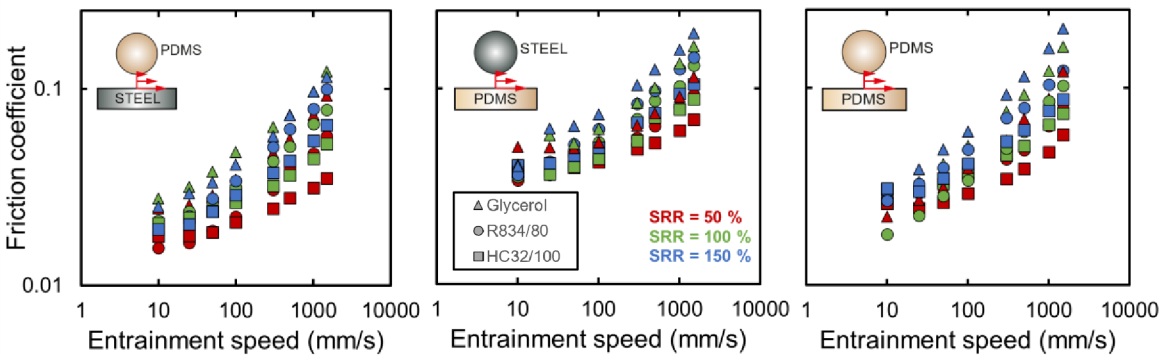

Fig. 5-19 Friction coefficient plotted as a function of entrainment speed and SRR in log-log scale for all configurations.

The effect of lubricant viscosity

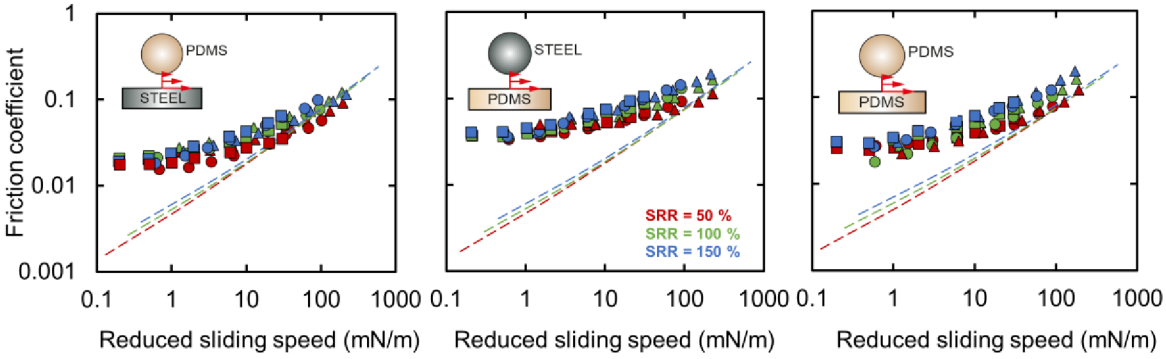

Fig. 5-20 Friction coefficient plotted as a function of reduced sliding speed and SRR in log-log scale for all configurations.

The effect of viscoelasticity

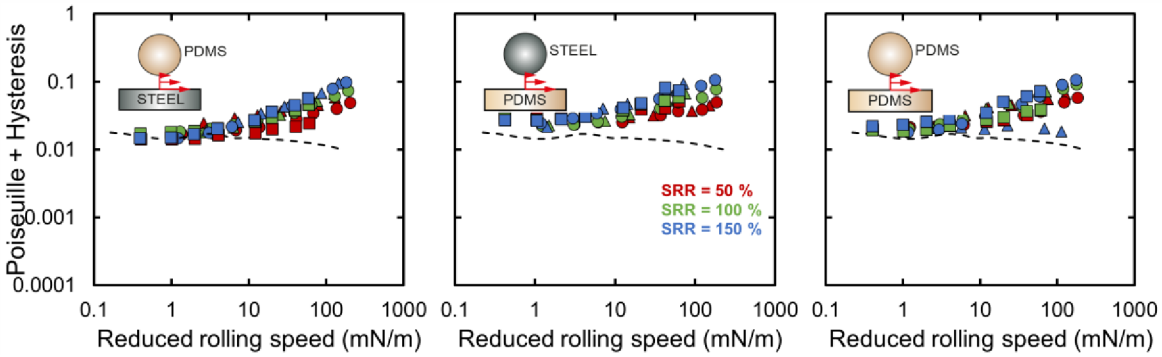

Fig. 5-21 Rolling friction coefficient plotted as a function of reduced rolling speed and SRR in log-log scale for all configurations.

The effect of material

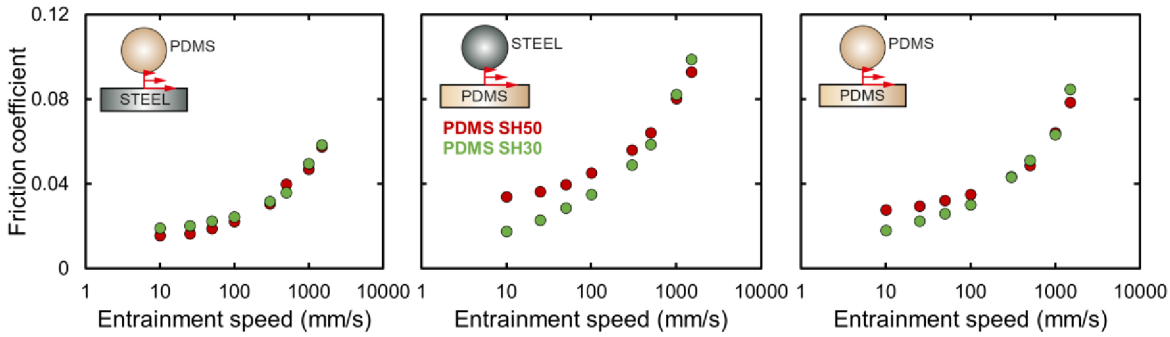

Fig. 5-22 Friction coefficient plotted as a function of entrainment speed and Shore hardness for all configurations.

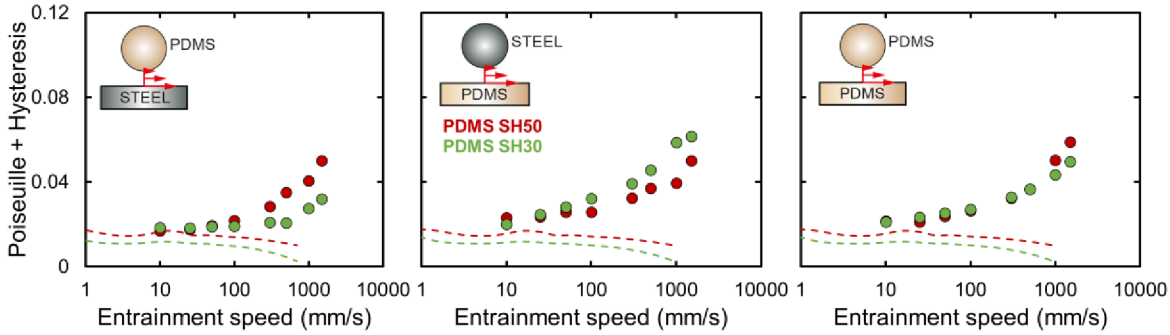

Fig. 5-23 Rolling friction coefficient plotted as a function of entrainment speed and Shore hardness for all configurations and compared to the theoretical prediction of elastic hysteresis by Persson [24].

5.3 Technical application measurements – Part II

The carried-out measurements from tab.4-5 are presented in the following subchapters concerning the effects of kinematic conditions, lubricant viscosity, and viscoelasticity, respectively.

5.3.1 The effects of kinematic conditions

The following figures show friction coefficient as a function of entrainment speed using the R834/80 lubricant with the fixed speed of the soft specimen.

Soft-on-hard configuration

The soft-on-hard configuration exhibits a low friction coefficient at the lowest entrainment speed, which should correspond to a pure-rolling contact. From this point, an increase in friction coefficient with increasing entrainment speed can be observed for all lubricants. In the case of the fixed ball speed (positive SRR), the produced friction coefficient is higher compared to the fixed disc speed (negative SRR).

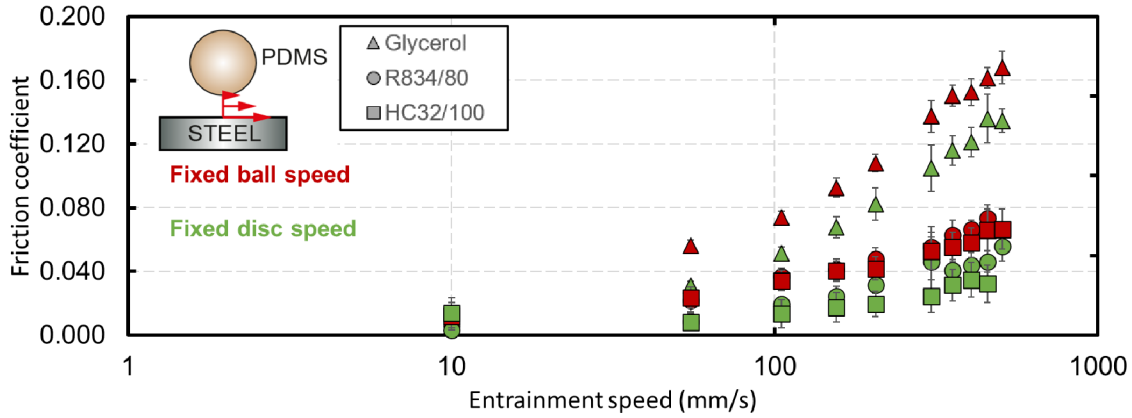

Fig. 5-24 Friction coefficient plotted as a function of log-entrainment speed for the fixed ball speed and the fixed disc speed scenarios using the PDMS SH50 in the soft-on-hard configuration lubricated by all three lubricants.

Hard-on-soft configuration

The friction coefficient of the hard-on-soft configuration also produces a low friction coefficient at low entrainment speed and with increasing entrainment speed the friction coefficient increases, wherein the case of the fixed ball speed the growth is more rapid compared to the fixed disc speed.

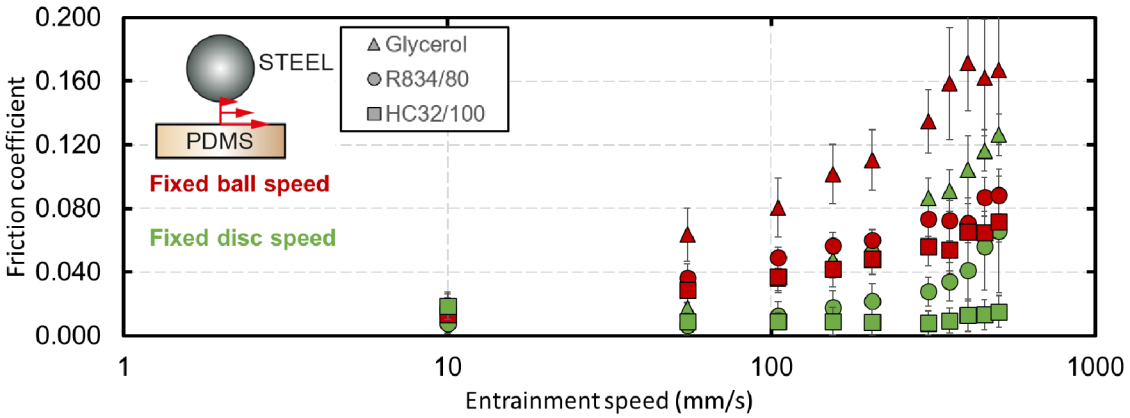

Fig. 5-25 Friction coefficient plotted as a function of log-entrainment speed for the fixed ball speed and the fixed disc speed scenarios using the PDMS SH50 in the hard-on-soft configuration lubricated by all three lubricants.

Soft-on-soft configuration

This configuration also produces a low friction coefficient at the lowest entrainment speed, where an increase in friction with increasing entrainment speed is observed. The differences between the fixed ball and disc speed's friction coefficient are not as significant.

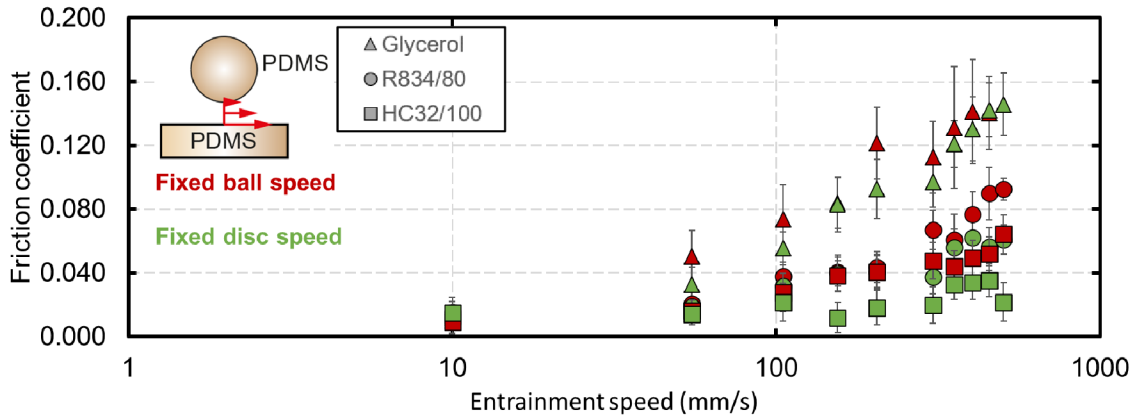

Fig. 5-26 Friction coefficient plotted as a function of log-entrainment speed for the fixed ball speed and the fixed disc speed scenarios using the PDMS SH50 in the soft-on-soft configuration lubricated by all three lubricants.

5.3.2 The effects of lubricant viscosity

The following figures display the friction coefficient as a function of reduced rolling speed (entrainment speed · lubricant viscosity) for the fixed speed of the soft specimen and then the fixed speed of the opposing specimen. The experimental data have been compared with theoretical predictions by de Vicente [16] represented by dashed lines, where the experimental data and the theoretical predictions are matched by colour for each lubricant.

Soft-on-hard configuration

In general, with increasing lubricant viscosity the friction coefficient increases for both scenarios. In the case of the fixed disc speed, a subtle decrease in friction can be observed at the beginning, but then friction increases also. At high reduced rolling speeds, the experimental data show good agreement with the theoretical predictions for the fixed ball speed case, however, for the case of the fixed disc speed the experimental data are shifted lower and the agreement is not as good except for glycerol. However, at the lowest reduced rolling speed there's a noticeable difference between the experimental and theoretical data. This difference increases with decreasing lubricant viscosity in both cases.

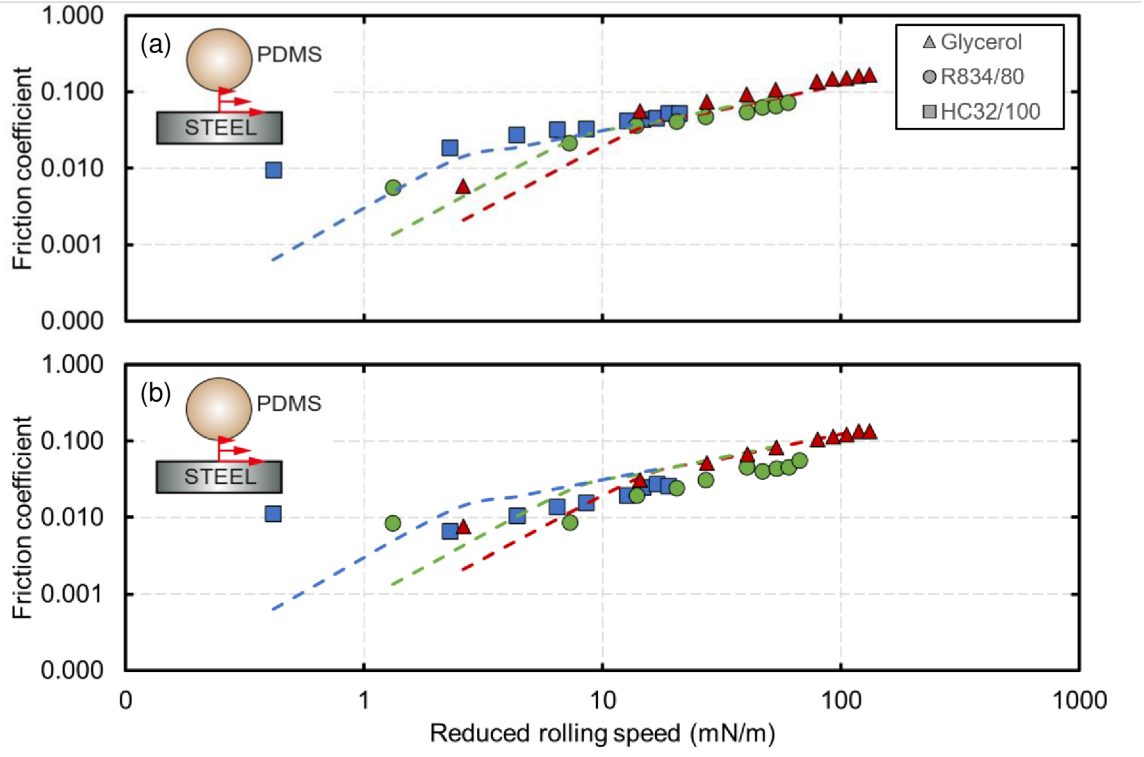

Fig. 5-27 Friction coefficient plotted as a function of log-reduced rolling speed in log-log for the soft-on-hard configuration while: (a) ball speed is fixed (b) disc speed fixed.

Hard-on-soft configuration

The hard-on-soft configuration shows similar behaviour as the previous configuration. Nevertheless, in the case of the fixed ball speed, the initial drop in friction coefficient is more significant than in the previous case. Similarly, the experimental data don't show good agreement with theory except for high reduced speed. In the case of the fixed disc speed, the experimental data show better overall agreement with theory, however at lower speeds a slight deviation can be observed. At the lowest reduced rolling speed, a noticeable difference between theoretical and experimental data can be also observed, wherein the case of the fixed ball speed the difference is sensitive to lubricant viscosity changes, however, the size of the difference is not as sensitive to viscosity changes in the case of the fixed disc speed.

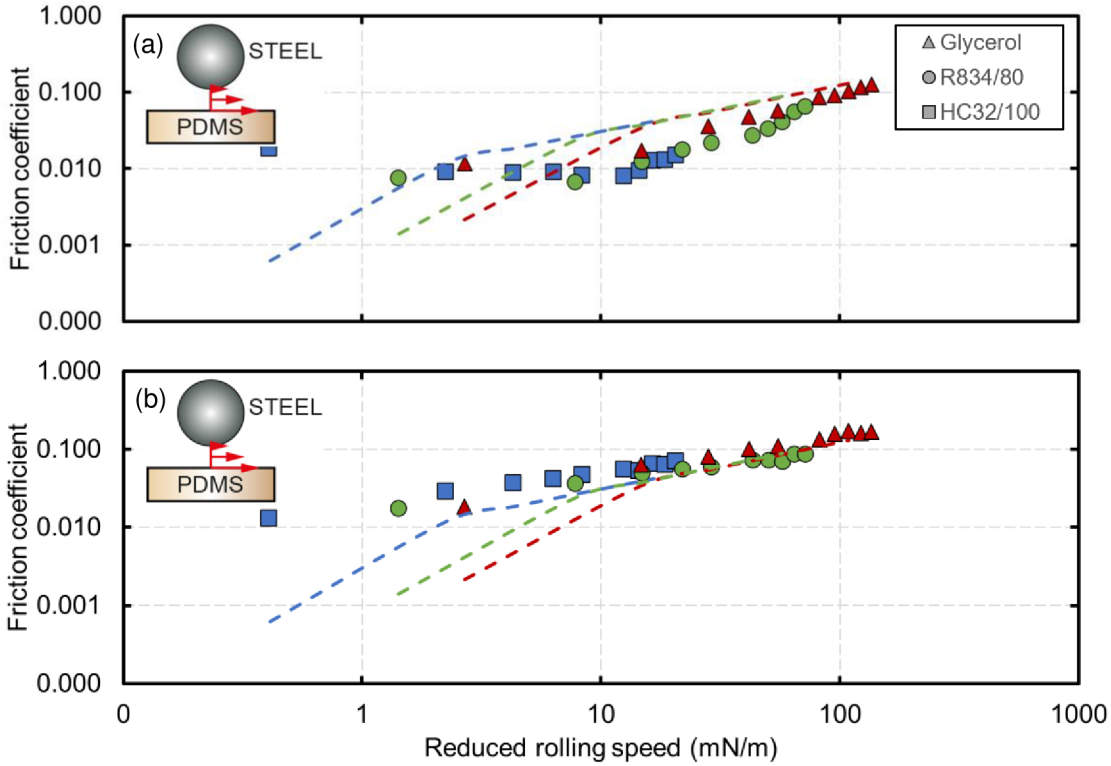

Fig. 5-28 Friction coefficient plotted as a function of log-reduced rolling speed in log-log for the hard-on-soft configuration while: (a) ball speed is fixed (b) disc speed fixed.

Soft-on-soft configuration

In the case of the fixed ball speed, the initial drop in friction can be also observed, however in this case the drop is not as significant as in the previous cases. At high reduced rolling speeds, the experimental data show better agreement as they approach the theoretical curve. In the case of the fixed disc speed, the experimental data coincide with the theoretical predictions for most of the measured points. At the lowest reduced rolling speed for the case of fixed ball speed, the differences between experimental and theoretical data also grow with decreasing lubricant viscosity, however, also not as rapidly as for the soft-on-hard configuration. In the case of the fixed disc speed, the difference doesn't seem to be affected by lubricant viscosity.

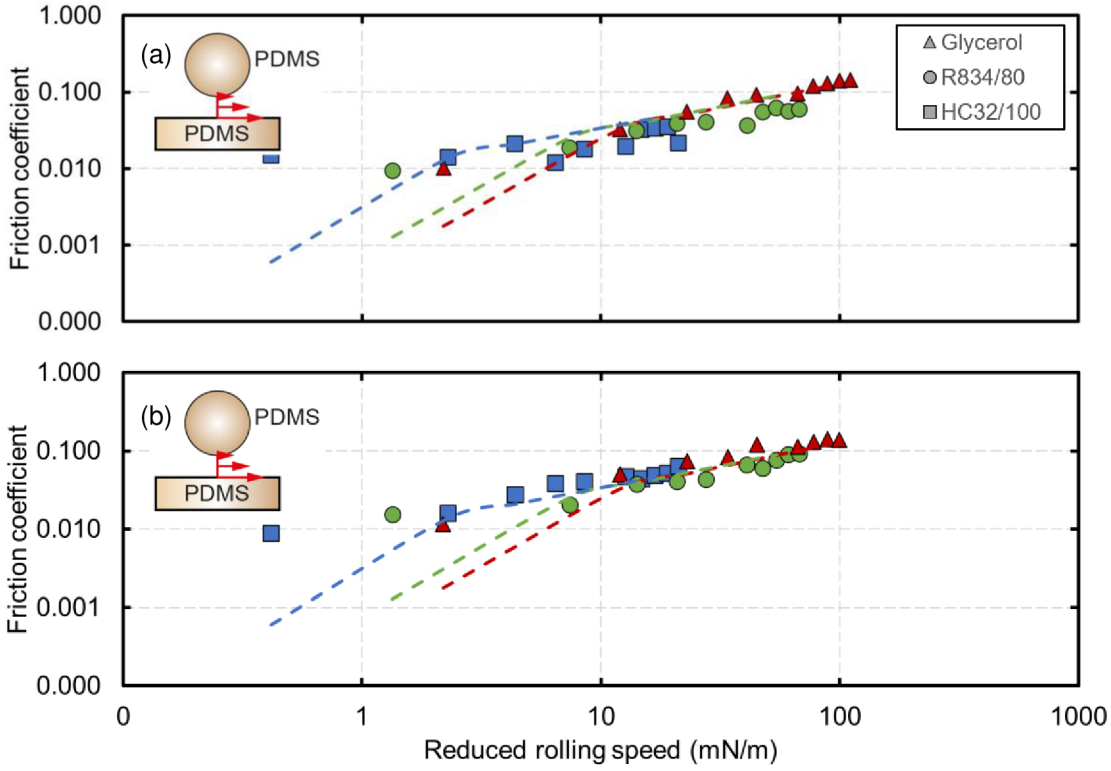

Fig. 5-29 Friction coefficient plotted as a function of log-reduced rolling speed in log-log for the soft-on-soft configuration while: (a) ball speed is fixed (b) disc speed fixed.

5.3.3 The effects of viscoelasticity

The following figures compare the sum of the Poiseuille friction component and elastic hysteresis, which corresponds to rolling friction, with predicted elastic hysteresis using Persson's theory [24] (eq.11). The sum of the two components is displayed as a function of reduced rolling speed for different lubricants. The elastic hysteresis is represented by a dashed line using a colour corresponding to each lubricant.

Soft-on-hard configuration

With increasing reduced rolling speed, the rolling friction increases roughly at the same rate. A slight difference in slope can be observed, where low viscosity produces a less steep slope. When the experimental data at their lowest speed are compared with the predicted elastic hysteresis, with increasing viscosity the difference between theoretical and experimental data increases as well.

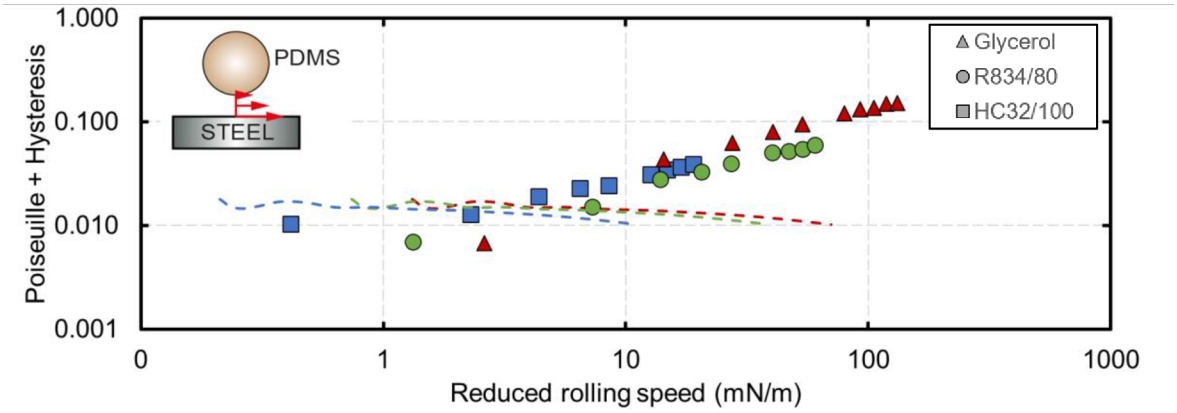

Fig. 5-30 Rolling friction (Poiseuille+Hysteresis) plotted as a function of log-reduced rolling speed for the soft-on-hard configuration compared with the elastic hysteresis predicted by Persson's theory [24].

Hard-on-soft configuration

The hard-on-soft configuration also exhibits similar behaviour, where with increasing reduced rolling speed the rolling friction increases also. However, at the lowest speed, the experimental data show good agreement with the theoretical hysteresis regardless of lubricant viscosity.

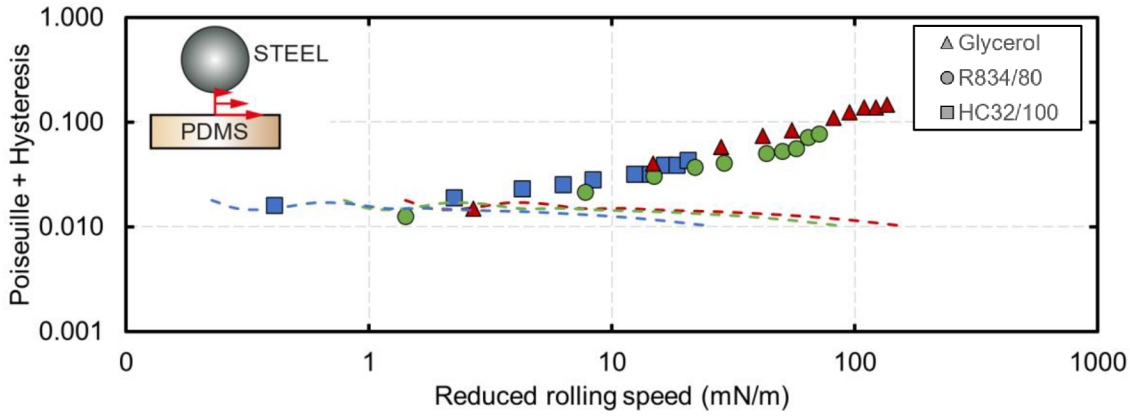

Fig. 5-31 Rolling friction (Poiseuille+Hysteresis) plotted as a function of log-reduced rolling speed for the hard-on-soft configuration compared with the elastic hysteresis predicted by Persson's theory [24].

Soft-on-soft configuration

The soft-on-soft configuration behaves similar to the hard-on-soft configuration, where the only difference can be observed at the lowest reduced rolling speeds, where the experimental data are slightly offset from the theoretical hysteresis curve. The value of the offsets seems to be constant with regards to viscosity.

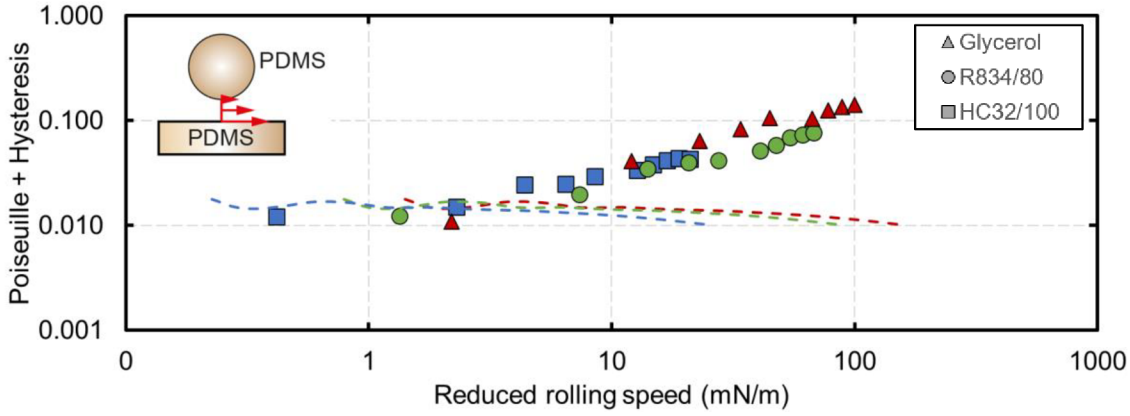

Fig. 5-32 Rolling friction (Poiseuille+Hysteresis) plotted as a function of log-reduced rolling speed for the soft-on-soft configuration compared with the elastic hysteresis predicted by Persson's theory [24].

5.3.4 Summarization

The effect of kinematic conditions

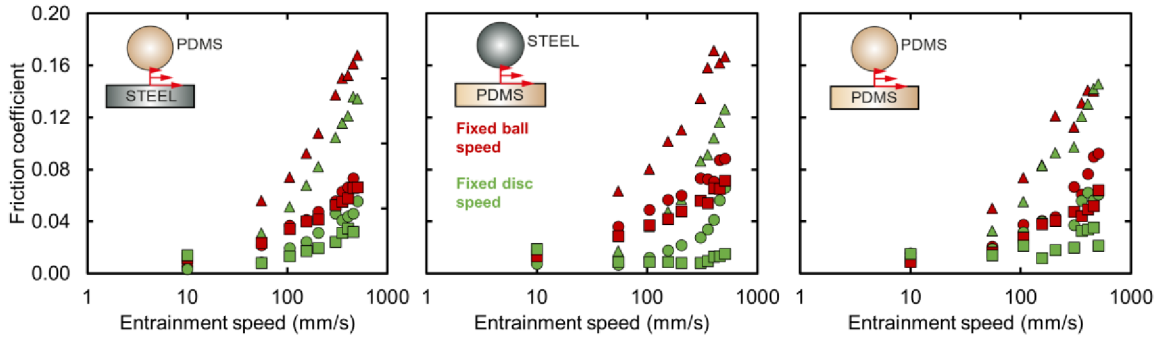

Fig. 5-33 Friction coefficient plotted as a function of log-entrainment speed for the fixed ball speed and the fixed disc speed scenarios for all configurations.

The effect of lubricant viscosity

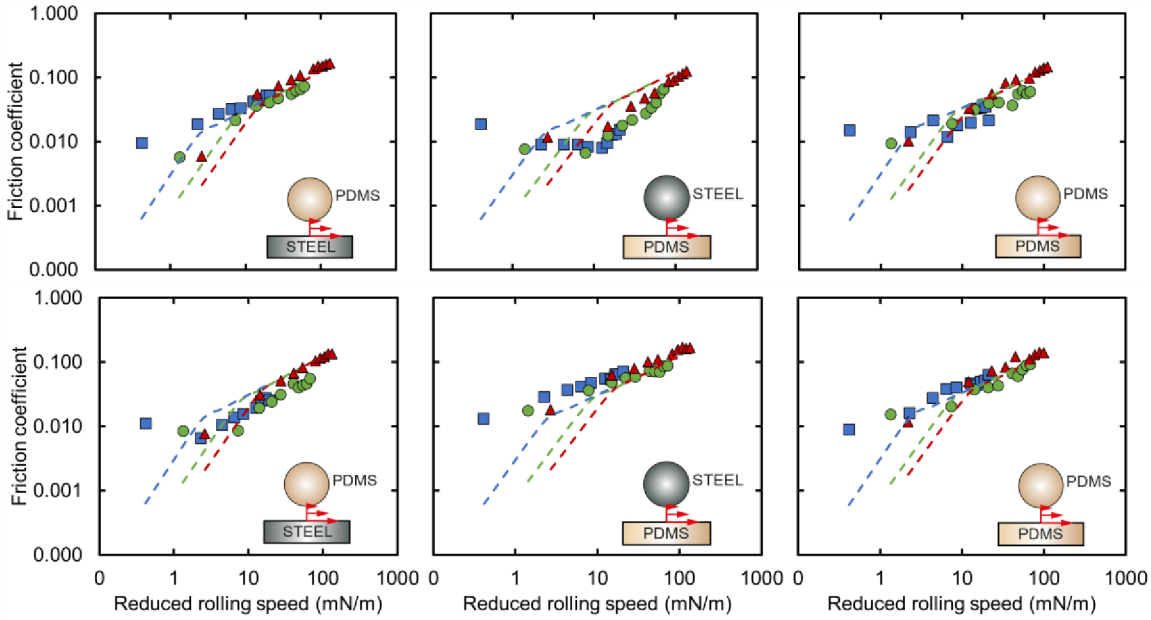

Fig. 5-34 Top row: Friction coefficient plotted as a function of reduced rolling speed in log-log scale with a fixed soft sample speed; Bottom row: Friction coefficient plotted as a function of reduced rolling speed in log-log scale with a fixed opposing sample speed.

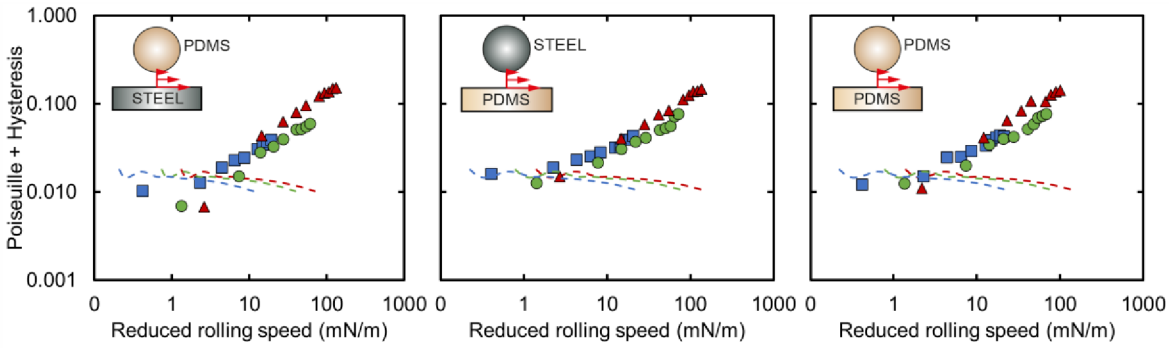

Fig. 5-35 Rolling friction coefficient plotted as a function of reduced rolling speed in log-log scale for all configurations compared with the elastic hysteresis predicted by Persson's theory [24].

5.4 Biological application measurements

The following chapters display the results from the individual measurements made for the three typical biological applications of compliant contacts, which are divided into three subchapters by case studies of eye, artificial knee and fascia, respectively. The experimental conditions were set according to tab.4-7 to suitably mimic real biological conditions.

5.4.1 Eye

The friction coefficient for both glycerol 40% and eye drops at SRR = 200% exhibit nearly identical behaviour, where with increasing sliding speed the friction coefficient decreases to low values. In general, the glycerol solution produces a slightly lower friction coefficient over the whole speed range. The elastic hysteresis does not significantly contribute to the total friction coefficient at low entrainments speeds, however, at higher sliding speeds it can be seen that the elastic hysteresis comes close to the experimental data.

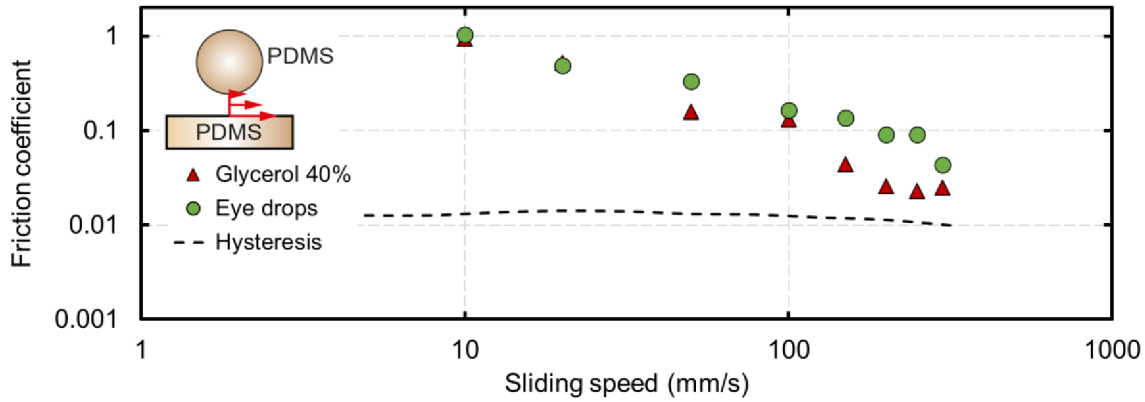

Fig. 5-36 Friction coefficient plotted as a function of log-sliding speed in the case study of the eye lubrication compared with the elastic hysteresis predicted by Persson's theory [24].

5.4.2 Artificial knee

The friction coefficient for all the lubricants is relatively stable throughout the whole entrainment speed spectrum except for the lowest entrainment speed, where a slight growth in friction can be observed. The highest friction coefficient is produced by the synovial fluid, followed by clear water, where these two lubricants are relatively close to each other in terms of friction. The PBS produces the lowest friction coefficient. The SRR was set to 100% as the defined cycle goes through a variety of SRR, this value was chosen based on the most common value.

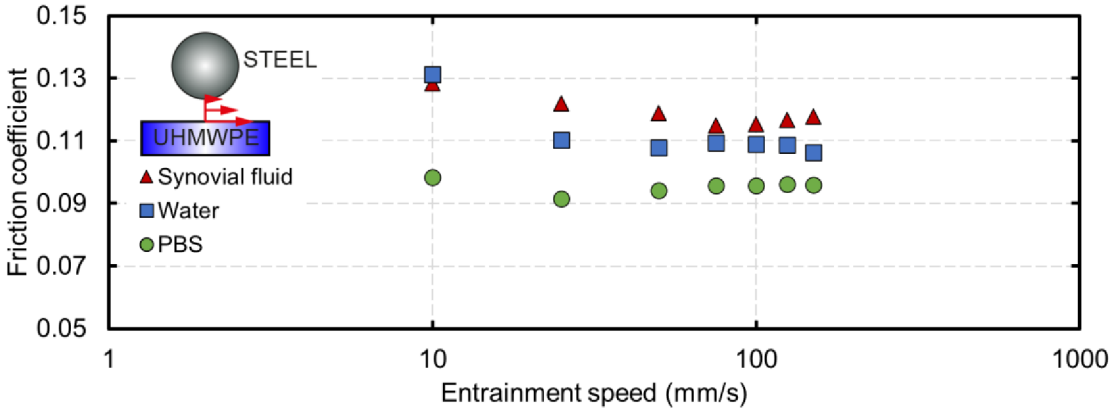

Fig. 5-37 Friction coefficient plotted as a function of log-entrainment speed in the case study of the knee lubrication.

5.4.3 Fascia

The two lubricants exhibited different behaviours as the hyaluronic acid‘s (HA 317) friction coefficient decreases with increasing sliding speed and eventually stables, the lubricant TOTM (Trioctyl trimellitate) produced an increasing friction coefficient with increasing sliding speed. At the lowest sliding speed, HA 317 produces a higher friction coefficient, however, the friction coefficient of HA 317 for the rest of the sliding speeds is lower than the TOTM’s friction coefficient. The dashed line represents the theoretical elastic hysteresis for this configuration. In this case, hysteresis is compared to the whole friction coefficient. It is evident that elastic hysteresis significantly contributes to the total friction measured.

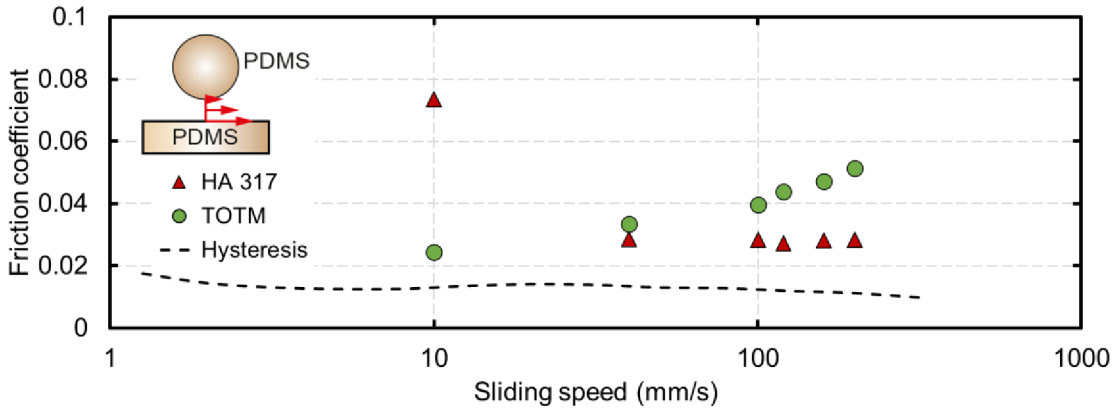

Fig. 5-38 Friction coefficient plotted as a function of log-sliding speed in the case study of the fascia lubrication compared with the elastic hysteresis predicted by Persson’s theory [24].

6 DISCUSSION

6.1 Technical applications

6.1.1 Lubrication regime

Before discussing any effects that were analysed in this work it is appropriate to reflect the lubrication regimes (λ parameter) in which the measurements were operated, which justifies certain considerations about the conditions in the contact.

A typical Stribeck curve begins with a boundary lubrication regime, where the film thickness of the lubricant is not sufficient enough to separate the surfaces of the two bodies in contact and thus, the load is mostly transmitted by the contacts of asperities, which results in a high friction coefficient. As the film thickness increases the surfaces of the contact bodies begin to move apart producing fewer asperity contacts transmitting the load and the portion of the load transmitted by the lubricant film increases. With further increase in film thickness, the surfaces are now separated, meaning that the load is not transmitted only by the fluid film. At this point, a rapid decrease in friction coefficient occurs. This lubrication regime is called elastohydrodynamic lubrication. At this point further increase in film thickness will slowly add to friction, however, now produced by the shear effects of the flowing lubricant in the contact.

According to Sadowski et al. [23] film breakdown occurs at $\lambda \approx 3$ leading to the creation of asperity contacts. However, the work of Selway et al. [21] showed that the static contact angle of the lubricant also contributes to the lubrication of the contact, as a lower static contact angle can enhance lubrication and the lubricant can stay in the contact even at very low speeds. Also, the measured surface roughness of the soft specimens may not remain constant as the bodies are soft and under pressure, the asperities can deform and thus producing different surface roughness [15].

From the shape of the experimental data in fig. 5-19 and 5-33 it is evident that even at the lowest speeds the friction coefficient remains low (0.01-0.04) and with an increase in entrainment speed the friction coefficient increases also, suggesting that the contact is found in the EHL regime from the beginning. In addition, at any moment with decreasing entrainment speed an increase in friction coefficient was not observed, which would indicate a change of the lubrication regime.

The lubrication parameters for the measurements in "Technical applications – Part I and Part II" were investigated using three different theories predicting film thickness: Hamrock-Dowson Central, Minimal [9] and Nijenbanning [33]. The studies of Myant et al. [35, 36] found that the produced film thickness in compliant contact using glycerol was lower compared to the predictions [9]. Also, the author found that the model's dependence on dimensionless speed and load deviated from the observed film thickness.

Fowell et al. [36] compared the theories of Nijenbanning and Hamrock-Dowson to his experimental data, which laid between the two predictions, whereas the work of Nečas et al. [37] showed that the experimental film thickness coincided with Nijenbanning's theory. Marian et al. [38] systematically reviewed available theoretical models for film thickness prediction where also Nijenbanning and Hamrock-Dowson theories were compared using Moes load parameter M and viscosity parameter L. The parameters of the carried out measurements in this work were in the Nijenbanning area displayed in fig.6-1 by a red rectangular. This suggests that the theory of Nijenbanning should predict the film thickness more accurately compared to the Hamrock-Dowson theory in the case of this work.

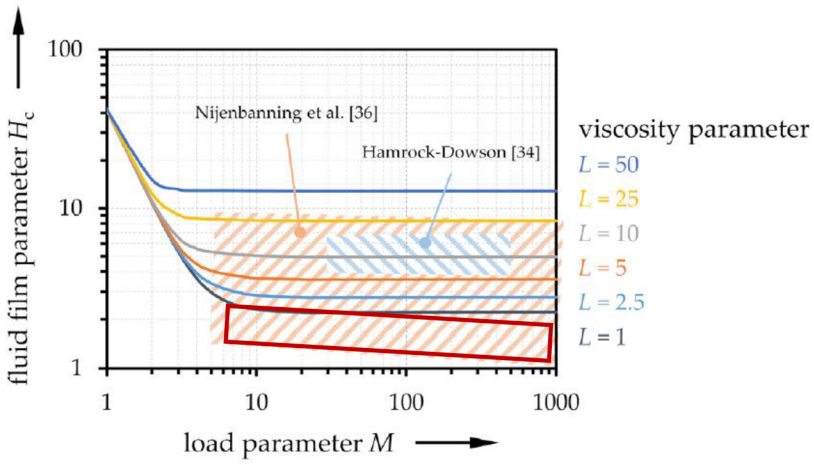

Fig. 6-1 Central lubrication gap vs. load parameter M for different viscosity parameters L displaying the validity regions of Nijenbanning [33] and Hamrock-Dowson [9] equations [38].

The calculated lubrication parameters using the Nijenbanning suggests that in the case of the S/H configuration lubricated by HC32/100 the lubrication parameter at the lowest speed is lower than 3 and according to Sadowski et al. [23] film breakdown should occur at this moment, where this prediction was made using the Hamrock-Dowson central equation. The rest of the entrainment speeds of the measurements should fall into the criteria $\lambda > 3$, meaning that the measurements should be in the EHD and full-film regime solely.

6.1.2 The effects of operating conditions and viscosity

The effects of operating conditions can be assigned to two quantities: entrainment speed and SRR.

The effects of entrainment speed on the measurements from “Technical applications” can be seen in fig. 5-19 and 5-33. For all three configurations, a steady increase in friction coefficient with entrainment speed can be seen for all three used lubricants. The effects of lubricant viscosity can be directly seen in fig. 5-20 and 5-34. Both the growth of the friction coefficient with entrainment speed and lubricant viscosity can be seen in these figures. These findings are consistent with the findings of both experimental studies by Bongaerts et al. [15], de Vicente et al. [16, 17], Myant et al. [18] and Sadowski et al. [23] and numerical studies by Putignano et al. [20, 25], Stupkiewicz et al. [39] and Scaraggi et al. [22].

The effect of the SRR can be also seen in fig. 5-20. The increase in friction coefficient with increasing SRR can be explained by the fact that the sliding speed in the contact increases, which produces more sliding friction (Couette friction component). If the sliding speed were to be zero, so would the Couette friction component. Also, the friction coefficient increases with SRR more rapidly. This can be explained by the fact, that high viscosity lubricants produce a thicker lubricating film which also increases the friction arising from the lubricant flow in the contact, especially the Couette component, which is in agreement with de Vicente et al. [16, 17].

6.1.3 The effect of configuration and viscoelasticity

The effect of configuration can be seen in the top row of fig.6-2 which directly compares different configurations at constant SRR. It is evident that the S/H configuration produces the lowest friction coefficient over the whole speed spectrum, followed by the S/S configuration and the highest friction coefficient is produced by the H/S configuration. Similar behaviour can be also observed in the work of Sadowski et al. [23].

The observed deviation between theory and experimental data described in fig.5-20 was also observed by de Vicente et al. [17] for the H/S configuration. However, it can be seen that this also applies to the S/H and S/S configurations. When the hysteretic effects calculated by Persson's theory [24] are added to the prediction of the de Vicente et al. [16] equation this shows good agreement between the newly obtained theoretical prediction and experimental data. However, the S/S and H/S still seem to produce more rolling friction than that predicted by theory. This suggests that the hysteretic effects of the soft disc specimen produce more hysteresis than the ball specimen, where the same behaviour was observed in fig.5-34 and 5-35 where the change in friction coefficient was most notable in the case of the H/S configuration. This could be a product of the geometry of the disc itself or by the fact that the disc rotates at a significantly lower frequency compared to the ball specimen and thus the ball and disc specimens have different viscoelastic properties at the given moment. This can be also seen in fig. 5-23 where S/S and H/S configurations produce higher friction than predicted. Similar behaviour can be seen in fig. 5-35.

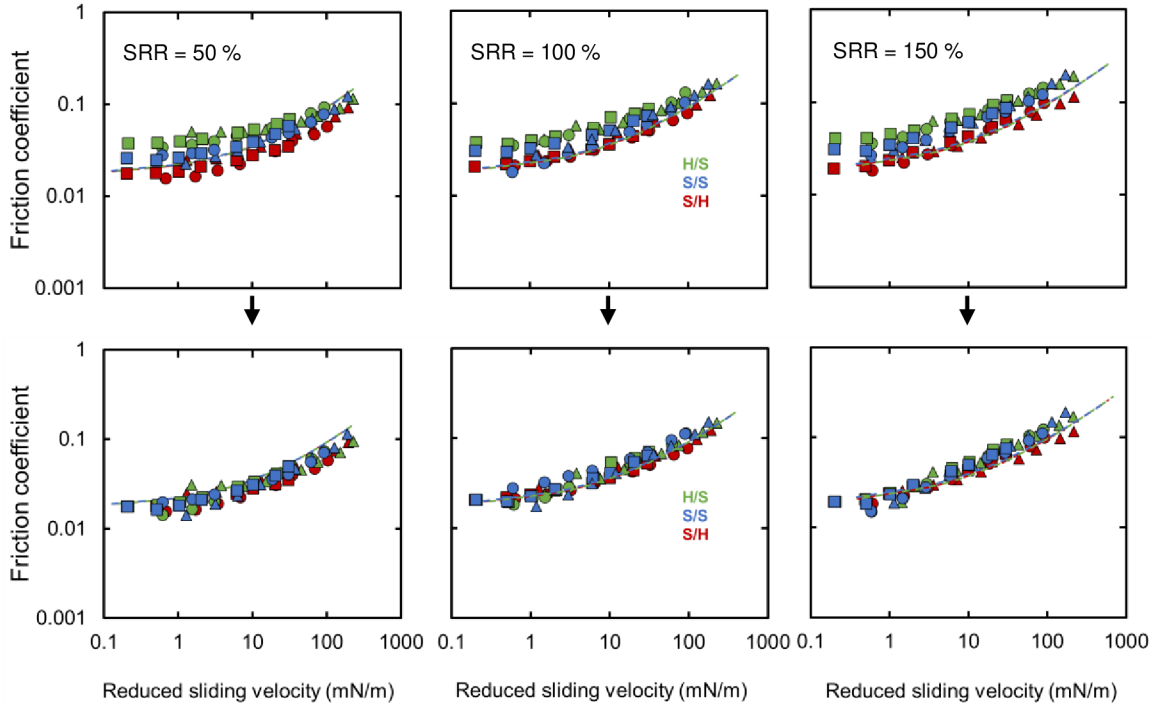

Fig. 6-2 Friction coefficient plotted as a function of reduced sliding speed for different SRR comparing the S/H, H/S and S/S configurations in a single plot; Experimental data are also compared to de Vicente et al. theory [16] with added hysteretic effect calculated by Persson theory [24]; top row displays friction coefficient as measured; bottom row displays friction coefficient shifted to a unified starting point considering the effects of hysteresis.

In the bottom row of fig.6-2, the experimental data of each configuration are shifted to a united "starting point" of the S/H configuration. This is made under the assumption that experimental data are corrected for hysteretic losses using Persson's theory [24] and that the S/H configuration behaves according to the EHL theory [23, 39] and thus was chosen as a "starting point". It was not possible to use the full form of the Persson equation [24] due to an insufficient material description, which will be discussed in chapter 6.3. If this assumption is correct, it is evident that configuration does not affect the shape of the Stribeck curve in the full-film regime and the friction coefficient for all three configurations increases identically, which would be in agreement with the observation made by Sadowski et al. [23].

The effect of the dynamic modulus of the material in the de Vicente et al. regression equation [16] was also analysed, where a static elastic modulus was compared to the dynamic elastic modulus from the DMA analysis. The results in fig.6-3 show that this does not have an effect considering the measured range of the used material on the predicted friction.

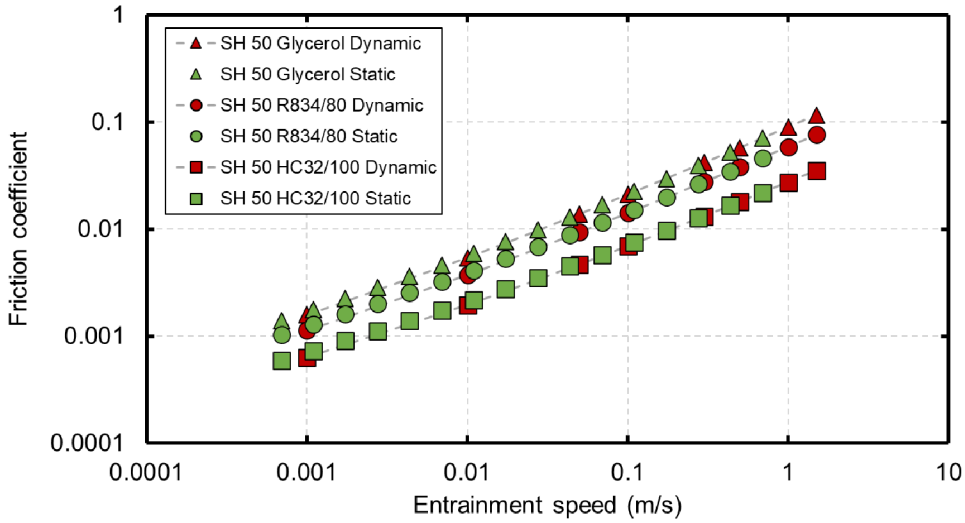

Fig. 6-3 Friction coefficient plotted as a function of entrainment speed predicted by de Vicente et al. [16] theory; Comparison of the use of static and dynamic elastic modulus.

To address the first hypothesis raised in this work, fig. 5-21 displays the rolling friction coefficient as a function of SRR. In general, with an increase in SRR the slope of the rolling friction coefficient becomes steeper, the experimental data of different SRR gradually move away from each other at higher speeds, which is most clearly seen in the S/H configuration and a similar trend can be observed in the H/S and S/S configurations. Nevertheless, the effect of SRR on the rolling friction seems not to be significant in terms of the viscoelastic response, which would noticeably modify the Stribeck curve as in fig.2-5 for example. This is caused by the viscoelastic property of the PDMS samples, as they seem to have a relatively stable dynamic modulus through the measured frequency range. The SRR could have an impact if the samples material would have a significantly changing dynamic modulus in the measured frequency range.

Nevertheless, de Vicente et al. [17] investigated the effect of the SRR on rolling friction using SRR from 10% to 50% and stated that rolling friction is essentially independent of the SRR (fig.6-4). However, the experimental data show that the SRR influences rolling friction for all three configurations for the chosen conditions, which is contrary to the findings of de Vicente et al. [17]

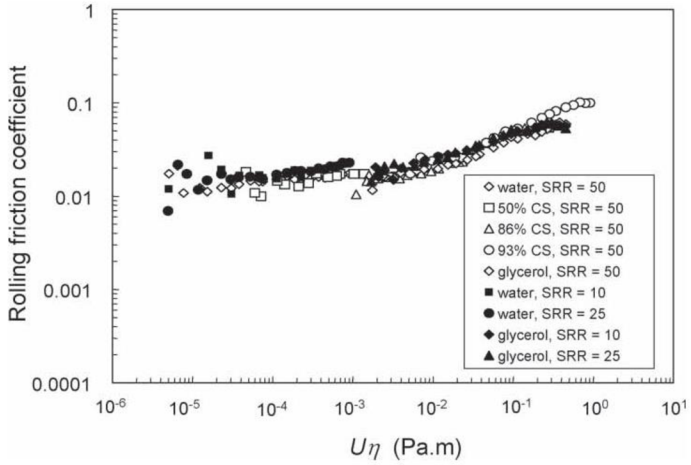

Fig. 6-4 Influence of SRR on rolling friction coefficient by de Vicente et al. [17].

To address the second hypothesis, fig. 5-21, 5-23 and 5-35 suggest that most of the rolling friction in the i-EHL lubrication regime is facilitated by elastic hysteresis as the experimental data at low speeds mostly coincide with the predictions made by Persson's theory [24] for the actual conditions of the measurements. This suggests that modifying the friction coefficient in the EHL regime is possible by tuning the viscoelastic properties of the material or using structured samples, which has been done in the work of Moyle et al. [27].

6.1.4 Experimental vs. Numerical data

From fig. 5-17 and 5-18, it can be seen that the numerical simulation is in good agreement with experimental data. However, the numerical simulation is not capable of including rolling friction at this moment and is going to be further developed. At this point, the effect had to be manually added using the Persson theory [24] as was done in fig.6-2. Despite this fact, the numerical simulation was better at predicting the trend of the friction coefficient evolution with speed, especially for the S/H configuration (fig.6-5). This could be explained by the fact that the numerical simulation uses the actual rheology of the used lubricant. The equation proposed by de Vicente et al. [16] was created using experimental data for the H/S configuration, so the agreement of the proposed theory and experimental data in terms of the friction trend is understandable. Also, for the H/S configuration using glycerol as a lubricant a deviation from the proposed trend by de Vicente et al. [16] can be observed. As the theory uses the Hamrock-Dowson [9] equation for film thickness in its calculations, which was reported by Myant [35, 36] that for glycerol a deviation in film thickness was also observed and the equation had to be modified to better describe the actual film thickness, this may explain the deviations origin. For the lubricants with lower viscosity, the trend seems to comply better with de Vicente's theory [16], where Myant et al. [35] also reported that the film thickness was in good agreement with the theory for lubricants with lower viscosities.

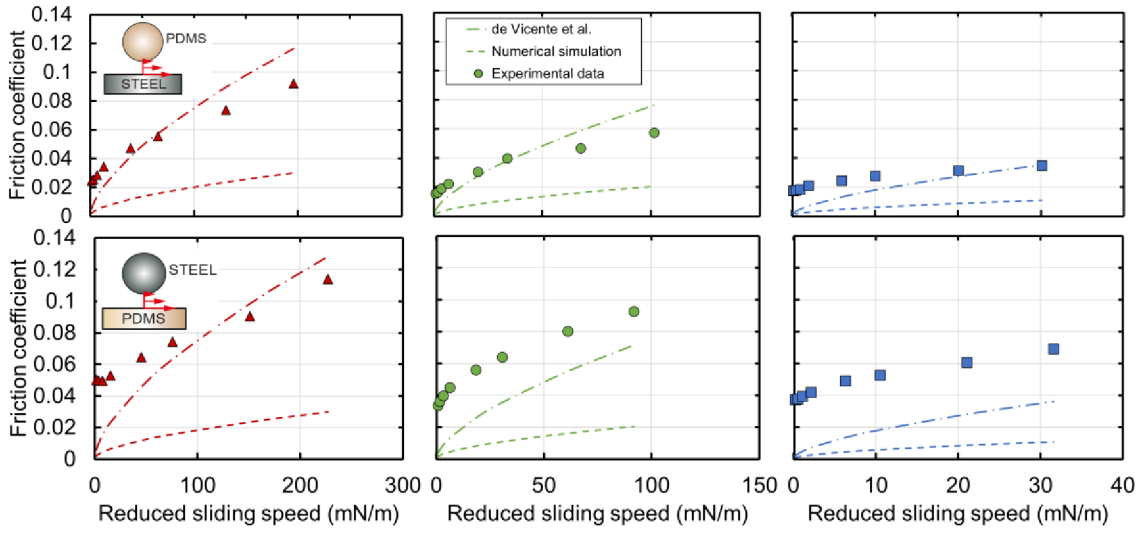

Fig. 6-5 Friction coefficient plotted as a function of reduced sliding speed; Experimental data are compared to both numerical simulation and theory of de Vicente et al. [16].

6.2 Biological applications

Three case studies from the field of compliant contacts in biotribology were conducted to examine the possibility of using non-biological lubricants while preserving the original behaviour and assessing the potential effect of elastic hysteresis.

The first measurement investigated the eye-lid case study comparing commercial eye drops and a glycerol-water solution. Fig. 5-36 shows good agreement between the two used lubricants suggesting that the glycerol-water solution could potentially be used instead of the commercial eye drops which could simplify its investigation concerning both friction and film thickness investigation. Based on the observations from both the literature concerning compliant contacts and their viscoelastic effects and the carried out experiments in the "Technical applications" viscoelastic effects should not be neglected as it has been proven, that the S/S configuration produces a notable amount of hysteresis. If not accounted for, this could lead to a wrong interpretation of data as they would not be corrected for elastic hysteresis.

The next study investigating the artificial knee case study (fig.5-37) does correspond with the observed behaviour in the work of Crockett et al. [42], where model synovial fluid produces the highest friction coefficient followed by water and then PBS producing the lowest friction coefficient. The viscoelastic properties were not available for the used UHMWPE specimen, so an estimation of the elastic hysteresis was done using the experimental data of Blaine [40], where the effect of viscoelasticity corresponds to a value around 0.0034 which can be neglected, suggesting that the viscoelastic effects do not play a significant role in this material pair. Nevertheless, to be precise, the UHMWPE specimen would have to be analysed using DMA to determine its viscoelastic properties and then the exact elastic hysteresis effect.

The last case study investigates friction between fascia. The contact was lubricated by hyaluronic acid solution and TOTM. In fig. 5-38 it is evident that two used lubricant do not correspond with each other. The lubricants should have similar viscosities, however, it seems that the contact pair is sensitive to the viscosity of the lubricant. The shape of the experimental data suggests that the hyaluronic acid solution has a slightly lower viscosity compared to TOTM. Also, non-Newtonian behaviour of the hyaluronic acid might be in play, which could affect the friction coefficient further. As well, the elastic hysteresis is responsible for roughly half of the measured friction coefficient at higher sliding speeds for HA 317 which suggests that at this level the hysteresis should be accounted for when interpreting the experimental data.

6.3 Limitations, measures, and future goals

One of the limitations throughout the measurements was the limited ability of the experimental device concerning the available license, which did not allow the setting of measurements to a bi-directional character, which would contribute to a more accurate description in terms of isolating the rolling and sliding friction components. Nevertheless, despite the limited experimental abilities, the present work went beyond the up-to-date reported studies.

During certain experiments, the temperature did not hold a constant stable value as at higher SRR more heat was generated and thus the temperature rose. This directly affected the viscosity of the lubricant and thus when comparing individual data, especially at the lower end of the speed spectrum could lead to unwanted discrepancies. However, the measuring device is capable of reading the temperature throughout the measurements, so these changes were taken into account while evaluating the experimental data.

Concerning glycerol as a lubricant. An unpleasant property of glycerol is that it binds air moisture, where a slight change in glycerol concentration leads to a sudden change in viscosity. To correct this effect while evaluating the experimental data using glycerol, its refractive index was measured to determine its actual concentration and the laboratory's humidity was measured. This information was then used to specifically determine the glycerol's viscosity and to address this phenomenon.

The measurements of the viscoelastic properties of the PDMS samples were limited to a frequency range to a maximum of 10 Hz, which in terms of measurements conditions does not cover a whole speed range, especially the ball speed range. As mentioned, to describe the viscoelastic properties through a wide frequency range, time-temperature superposition (TTS) can be used. However, to do so, the measurements of the viscoelastic properties (DMA) have to be found in a temperature range between (T_g, T_g+100°C), where T_g of PDMS is around -140°C. The required temperature range could not be reached by the measurement device and thus the TTS could not be applied. If this would've been possible, the viscoelastic properties could've been described through the required frequency range that would cover the experiments and also enable the use of the full equation proposed by Persson [24] which would enable for more precise assessment of the viscoelastic response of each configuration.

During the measurements, some investigated rolling speeds and SRRs destabilized the conditions, where the ball would begin to bounce on the disc and eventually the whole device would begin to resonate. This made it difficult to measure in certain settings which had to be modified. Also, in some instances, the load of 1N proved to be unstable, so in future investigations, there are two paths to solving this problem, where one is the use of a Low-load beam in the MTM device capable of holding lower loads or adjusting the load to a more stable value.

Prediction of film thickness is one of the necessary tools to accurately predict fluid film friction in compliant contacts. Both literature and experimental data found certain disagreements between experimental data and predictions, which origin could be the inaccurately predicted film thickness and thus inaccurately predicted friction. The study of lubrication of soft contacts could shed more light on this problem as soft lubrication is still not completely explored.

Another possibility could lie in further developing numerical simulations which are also a powerful tool capable of predicting both film thickness and friction and in today's world of ever-improving computing.

7 CONCLUSION

This work investigated the effects of viscoelasticity and operating conditions on friction in compliant contacts with emphasis on the effects of configuration and SRR. This choice is based on the analysis of the current literature investigating compliant contacts. To predict fluid friction in compliant contacts, de Vicente et al. [16, 17] proposed a regression equation of sliding and rolling friction based on the experimental data using the hard-on-soft configuration, where the authors stated that SRR does not affect rolling friction, however, the SRR was investigated only up to 50%. Many investigations only used certain configurations and have not assessed the effect of the configuration itself. Sadowski et al. [23] showed that after correcting for the viscoelastic effects the configuration should not affect friction in the full-film regime. Nevertheless, the author's measurements were carried out under pure sliding conditions, and thus no experimental works are directly comparing the effect of configuration under varying sliding-rolling conditions.

The first part of the work's investigation focuses on both the effect of configuration and SRR set to 50%, 100% and 150%. The SRR increased the friction coefficient as one could expect, but the experimental data suggest that the SRR does affect the rolling friction in compliant contacts which is contrary to the current state of knowledge. The obtained experimental data show that configuration affects friction coefficient when not corrected for the elastic hysteresis which may not be accounted for in certain applications. In the case of the work's measurements, the configurations using a soft disc tend to produce higher hysteresis throughout all the SRRs and used lubricants. The effect of configuration has been further analysed in the second part of the measurements which confirmed the described behaviour.

The experimental data have been also used to support the development of a numerical solver of Friedrich-Alexander-University of Erlangen - Nürnberg, Germany, which has shown the potential to be a powerful tool for predicting friction coefficient in compliant contacts.

The last part of the measurements investigated compliant contacts in typical biological applications with attention paid to the possibility of substituting the biological lubricant and the effect of viscoelasticity. For example, the results from the eye case study suggest that for the used conditions the eye drops may be replaced with the glycerol-water solution which would have the potential to simplify future investigations.

To improve friction coefficient prediction in compliant contact further investigation of film thickness and the overall behaviour of the contact could be a possible solution unravelling more information about the contacts nature which could be used in further development of the numerical solver. The problem of the lubricated compliant contact is still relatively unexplored and further investigations may be required.

Let's see what the future holds.

8 BIBLIOGRAPHY

[1] HOLMBERG, K. and A. ERDEMIR. Influence of tribology on global energy consumption, costs and emissions. *Friction*. 2017, 5(3), 263–284. ISSN 22237704.

[2] KWACZ, M. and Z. RYMUZA. Frictional behaviour of miniature journal polymer-on-polymer bearings. *Polymer Tribology*. 2009, 267–311.ISBN 9781848162044

[3] TOLPEKINA, T. V. and B. N.J. PERSSON. Adhesion and friction for three tire tread compounds. *Lubricants*. 2019, 7(3), 1–25. ISSN 20754442.

[4] ALHARBI, K. A. M. Wear and Mechanical Contact Behavior of Polymer Gears. *Journal of Tribology*. 2019, 141(1), 1–10. ISSN 0742-4787.

[5] LICUP, A. J., S. MÜNSTER, A. SHARMA, M. SHEINMAN, L. M. JAWERTH, B. FABRY, D. A. WEITZ a F. C. MACKINTOSH. Stress controls the mechanics of collagen networks. *Proceedings of the National Academy of Sciences of the United States of America*. 2015, 112(31), 9573–9578. ISSN 10916490.

[6] PULT, H., S. G.P. TOSATTI, N. D. SPENCER, J. M. ASFOUR, M. EBENHOCH a P.J. MURPHY. Spontaneous Blinking from a Tribological Viewpoint. *Ocular Surface*. 2015, 13(3), 236–249. ISSN 19375913.

[7] ARSHAD, K.A., J. K. HIRWANI and S. K. SINHA. Effects of UHMWPE Filler on the Tribological and Mechanical Properties of Biocompatible Epoxies. *Tribology Transactions*. 2020, 63(2), 382–392. ISSN 1547397X.

[8] RUS, D. and M. T. TOLLEY. Design, fabrication and control of soft robots. *Nature*. 2015, 521(7553), 467–475. ISSN 14764687.

[9] HAMROCK, B. J. and D. DOWSON. Elastohydrodynamic lubrication of elliptical contacts for materials of low elastic modulus: I-Starved conjunction. *Journal of Tribology*. 1979, 101(1), 92–98. ISSN 15288897.

[10] STACHOWIAK, G. and A. BATCHELOR. *Engineering tribology*. 4th ed. Oxford: Butterworth-Heinemann, 2014. ISBN 978-0-12-397047-3.

[11] MEYERS, M.A. and K.K. CHAWLA. *Mechanical behaviour of materials*. 2nd ed. Cambridge: Cambridge University Press, 2009. ISBN 978-0-511-45557-5.

[12] FRANCK, A. and T.I. GERMANY. Viscoelasticity and dynamic mechanical testing. *TA Instruments*. 1993, 1–7. Available from: http://www.tainstruments.com/pdf/literature/AAN004_Viscoelasticity_and_DMA.pdf

[13] MENARD, K. P and N. MENARD. Dynamic Mechanical Analysis. In: *Encyclopedia of Analytical Chemistry*. Chichester, UK: John Wiley & Sons, Ltd, 2017, s. 1–25. ISBN 9780470027318

[14] WILLIAMS, M. L., R. F. LANDEL and J. D. FERRY. The Temperature Dependence of Relaxation Mechanisms in Amorphous Polymers and Other Glass-forming Liquids. *Journal of the American Chemical Society*. 1955, 77(14), 3701–3707. ISSN 0002-7863.

[15] BONGAERTS, J. H.H., K. FOURTOUNI and J. R. STOKES. Soft-tribology: Lubrication in a compliant PDMS-PDMS contact. *Tribology International*. 2007, 40(10-12), 1531–1542. ISSN 0301679X.

[16] DE VICENTE, J., J. R. STOKES and H. A. SPIKES. The frictional properties of Newtonian fluids in rolling - Sliding soft-EHL contact. *Tribology Letters*. 2005, 20(3-4), 273–286. ISSN 10238883.

[17] DE VICENTE, J., J. R. STOKES and H. A. SPIKES. Rolling and sliding friction in compliant, lubricated contact. *Proceedings of the Institution of Mechanical Engineers, Part J: Journal of Engineering Tribology*. 2006, 220(2), 55–63. ISSN 13506501.

[18] MYANT, C., H. A. SPIKES and J. R. STOKES. Influence of load and elastic properties on the rolling and sliding friction of lubricated compliant contacts. *Tribology International*. 2010, 43(1-2), 55–63. ISSN 0301679X.

[19] GREENWOOD, J. A. and D. TABOR. The friction of hard sliders on lubricated rubber: The importance of deformation losses. *Proceedings of the Physical Society*. 1958, 71(6), 989–1001. ISSN 03701328.

[20] PUTIGNANO, C. and D. DINI. Soft Matter Lubrication: Does Solid Viscoelasticity Matter? *ACS Applied Materials and Interfaces*. 2017, 9(48), 42287–42295. ISSN 19448252.

[21] SELWAY, N., V. CHAN and J. R. STOKES. Influence of fluid viscosity and wetting on multiscale viscoelastic lubrication in soft tribological contacts. *Soft Matter*. 2017, 138), 1702–1715. ISSN 17446848.

[22] SCARAGGI, M. and B. N.J. PERSSON. Theory of viscoelastic lubrication. *Tribology International*. 2014, 72, 118–130. ISSN 0301679X.

[23] SADOWSKI, P. and S. STUPKIEWICZ. Friction in lubricated soft-on-hard, hard-on-soft and soft-on-soft sliding contacts. *Tribology International*. 2019, 129, 246–256. ISSN 0301679X.

[24] PERSSON, B. N.J. Rolling friction for hard cylinder and sphere on viscoelastic solid. *European Physical Journal E*. 2010, 33(4), 327–333. ISSN 1292895X.

[25] PUTIGNANO, C. Soft lubrication: A generalized numerical methodology. *Journal of the Mechanics and Physics of Solids*. 2020, 134, 1-12. ISSN 00225096.

[26] KIM, A. R., A. CHOLEWINSKI, S. K. MITRA and B. ZHAO. Viscoelastic tribopairs in dry and lubricated sliding friction. *Soft Matter*. 2020, 16(32), 7447–7457. ISSN 17446848.

[27] MOYLE, N., H. WU, C. KHRIPIN, F. BREMOND, C. Y. HUI and A. JAGOTA. Enhancement of elastohydrodynamic friction by elastic hysteresis in a periodic structure. *Soft Matter*. 2020, 16(6), 1627–1635. ISSN 17446848.

[28] MASEN, M. and P. M.E. CANN. Friction Measurements with Molten Chocolate. *Tribology Letters*. 2018, 66(1), 1–13. ISSN 10238883.

[29] URUEÑA VARGAS, J. M. . *POLYMER FLUCTUATION LUBRICATION MECHANISMS IN GEMINI HYDROGELS*. Florida, 2014. Dissertation. UNIVERSITY OF FLORIDA. Available from: https://ufdcimages.uflib.ufl.edu/UF/E0/04/75/44/00001/URUENA_J.pdf.

[30] MURAKAMI, T., H. HIGAKI, Y. SAWAE, N. OHTSUKI, S. MORIYAMA and Y. NAKANISHI. Adaptive multimode lubrication in natural synovial joints and artificial joints. *Proceedings of the Institution of Mechanical Engineers, Part H: Journal of Engineering in Medicine*. 1998, 212(1), 23–35. ISSN 09544119.

[31] JAHN, S. and J. KLEIN. Lubrication of articular cartilage. *Physics Today*. 2018, 71(4), 48–54. ISSN 00319228.

[32] HILŠER, P., A. SUCHÁNKOVÁ, K. MENDOVÁ, K. E. FILIPIČ, M. DANIEL and M. VRBKA. A new insight into more effective viscosupplementation based on the synergy of hyaluronic acid and phospholipids for cartilage friction reduction. *Biotribology*. 2021, 25(1). 1-11. ISSN 23525738.

[33] NIJENBANNING, G, C.H. VENNER and H MOES. Film thickness in elastohydrodynamically lubricated elliptic contacts. *Wear*. 1994, 176(2), 217–229. ISSN 00431648.

[34] MARIAN, M., C. ORGELDINGER, B. ROTHAMMER, D. NEČAS, M. VRBKA, I. KŘUPKA, M. HARTL, M. A. WIMMER, S. TREMMEL and S. WARTZACK. Towards the understanding of lubrication mechanisms in total knee replacements – Part II: Numerical modelling. *Tribology International*. 2021, 156(9). 1-12.ISSN 0301679X.

[35] MYANT, C., T. REDDYHOFF and H. A. SPIKES. Laser-induced fluorescence for film thickness mapping in pure sliding lubricated, compliant, contacts. *Tribology International*. 2010, 43(11), 1960–1969. ISSN 0301679X.

[36] MYANT, C., M. FOWELL, H. A. SPIKES and J. R. STOKES. An investigation of lubricant film thickness in sliding compliant contacts. *Tribology Transactions*. 2010, 53(5), 684–694. ISSN 10402004.

[37] NEČAS, D., T. JAROS, K. DOČKAL, P. SPERKA, M. VRBKA, I. KRUPKA and M. HARTL. The effect of kinematic conditions on film thickness in compliant lubricated contact. *Journal of Tribology*. 2018, 140(5), 1–8. ISSN 15288897.

[38] MARIAN, M., M. BARTZ, S. WARTZACK and A. ROSENKRANZ. Non-dimensional groups, film thickness equations and correction factors for elastohydrodynamic lubrication: A review. *Lubricants*. 2020, 8(10), 1–20. ISSN 20754442.

[39] STUPKIEWICZ, S., J. LENGIEWICZ, P. SADOWSKI and S. KUCHARSKI. Finite deformation effects in soft elastohydrodynamic lubrication problems. *Tribology International*. 2016, 93, 511–522. ISSN 0301679X.

[40] BLAINE, R. Dynamic mechanical properties of an ultra high molecular weight polyethylene reference material SRM 8456. *Journal of Thermal Analysis and Calorimetry*. 2012, 109(3), 1111–1115. ISSN 1388-6150.

[41] *Dynamic Mechanical Analysis* [online]. [cit. 2021-5-20]. Available from: https://polymerdatabase.com/polymer physics/DMA.html

[42] CROCKETT, R., ROBA, M. and M. NAKA et al.. *Journal of Biomedical Materials Research - Part A*. 2009, 89(4), 1011-1018. ISSN 15493296

9 LIST OF ABBREVIATIONS, SYMBOLS AND QUANTITIES USED

9.1 Abbreviations

DMA	Dynamic mechanical analysis
i-EHL	Isoviscous elastohydrodynamic lubrication
MTM	Mini traction machine
PDMS	Polydimethylsiloxane
PEEK	Polyetheretherketon
PMMA	Polymethylmethacrylate
PVA	Polyvinyl alcohol
SFB	Dynamic viscosity
SRR	Slide-to-roll ratio
TOTM	Trioctyl Trimellitate
TPPS	Two-phase periodic structure
TTS	Time-temperature superposition
UHMWPE	Ultra-high-molecular-weight polyethylene
UMT2	Universal macro-tribometer
VEHL	Visco-elastohydrodynamic lubrication

9.2 Physical quantities

δ	Phase difference angle
$E(\omega)$	Dynamic modulus
E', E''	Storage, Loss modulus
E_0	Low-frequency modulus
E_{red}	Reduced elastic modulus
E', E''	Phase difference angle
$F_{E,Fluid}$	Friction force from fluid
η	Dynamic viscosity
f	Frequency
G_E, G_V	Dimensionless elastic parameter, Dimensionless viscosity parameter
h	Film thickness
h_c, h_{min}	Hamrock-Dowson Central film thickness, Hamrock-Dowson Minimal film thickness
h_{nij}	Nijenbanning film thickness
k	Ellipticity parameter
λ	Lubrication parameter
p_a	Average contact pressure
$R_{a,ball}, R_{a,disc}$	Ball, Disc surface roughness
R'_x	Reduced radius of curvature
SRR	Slide-to-roll ratio
$tan(\delta)$	Proportion between loss and storage moduli
τ_{zi}	Slide-to-roll ratio
u	Entrainment (rolling) speed
u_b	Ball speed
u_d	Disc speed

$\overline{U}$	Dimensionless speed
$\mu_{Couette}$	Couette (Sliding) friction component
μ_{Hyst}	Hysteretic friction component
$\mu_{Poiseuille}$	Poiseuille (Rolling) friction component
w	Normal load
$\overline{W}$	Dimensionless load

10 LIST OF FIGURES AND GRAPHS

11 LIST OF TABLES

12 LIST OF ATTACHMENTS

1) Nijenbanning film thickness equation parameters

2) Lambda parameters – Technical applications – Part I

3) Lambda parameters – Technical applications – Part II

13 ATTACHMENTS

13.1 Nijenbanning film thickness equation parameters

This chapter supplements the parameters used in the Nijenbanning [33] film thickness equation (eq.8).

13.1.1 Moes parameters

$$M = \frac{F}{E_{red} R'^{2}_{x}} \left(\frac{\eta_0 u}{E_{red} R'_x} \right)^{-3/4}$$

$$L = \alpha E_{red} \left(\frac{\eta_0 u}{E_{red} R'_x} \right)^{1/4}$$

13.1.2 Film thickness parameters

$$D = {R'_x}/{R'_y}$$

Rigid isoviscous

$$C_c^{RI} = 145(1 + 0.796 D^{14/15})^{-15/7}$$

$$\bar{h}_{RIc} = C_c^{RI}(D) M^{-2}$$

Elastic isoviscous

$$C_c^{EI} = 3.18(1 + 0.006\, lnD + 0.63 D^{4/7})^{-14/25} D^{-1/15}$$

$$\bar{h}_{EIc} = C_c^{EL}(D) M^{-2/15}$$

Rigid piezoviscous

$$C_c^{RP} = 1.29(1 + 0.691 D)^{-2/3}$$

$$\bar{h}_{RPc} = C_c^{RP}(D) L^{2/3}$$

Elastic piezoviscous

$$C_c^{EP} = 1.48(1 + 0.006 lnD + 0.63 D^{4/7})^{-7/20} D^{-1/24}$$

$$\bar{h}_{EPc} = C_c^{EP}(D) M^{-1/12} L^{3/4}$$

Additional parameters for smooth transitions

$$s = 1.5\left[1 + exp\left(-1.2\frac{\bar{h}_{EIc}}{\bar{h}_{RIc}}\right)\right]$$

$$\bar{h}_{\infty} = 1.8D^{-1}$$

13.2 Lambda parameters - Technical applications – Part I

Nijenbanning, Hamrock Dowson Central and Hamrock Dowson Minimum equations were used to determine the lubrication parameter λ.

13.2.1 Lambda calculated by Nijenbanning equation

SRR 50%

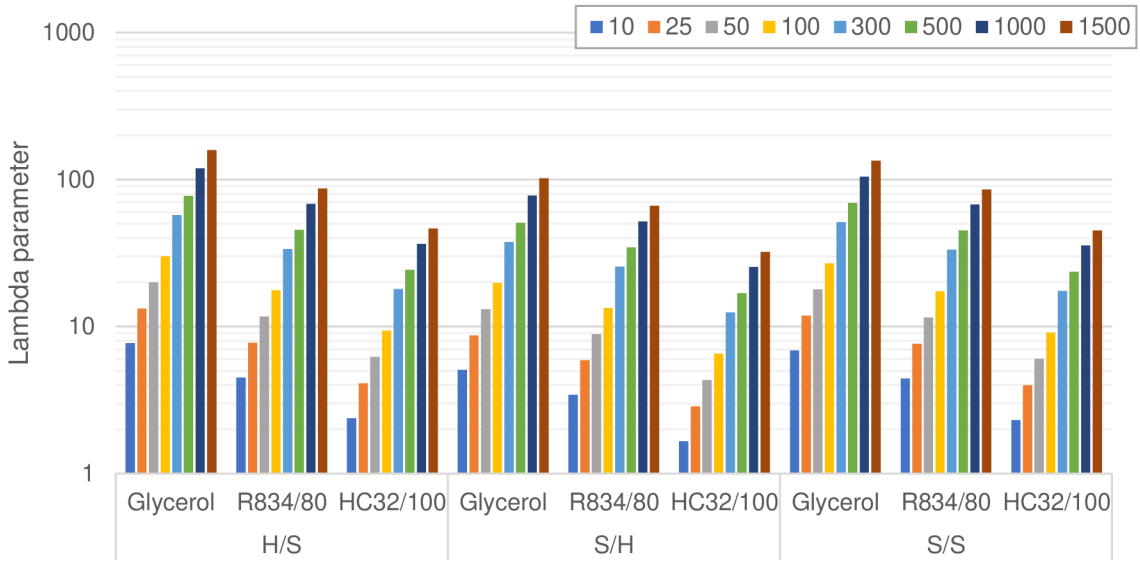

Fig. 13-1 Lambda parameters plotted for different configurations and lubricants at different speeds for SRR = 50 % using Nijenbanning equation.

Tab. 13-1 Lambda parameters determined by Nijenbanning equation for film thickness for SRR = 50%.

Configuration	**Lubricant**	**Entrainment speed** mm/s							
		10	25	50	100	300	500	1000	1500
H/S	Glycerol	7.71	13.29	20.01	30.09	57.33	77.57	119.24	158.40
	R834/80	4.50	7.76	11.71	17.65	33.69	45.46	68.34	87.09
	HC32/100	2.38	4.11	6.22	9.39	17.99	24.31	36.53	46.34
S/H	Glycerol	5.07	8.73	13.15	19.78	37.68	50.92	77.70	101.92
	R834/80	3.42	5.90	8.90	13.41	25.60	34.54	51.96	66.33
	HC32/100	1.66	2.86	4.32	6.53	12.51	16.91	25.42	32.24
S/S	Glycerol	6.88	11.87	17.89	26.94	51.37	69.32	104.59	134.40
	R834/80	4.43	7.65	11.56	17.43	33.32	44.98	67.53	85.76
	HC32/100	2.31	3.99	6.03	9.10	17.47	23.62	35.53	45.08

SRR 100%

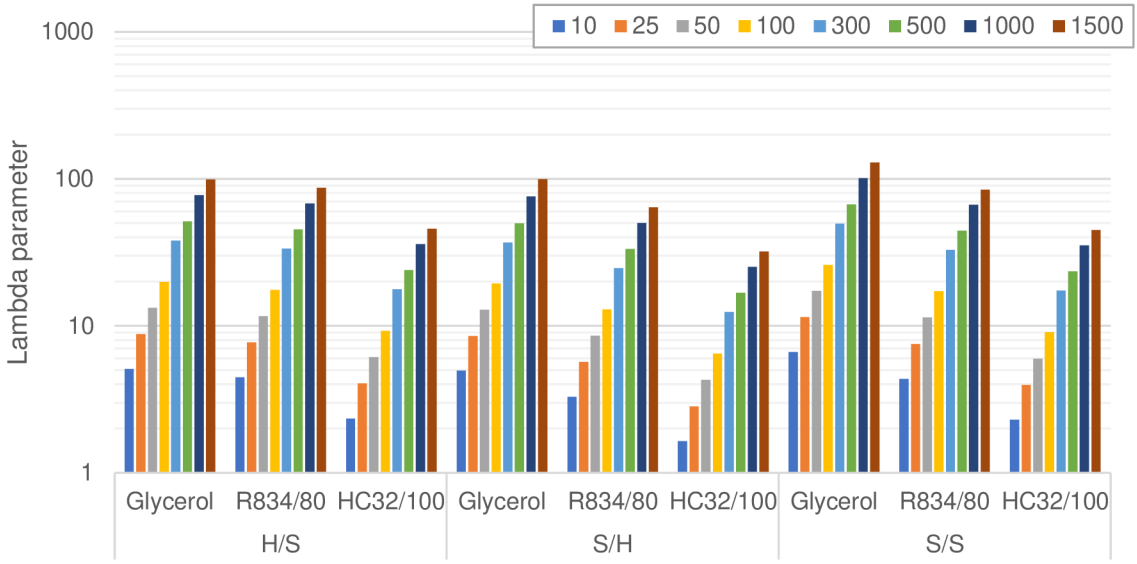

Fig. 13-2 Lambda parameters plotted for different configurations and lubricants at different speeds for SRR = 100 % using Nijenbanning equation.

Tab. 13-2 Lambda parameters determined by Nijenbanning equation for film thickness for SRR = 100%.

Configuration	**Lubricant**	**Entrainment speed** mm/s							
		10	25	50	100	300	500	1000	1500
H/S	Glycerol	5.09	8.77	13.23	19.93	38.03	51.31	77.26	98.84
	R834/80	4.48	7.72	11.65	17.56	33.53	45.24	68.00	86.65
	HC32/100	2.35	4.05	6.13	9.25	17.73	23.97	36.02	45.68
S/H	Glycerol	4.96	8.55	12.88	19.37	36.92	49.87	75.99	99.42
	R834/80	3.30	5.69	8.59	12.94	24.70	33.33	50.11	63.90
	HC32/100	1.64	2.84	4.29	6.47	12.40	16.76	25.20	31.96
S/S	Glycerol	6.64	11.44	17.26	25.99	49.56	66.87	100.80	129.29
	R834/80	4.37	7.54	11.39	17.17	32.83	44.32	66.55	84.50
	HC32/100	2.29	3.96	5.99	9.04	17.35	23.47	35.29	44.78

SRR 150%

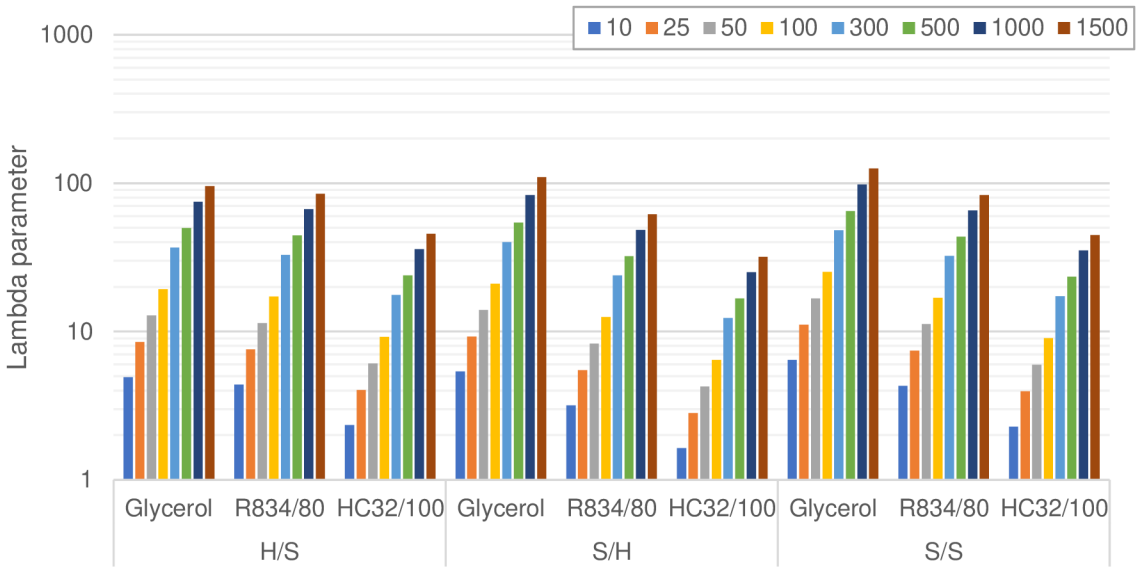

Fig. 13-3 Lambda parameters plotted for different configurations and lubricants at different speeds for SRR = 150 % using Nijenbanning equation.

Tab. 13-3 Lambda parameters determined by Nijenbanning equation for film thickness for SRR = 150%.

Configuration	**Lubricant**	**Entrainment speed** mm/s							
		10	25	50	100	300	500	1000	1500
H/S	Glycerol	4.92	8.49	12.81	19.30	36.83	49.69	74.77	95.55
	R834/80	4.39	7.57	11.42	17.21	32.87	44.36	66.66	84.90
	HC32/100	2.34	4.04	6.11	9.22	17.68	23.90	35.91	45.55
S/H	Glycerol	5.38	9.27	13.96	21.00	40.01	54.10	82.96	109.75
	R834/80	3.19	5.50	8.30	12.51	23.89	32.24	48.46	61.74
	HC32/100	1.63	2.82	4.26	6.44	12.34	16.68	25.08	31.81
S/S	Glycerol	6.43	11.10	16.74	25.21	48.08	64.87	97.72	125.16
	R834/80	4.30	7.43	11.21	16.91	32.34	43.66	65.55	83.22
	HC32/100	2.28	3.95	5.97	9.02	17.31	23.41	35.21	44.67

13.2.2 Lambda calculated by Hamrock Dowson Central equation

SRR 50%

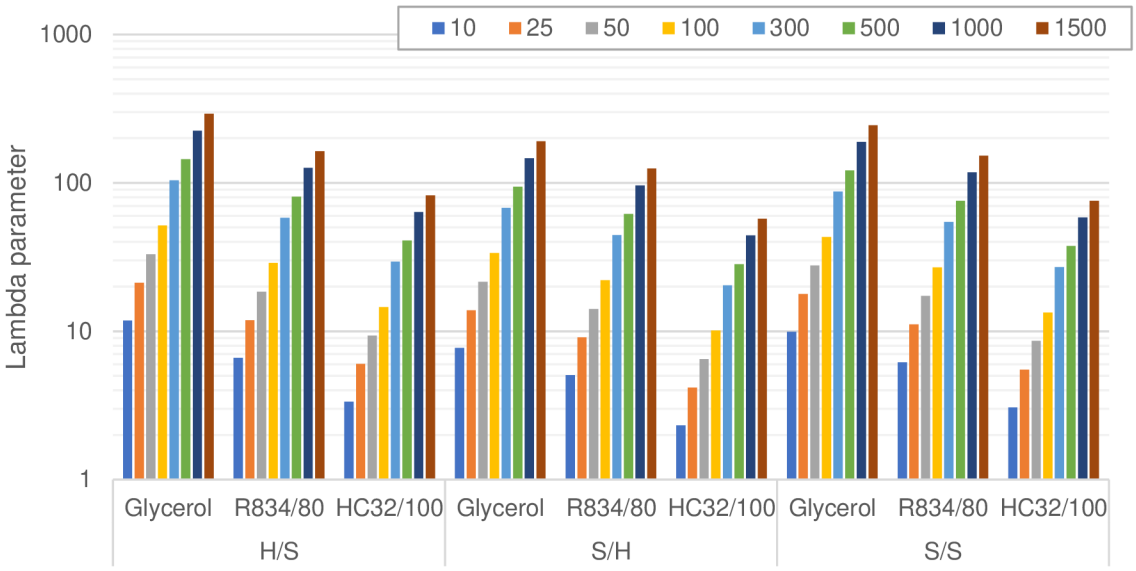

Fig. 13-4 Lambda parameters plotted for different configurations and lubricants at different speeds for SRR = 50% using Hamrock Dowson Central equation.

Tab. 13-4 Lambda parameters determined by Hamrock Dowson Central equation for film thickness for SRR = 50%.

Configuration	**Lubricant**	**Entrainment speed** mm/s							
		10	25	50	100	300	500	1000	1500
H/S	Glycerol	11.81	21.22	33.07	51.53	104.10	144.36	224.96	291.61
	R834/80	6.61	11.88	18.51	28.85	58.28	80.82	125.94	163.25
	HC32/100	3.34	6.00	9.36	14.58	29.45	40.84	63.65	82.50
S/H	Glycerol	7.70	13.84	21.57	33.61	67.90	94.15	146.72	190.19
	R834/80	5.05	9.08	14.14	22.04	44.53	61.74	96.22	124.72
	HC32/100	2.32	4.17	6.49	10.12	20.44	28.35	44.17	57.26
S/S	Glycerol	9.91	17.81	27.75	43.25	87.37	121.15	188.80	244.74
	R834/80	6.18	11.11	17.31	26.98	54.49	75.57	117.76	152.65
	HC32/100	3.07	5.51	8.59	13.39	27.04	37.50	58.43	75.74

SRR 100%

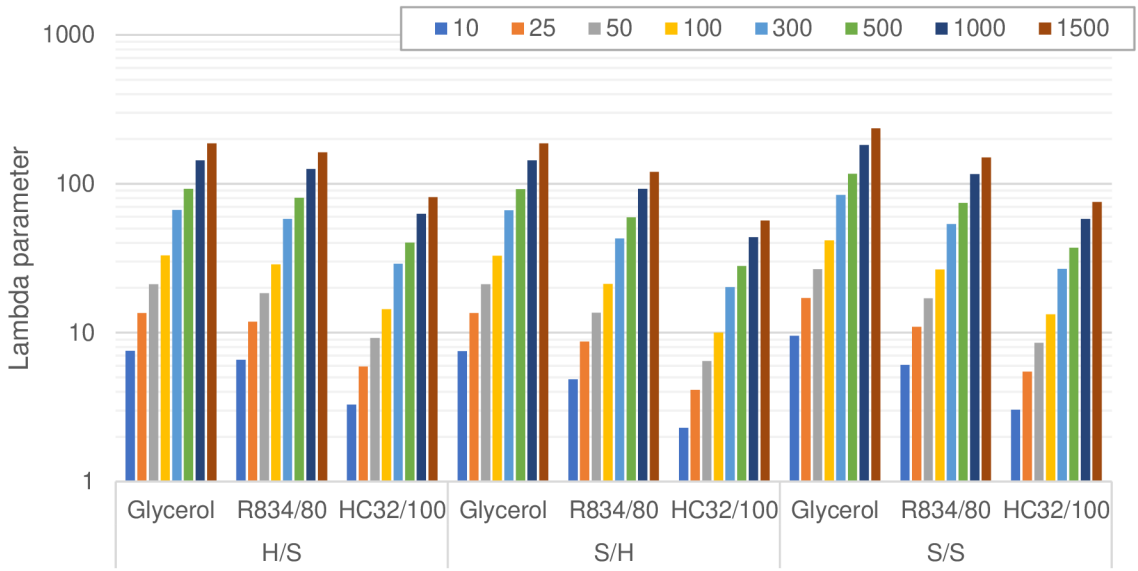

Fig. 13-5 Lambda parameters plotted for different configurations and lubricants at different speeds for SRR = 100% using Hamrock Dowson Central equation.

Tab. 13-5 Lambda parameters determined by Hamrock Dowson Central equation for film thickness for SRR = 100%.

Configuration	**Lubricant**	**Entrainment speed** mm/s							
		10	25	50	100	300	500	1000	1500
H/S	Glycerol	7.54	13.56	21.13	32.93	66.52	92.24	143.75	186.33
	R834/80	6.57	11.82	18.42	28.70	57.97	80.39	125.28	162.40
	HC32/100	3.29	5.91	9.21	14.36	29.00	40.22	62.67	81.24
S/H	Glycerol	7.53	13.53	21.09	32.87	66.39	92.06	143.46	185.97
	R834/80	4.86	8.73	13.60	21.20	42.82	59.38	92.53	119.94
	HC32/100	2.30	4.13	6.43	10.02	20.24	28.07	43.75	56.71
S/S	Glycerol	9.53	17.13	26.69	41.59	84.02	116.51	181.56	235.35
	R834/80	6.08	10.93	17.04	26.55	53.62	74.36	115.88	150.21
	HC32/100	3.04	5.47	8.53	13.29	26.85	37.23	58.01	75.20

SRR 150%

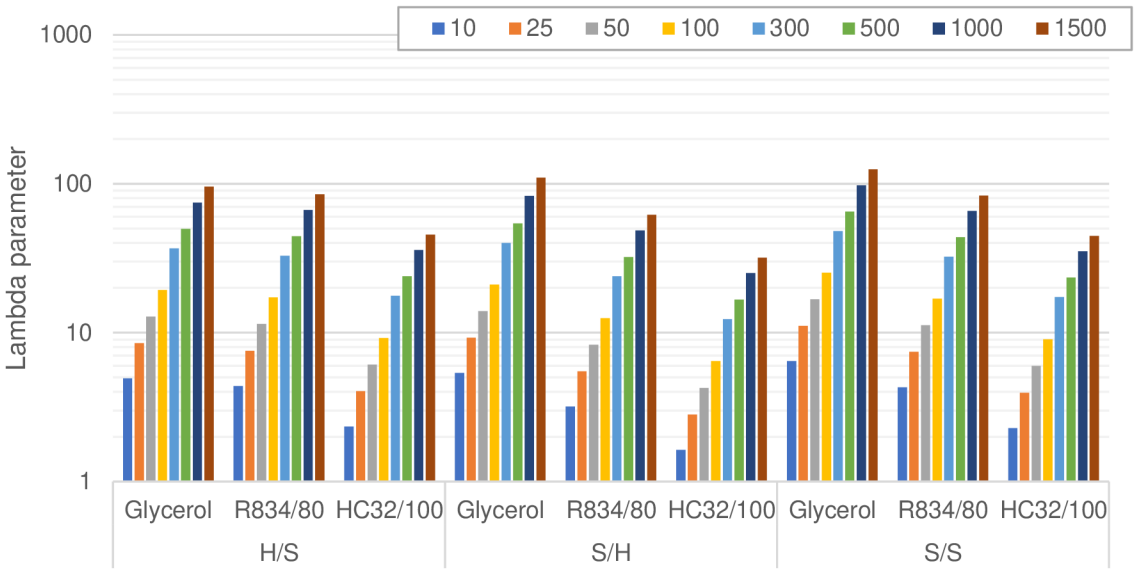

Fig. 13-6 Lambda parameters plotted for different configurations and lubricants at different speeds for SRR = 150% using Hamrock Dowson Central equation

Tab. 13-6 Lambda parameters determined by Hamrock Dowson Central equation for film thickness for SRR = 150%.

Configuration	**Lubricant**	**Entrainment speed** mm/s							
		10	25	50	100	300	500	1000	1500
H/S	Glycerol	4.92	8.49	12.81	19.30	36.83	49.69	74.77	95.55
	R834/80	4.39	7.57	11.42	17.21	32.87	44.36	66.66	84.90
	HC32/100	2.34	4.04	6.11	9.22	17.68	23.90	35.91	45.55
S/H	Glycerol	5.38	9.27	13.96	21.00	40.01	54.10	82.96	109.75
	R834/80	3.19	5.50	8.30	12.51	23.89	32.24	48.46	61.74
	HC32/100	1.63	2.82	4.26	6.44	12.34	16.68	25.08	31.81
S/S	Glycerol	6.43	11.10	16.74	25.21	48.08	64.87	97.72	125.16
	R834/80	4.30	7.43	11.21	16.91	32.34	43.66	65.55	83.22
	HC32/100	2.28	3.95	5.97	9.02	17.31	23.41	35.21	44.67

13.2.3 Lambda calculated by Hamrock Dowson Minimum equation

SRR 50%

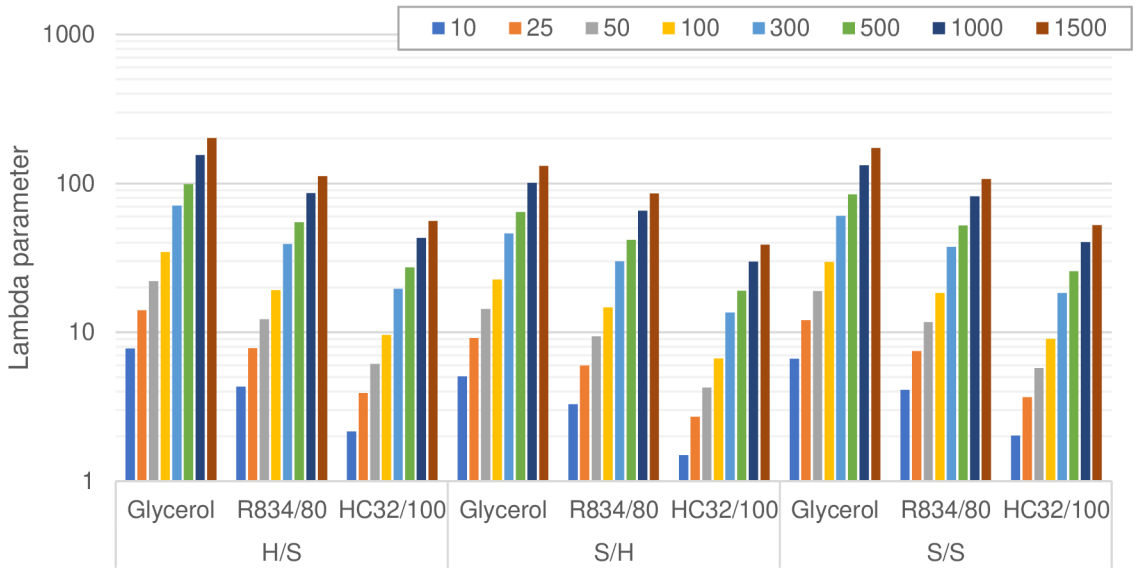

Fig. 13-7 Lambda parameters plotted for different configurations and lubricants at different speeds for SRR = 50% using Hamrock Dowson Minimum equation.

Tab. 13-7 Lambda parameters determined by Hamrock Dowson Minimum equation for film thickness for SRR = 50%.

Configuration	**Lubricant**	**Entrainment speed** mm/s							
		10	25	50	100	300	500	1000	1500
H/S	Glycerol	7.76	14.07	22.08	34.65	70.77	98.63	154.77	201.45
	R834/80	4.30	7.81	12.25	19.22	39.26	54.72	85.87	111.76
	HC32/100	2.15	3.90	6.13	9.61	19.63	27.36	42.93	55.88
S/H	Glycerol	5.05	9.16	14.38	22.57	46.09	64.24	100.80	131.20
	R834/80	3.29	5.97	9.37	14.70	30.03	41.85	65.67	85.47
	HC32/100	1.49	2.71	4.25	6.67	13.62	18.98	29.78	38.77
S/S	Glycerol	6.64	12.05	18.91	29.67	60.60	84.47	132.55	172.52
	R834/80	4.11	7.46	11.71	18.37	37.52	52.30	82.06	106.81
	HC32/100	2.02	3.66	5.75	9.02	18.42	25.67	40.28	52.42

SRR 100%

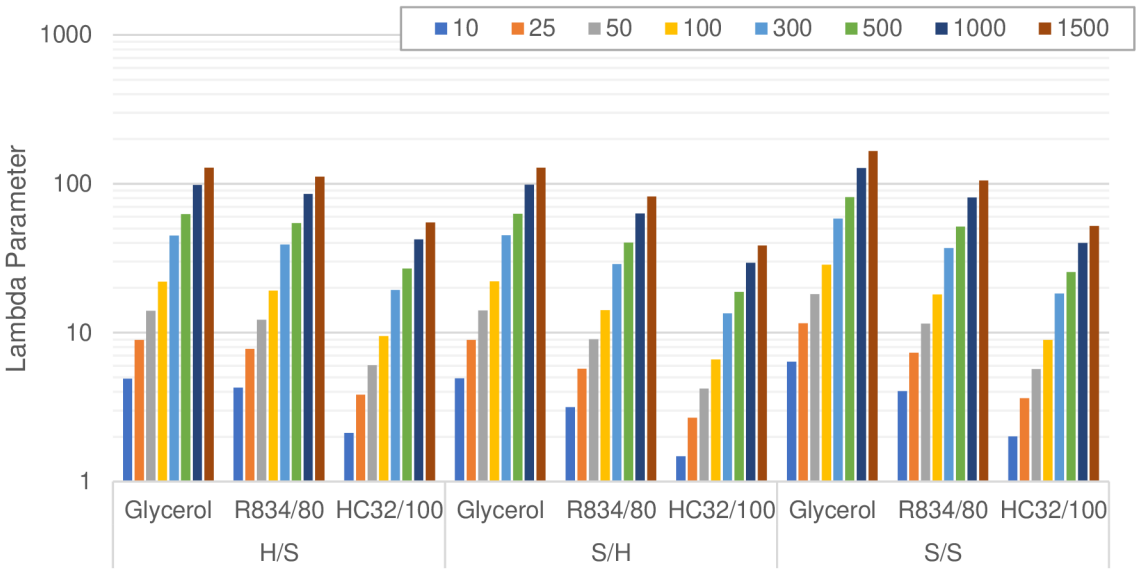

Fig. 13-8 Lambda parameters plotted for different configurations and lubricants at different speeds for SRR = 100% using Hamrock Dowson Minimum equation.

Tab. 13-8 Lambda parameters determined by Hamrock Dowson Minimum equation for film thickness for SRR = 100%.

Configuration	**Lubricant**	**Entrainment speed** mm/s							
		10	25	50	100	300	500	1000	1500
H/S	Glycerol	4.92	8.93	14.01	21.99	44.90	62.59	98.21	127.82
	R834/80	4.28	7.77	12.19	19.12	39.05	54.43	85.41	111.16
	HC32/100	2.12	3.84	6.03	9.46	19.33	26.94	42.27	55.01
S/H	Glycerol	4.94	8.96	14.06	22.06	45.05	62.79	98.53	128.24
	R834/80	3.16	5.74	9.00	14.13	28.86	40.22	63.11	82.14
	HC32/100	1.48	2.68	4.21	6.60	13.48	18.80	29.49	38.39
S/S	Glycerol	6.38	11.58	18.17	28.52	58.24	81.18	127.39	165.80
	R834/80	4.05	7.34	11.52	18.07	36.91	51.45	80.74	105.08
	HC32/100	2.00	3.64	5.70	8.95	18.28	25.48	39.98	52.04

SRR 150%

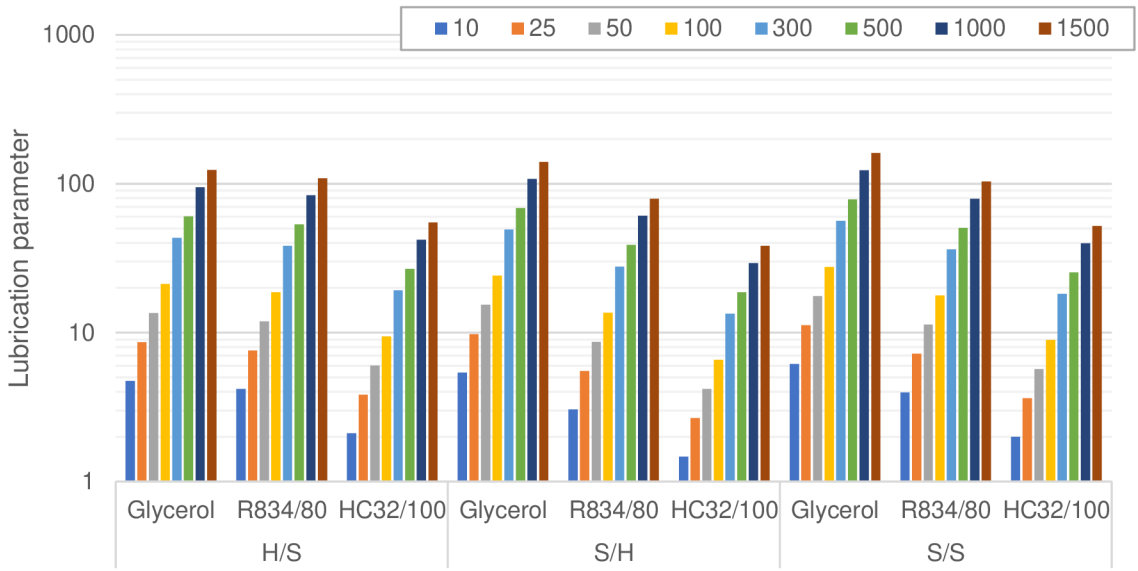

Fig. 13-9 Lambda parameters plotted for different configurations and lubricants at different speeds for SRR = 150% using Hamrock Dowson Minimum equation.

Tab. 13-9 Lambda parameters determined by Hamrock Dowson Minimum equation for film thickness for SRR = 150%.

Configuration	**Lubricant**	**Entrainment speed** mm/s							
		10	25	50	100	300	500	1000	1500
H/S	Glycerol	4.75	8.62	13.52	21.22	43.33	60.40	94.77	123.35
	R834/80	4.19	7.60	11.92	18.71	38.21	53.25	83.56	108.76
	HC32/100	2.11	3.83	6.01	9.43	19.26	26.85	42.13	54.84
S/H	Glycerol	5.40	9.79	15.37	24.11	49.24	68.64	107.70	140.18
	R834/80	3.05	5.53	8.68	13.62	27.81	38.77	60.83	79.17
	HC32/100	1.47	2.67	4.19	6.57	13.41	18.70	29.34	38.18
S/S	Glycerol	6.17	11.20	17.57	27.58	56.32	78.50	123.17	160.32
	R834/80	3.98	7.22	11.33	17.77	36.30	50.60	79.40	103.34
	HC32/100	2.00	3.63	5.69	8.93	18.23	25.41	39.87	51.90

13.3 Lambda parameters - Technical applications – Part II

Nijenbanning, Hamrock Dowson Central and Hamrock Dowson Minimum equations were used to determine the lubrication parameter λ.

13.3.1 Lambda calculated by Nijenbanning equation

Fixed ball speed

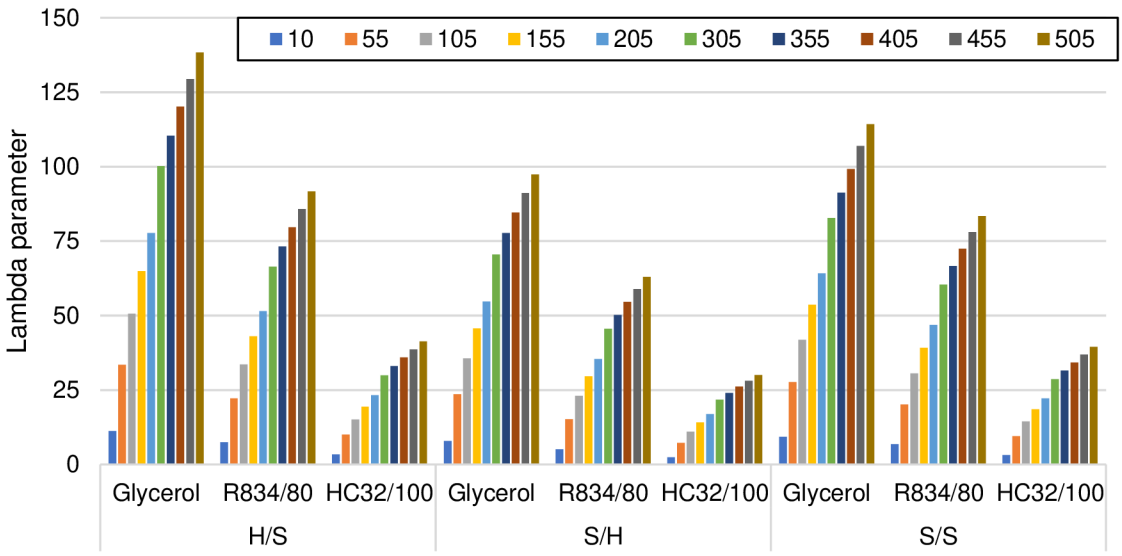

Fig. 13-10 Lambda parameters plotted for different configurations and lubricants at different speeds for fixed ball speed using Nijenbanning equation.

Tab. 13-10 Lambda parameters determined by Nijenbanning equation for film thickness for fixed ball speed.

Configuration	**Lubricant**	**Entrainment speed** mm/s									
		10	55	105	155	205	305	355	405	455	505
H/S	Glycerol	11.2	33.5	50.6	65.0	77.7	100.2	110.4	120.1	129.4	138.4
	R834/80	7.5	22.2	33.6	43.1	51.5	66.4	73.2	79.7	85.8	91.7
	HC32/100	3.4	10.0	15.1	19.4	23.2	29.9	33.0	35.9	38.7	41.3
S/H	Glycerol	7.9	23.6	35.7	45.7	54.7	70.5	77.7	84.6	91.1	97.4
	R834/80	5.1	15.2	23.0	29.6	35.4	45.6	50.3	54.7	58.9	63.0
	HC32/100	2.4	7.3	11.0	14.1	16.9	21.8	24.0	26.1	28.1	30.1
S/S	Glycerol	9.3	27.7	41.8	53.7	64.2	82.8	91.2	99.2	106.9	114.3
	R834/80	6.8	20.2	30.5	39.2	46.9	60.4	66.6	72.5	78.1	83.5
	HC32/100	3.2	9.5	14.4	18.5	22.2	28.6	31.5	34.3	36.9	39.5

Fixed disc speed

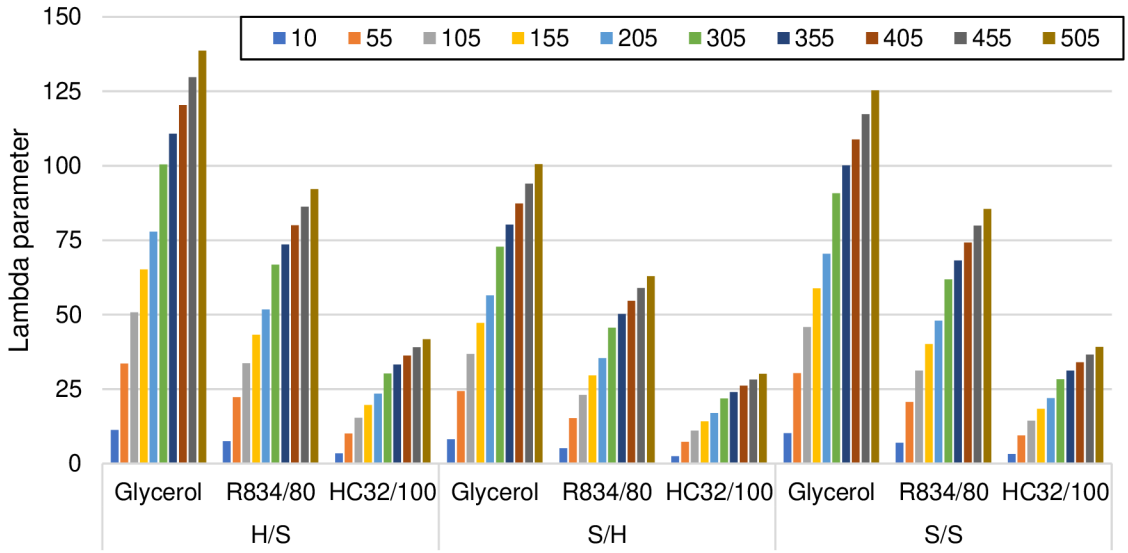

Fig. 13-11 Lambda parameters plotted for different configurations and lubricants at different speeds for fixed disc speed using Nijenbanning equation

Tab. 13-11 Lambda parameters determined by Nijenbanning equation for film thickness for fixed disc speed.

Configuration	**Lubricant**	**Entrainment speed** mm/s									
		10	55	105	155	205	305	355	405	455	505
H/S	Glycerol	11.3	33.6	50.8	65.1	77.9	100.4	110.7	120.4	129.8	138.7
	R834/80	7.5	22.3	33.7	43.3	51.8	66.7	73.5	80.0	86.2	92.2
	HC32/100	3.4	10.1	15.3	19.6	23.4	30.2	33.3	36.3	39.1	41.7
S/H	Glycerol	8.2	24.3	36.8	47.2	56.4	72.8	80.2	87.3	94.0	100.5
	R834/80	5.1	15.2	23.0	29.6	35.4	45.6	50.3	54.7	58.9	63.0
	HC32/100	2.5	7.3	11.0	14.2	16.9	21.8	24.1	26.2	28.2	30.2
S/S	Glycerol	10.2	30.3	45.9	58.9	70.4	90.8	100.0	108.8	117.3	125.4
	R834/80	6.9	20.7	31.3	40.1	48.0	61.9	68.2	74.2	79.9	85.4
	HC32/100	3.2	9.5	14.3	18.4	22.0	28.3	31.2	34.0	36.6	39.1

13.3.2 Lambda calculated by Hamrock Dowson Central equation

Fixed ball speed

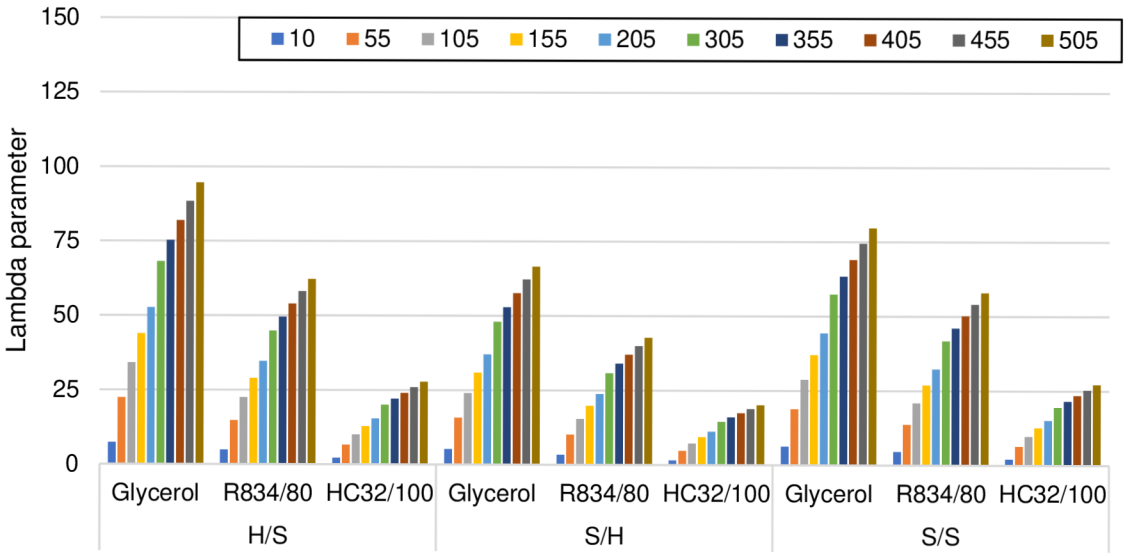

Fig. 13-12 Lambda parameters plotted for different configurations and lubricants at different speeds for fixed ball speed using Hamrock Dowson Central equation

Tab. 13-12 Lambda parameters determined by Hamrock Dowson Central equation for film thickness for fixed ball speed.

Configuration	**Lubricant**	**Entrainment speed** mm/s									
		10	55	105	155	205	305	355	405	455	505
H/S	Glycerol	7.4	22.4	34.1	43.9	52.6	68.1	75.2	81.9	88.4	94.6
	R834/80	4.9	14.7	22.4	28.9	34.7	44.9	49.5	54.0	58.2	62.3
	HC32/100	2.2	6.6	10.0	12.9	15.4	20.0	22.0	24.0	25.9	27.7
S/H	Glycerol	5.2	15.8	24.0	30.9	37.0	48.0	52.9	57.7	62.2	66.6
	R834/80	3.3	10.1	15.4	19.8	23.8	30.8	34.0	37.0	39.9	42.7
	HC32/100	1.6	4.8	7.3	9.4	11.2	14.5	16.0	17.5	18.8	20.2
S/S	Glycerol	6.2	18.9	28.7	37.0	44.4	57.4	63.4	69.0	74.5	79.7
	R834/80	4.5	13.7	20.9	26.9	32.2	41.7	46.1	50.2	54.1	57.9
	HC32/100	2.1	6.4	9.8	12.6	15.1	19.5	21.5	23.4	25.3	27.1

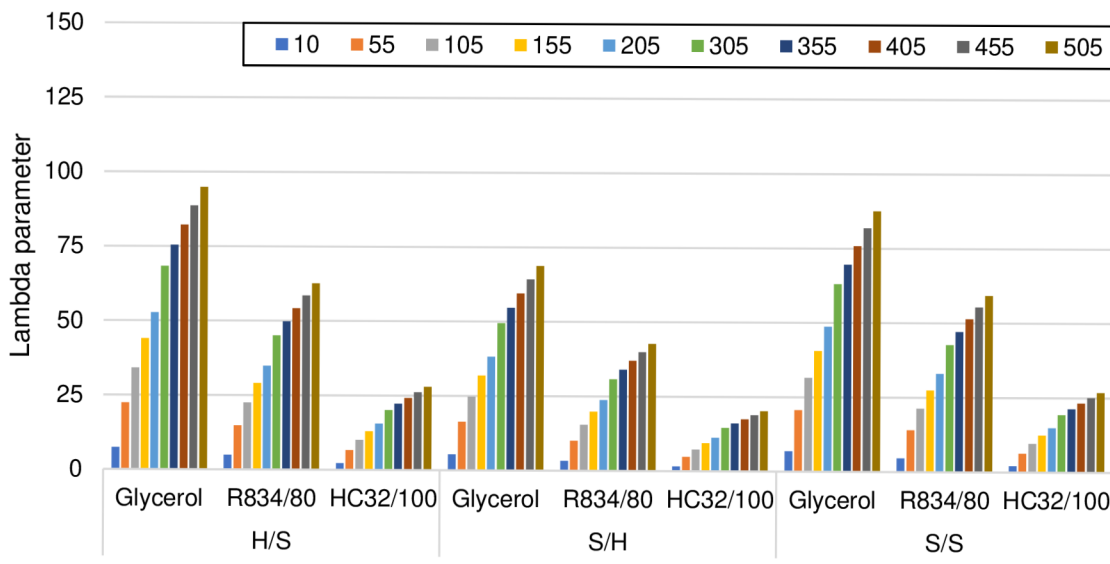

Fig. 13-13 Lambda parameters plotted for different configurations and lubricants at different speeds for fixed disc speed using Hamrock Dowson Central equation.

Tab. 13-13 Lambda parameters determined by Hamrock Dowson Central equation for film thickness for fixed disc speed.

Configuration	**Lubricant**	**Entrainment speed** mm/s									
		10	55	105	155	205	305	355	405	455	505
H/S	Glycerol	7.4	22.4	34.2	44.0	52.8	68.3	75.4	82.1	88.6	94.8
	R834/80	4.9	14.8	22.5	29.0	34.8	45.1	49.8	54.2	58.5	62.6
	HC32/100	2.2	6.6	10.1	13.0	15.6	20.2	22.3	24.3	26.2	28.0
S/H	Glycerol	5.4	16.3	24.8	31.9	38.2	49.5	54.6	59.5	64.2	68.7
	R834/80	3.3	10.1	15.4	19.8	23.8	30.8	34.0	37.0	39.9	42.7
	HC32/100	1.6	4.8	7.3	9.4	11.3	14.6	16.1	17.5	18.9	20.2
S/S	Glycerol	6.8	20.7	31.5	40.6	48.7	63.1	69.6	75.8	81.8	87.5
	R834/80	4.6	14.0	21.4	27.5	33.0	42.7	47.2	51.4	55.4	59.3
	HC32/100	2.1	6.3	9.7	12.4	14.9	19.3	21.3	23.2	25.1	26.8

13.3.3 Lambda calculated by Hamrock Dowson Minimum equation

Fixed ball speed

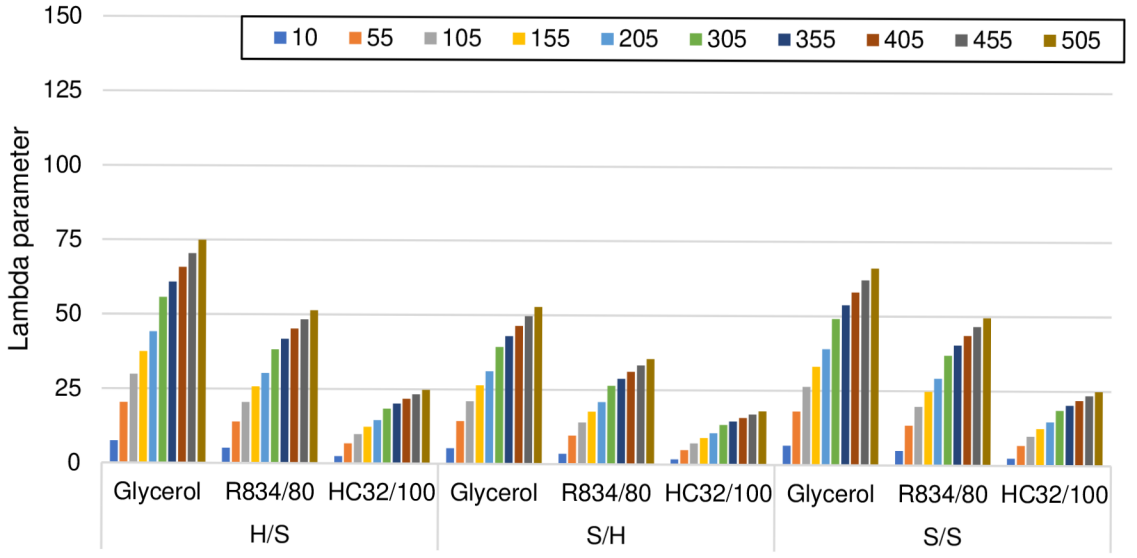

Fig. 13-14 Lambda parameters plotted for different configurations and lubricants at different speeds for fixed ball speed using Hamrock Dowson Minimum equation.

Tab. 13-14 Lambda parameters determined by Hamrock Dowson Minimum equation for film thickness for fixed ball speed.

Configuration	**Lubricant**	**Entrainment speed** mm/s									
		10	55	105	155	205	305	355	405	455	505
H/S	Glycerol	7.4	20.4	29.8	37.4	44.1	55.7	60.9	65.8	70.5	74.9
	R834/80	5.1	13.9	20.4	25.7	30.3	38.2	41.8	45.1	48.3	51.3
	HC32/100	2.4	6.6	9.8	12.3	14.5	18.4	20.1	21.7	23.2	24.7
S/H	Glycerol	5.2	14.3	21.0	26.4	31.1	39.3	42.9	46.4	49.7	52.8
	R834/80	3.5	9.6	14.1	17.7	20.8	26.3	28.8	31.1	33.3	35.4
	HC32/100	1.7	4.8	7.1	8.9	10.5	13.3	14.6	15.8	16.9	18.0
S/S	Glycerol	6.5	17.9	26.3	33.0	38.9	49.2	53.7	58.1	62.2	66.1
	R834/80	4.9	13.4	19.7	24.7	29.2	36.9	40.3	43.5	46.6	49.5
	HC32/100	2.4	6.7	9.8	12.4	14.6	18.5	20.2	21.9	23.4	24.9

Fixed disc speed

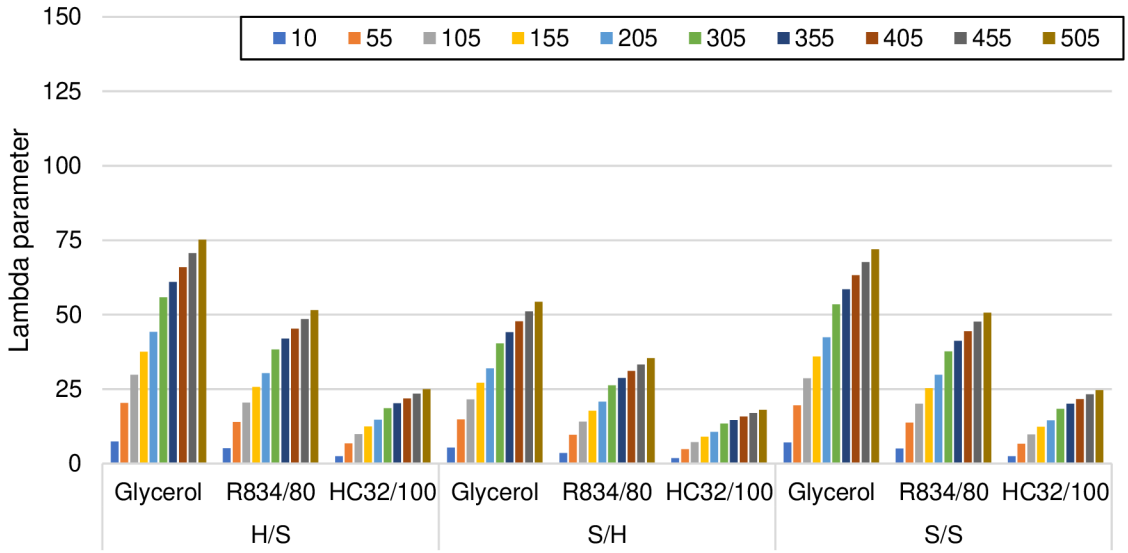

Fig. 13-15 Lambda parameters plotted for different configurations and lubricants at different speeds for fixed disc speed using Hamrock Dowson Minimum equation.

Tab. 13-15 Lambda parameters determined by Hamrock Dowson Minimum equation for film thickness for fixed disc speed.

Configuration	**Lubricant**	**Entrainment speed** mm/s									
		10	55	105	155	205	305	355	405	455	505
H/S	Glycerol	7.4	20.4	29.8	37.5	44.2	55.8	61.0	65.9	70.6	75.1
	R834/80	5.1	14.0	20.5	25.8	30.4	38.4	41.9	45.3	48.5	51.6
	HC32/100	2.4	6.7	9.9	12.4	14.6	18.5	20.3	21.9	23.5	24.9
S/H	Glycerol	5.4	14.8	21.6	27.2	32.0	40.4	44.2	47.7	51.1	54.4
	R834/80	3.5	9.6	14.1	17.7	20.8	26.3	28.8	31.1	33.3	35.4
	HC32/100	1.8	4.8	7.1	9.0	10.6	13.4	14.6	15.8	16.9	18.0
S/S	Glycerol	7.1	19.5	28.6	36.0	42.4	53.5	58.5	63.2	67.7	71.9
	R834/80	5.0	13.7	20.1	25.3	29.8	37.7	41.2	44.5	47.6	50.6
	HC32/100	2.4	6.6	9.7	12.3	14.5	18.3	20.1	21.7	23.2	24.7